Production of an upgraded bio-oil by catalytic pyrolysis of forest residues

by

Farai Chireshe

Thesis presented in partial fulfilment
of the requirements for the Degree

of

MASTER OF ENGINEERING
(CHEMICAL ENGINEERING)

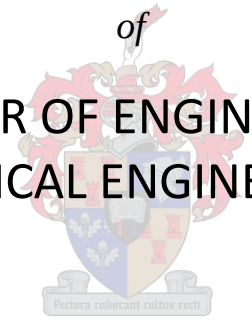

in the Faculty of Engineering
at Stellenbosch University

Supervisor
Prof. Johann F. Görgens

Co-Supervisor
Dr. François-Xavier Collard

April 2019

Declaration

By submitting this thesis electronically, I declare that the entirety of the work contained therein is my own, original work, that I am the sole author thereof (save to the extent explicitly otherwise stated), that reproduction and publication thereof by Stellenbosch University will not infringe any third party rights and that I have not previously in its entirety or in part submitted it for obtaining any qualification.

Date: April 2019

Plagiarism Declaration

1. Plagiarism is the use of ideas, material and other intellectual property of another's work and to present is as my own.

2. I agree that plagiarism is a punishable offence because it constitutes theft.

3. I also understand that direct translations are plagiarism.

4. Accordingly all quotations and contributions from any source whatsoever (including the internet) have been cited fully. I understand that the reproduction of text without quotation marks (even when the source is cited) is plagiarism.

5. I declare that the work contained in this assignment, except where otherwise stated, is my original work and that I have not previously (in its entirety or in part) submitted it for grading in this module/assignment or another module/assignment.

Student number: 21451230

Initials and surname: F CHIRESHE

Signature: ……..

Date: 15 February 2019

Abstract

Forest plantations generate solid residues which are usually disposed of by combustion. Sometimes these residues are simply left in the forest, where they contribute little to soil fertility, and yet pose a significant fire hazard. Unlike combustion, which produces heat and is limited to onsite use only, pyrolysis can be used to convert the forestry residues to produce a bio-oil that is easier to transport and use offsite. However, bio-oil has limitations in its use as a liquid fuel because its high oxygen content (about 40 wt. %), gives it undesirable qualities such as high acidity, oxidative instability and low energy content. The aim of the project was to catalytically upgrade the bio-oil by lowering its oxygen content so that it can be co-processed in a conventional crude oil refinery to produce transportation fuels.

Eucalyptus grandis was chosen as the feedstock based on it being the most abundant species used in the regions with the most forestry residue in South Africa. From literature, 3 catalysts: CaO, MgO and Al_2O_3 were selected based on their ability to promote deoxygenation. Screening tests were carried out in a batch reactor, under intermediate pyrolysis conditions at 550 °C and 30 wt.% catalyst concentration. The improvement in the bio-oil HHV in the catalyst screening was similar for all the catalysts; it increased from 21.8 MJ/kg without catalyst to between 26.3 – 26.8 MJ/kg for all 3 catalysts. Optimisation experimental designs (CCD) were then carried out for each of CaO and MgO to maximise bio-oil quality in terms of HHV at an acceptable yield. Temperature was varied from 444 – 656 °C and the catalyst concentration from 1.7 – 58.3 wt.%. For MgO deoxygenation occurred mainly via decarboxylation reactions and the maximum HHV was at 26.9 MJ/kg at 560.0 °C and 33.8 wt.% catalyst concentration, at a yield of 19.4 wt.%. For CaO, dehydration reactions were dominant and the maximum HHV was 27.5 MJ/kg at 490.0 °C and 59.0 wt.% CaO concentration. The bio-oil yield was 13.4 wt.% which was low to achieve the target bio-oil blending ratio. A statistical desirability function was then used, and the desirable optimum conditions were found to be those of the catalyst screening. The best performing catalyst was found to be CaO based on energy conversion assessment and the better applicability of char derived from CaO catalytic pyrolysis in soil amendment.

A pilot reactor with a 1 kg/hr capacity was then used to scale up the process from bench scale. Better contact between the solid catalyst and organic volatiles in the pilot reactor meant that the optimum reaction at bench (550 °C) had to be reduced to 500 °C to limit the effect of severe catalytic cracking. The resultant bio-oil had an oxygen content of 12.6 wt.%, a water content of 19.7 wt.% at a yield of 15.6 wt.%, which meet the specifications required for successful co-processing in a crude oil refinery at a 10 wt.% blending ratio. However, it is recommended that the bio-oil be tested for co-processing in a Fluid Catalytic Cracking unit (FCC).

Abstrak

Bosplantasies genereer soliede residu's wat gewoonlik deur verbranding verwyder word. Soms word hierdie residu's gewoon in die woud gelos, waar dit min bydrae tot grond vrugbaarheid, maar 'n beduidende brandgevaar inhou. Anders as verbranding wat hitte produseer en beperk is tot gebruik slegs op die perseel, kan pirolise gebruik word om die bosbou residu om te skakel na bio-olie wat makliker is om te vervoer en te gebruik weg van die terrein. Bio-olie het wel beperkinge in sy gebruik as 'n vloeistof-brandstof as gevolg van sy hoë suurstofinhoud (omtrent 40 wt.%) wat dit onwenslike kwaliteite soos hoë suurheid, oksidatiewe onstabiliteit en lae energie-inhoud gee. Die doel van hierdie projek was die katalitiese opgradering van die bio-olie deur sy suurstofinhoud te verlaag sodat dit in 'n konvensionele ru-olie raffinadery geko-prosesseer kan word om vervoer brandstof te produseer.

Eucalyptis grandis is gekies as die voermateriaal omdat dit die oorvloedigste spesie is wat gebruik word in die omgewings met die meeste bosbou residu in Suid-Afrika. Uit literatuur is drie kataliste — CaO, MgO en Al_3O_2 — gekies gebaseer op hul vermoë om deoksigenering te bevorder. Siftingstoetse is uitgevoer in 'n lotreaktor, onder intermediêre pirolise toestande by 550 °C en 30 wt.% kataliskonsentrasie. Die verbetering in die bio-olie hoër warmte waarde (HHV) in die katalissifting was soortgelyk vir al die kataliste; dit het verhoog van 21.8 MJ/kg tot tussen 26.3 en 26.8 MJ/kg vir al drie kataliste. Optimering eksperimentele ontwerpe (CCD) is toe uitgevoer vir elk van CaO en MgO om bio-olie kwaliteit in terme van HHV by 'n aanvaarbare opbrengs, te maksimeer. Temperatuur is gevarieer van 444 °C tot 656 °C en die kataliskonsentrasie van 1.7 wt.% tot 58.3 wt%. Vir MgO het deoksigenering hoofsaaklik voorgekom via dekarboksilasiereaksies en die maksimum HHV was 26.9 MJ/kg by 560.0 °C en 33.8 wt.% kataliskonsentrasie, by 'n opbrengs van 19.4 wt.%. Vir CaO was dehidrasiereaksies dominant en die maksimum HHV was 27.5 MJ/kg by 490.0 °C en 59.0 wt.% CaO-konsentrasie. Die bio-olie opbrengs was 13.4 wt.% wat te laag was om die doelwit bio-olievermengingverhouding te bereik. 'n Statistiese wenslikheidsfunksie is toe gebruik, en die gewenste optimale toestande is bevind om dié van die katalissifting te wees. Die beste presterende katalis is gevind om CaO te wees gebaseer op energie-omsetting-assessering en beter toepassing van verkoolsel wat van CaO katalitiese pirolise af kom in grondwysinging.

’n Loodsreaktor met ’n 1 kg/hr-kapasiteit is toe gebruik om die proses op te skaal vanaf banktoetsskaal. Beter kontak tussen die soliede katalis en organiese vlugtige stowwe in die loodsreaktor het beteken dat die optimale temperatuur by banktoetsskaal (550 °C) verlaag moes word na 500 °C om die effek van ernstige katalitiese kraking te beperk. Die resulterende bio-olie het ’n suurstof inhoud van 12.6 wt.%, ’n waterinhoud van 19.7 wt.% by ’n opbrengs van 15.6 wt.% gehad, wat die spesifikasies vereis vir suksesvolle ko-prosessering in ’n ru-olie raffinadery by ’n 10 wt.%, haal. Dit word egter aanbeveel dat die bio-olie getoets word vir ko-prosessering in ’n vloeistof katalise breking (FCC)-eenheid.

Acknowledgments

Firstly, I would to thank the Lord for guiding me throughout this project, giving me strength in times that were challenging, which was most of the time!

I would also like to thank the Paper Manufacturers Association of South Africa (PAMSA) and the Department of Science and Technology (DST) for funding this research project. I am eternally grateful to my supervisors Prof JF Görgens and Dr F-X Collard for their advice and guidance throughout this entire project. Thank you to all the staff from the Process Engineering and Forestry and Wood Science Departments, who contributed to making this project a success. Special thanks to Mr Henry Solomon for the help with sample preparation and lignocellulosic characterisation, Ms Levine Simmers for doing Karl Fischer analysis of the bio-oils, Ms Hanlie Botha and Mr Jaco Van Rooyen for proximate analysis, the workshop team, Messrs Jos Weerdenburg, Anton Cordier and Bevan Koopman for assistance with troubleshooting the pilot plant reactor. Thanks to my colleagues from the pyrolysis research group for the advice and discussions we had around this project. Special mention goes to Mses Salomie Van der Westhuizen, Dominique Trew and Wendy Mfana for assistance with gas analysis and running the pilot scale experiments.

Lastly, I would like to thank my family and friends for the emotional support which helped me carry on throughout the project. I dedicate this thesis to my parents, Regis and Excellent and my brother Tatenda who encouraged me to embark on this Masters journey. To the love of my life Michelle, who was there every step of the way, thank you, I would not have done it without you.

Table of Contents

List of Figures

List of Tables

List of Acronyms and Abbreviations

ANOVA	Analysis of Variance
ASTM	American Society for Testing and Materials
BTX	Benzene Toluene Xylene
C/B	Catalyst to Biomass Ratio
CP	Catalytic Pyrolysis
C_{cat}	Catalyst Concentration
CCD	Central Composite Design
E. grandis	*Eucalyptus grandis*
EC	Energy Conversion
ESP	Electrostatic Precipitator
daf	dry ash free basis
db	dry basis
FCC	Fluid Catalytic Cracker
GC	Gas Chromatography
HHV	Higher Heating Value
$HHV_{O\text{-}PHASE}$	Higher Heating Value of the organic phase
LCO	Light Cycle Oil
LHV	Lower Heating Value
L.O.I	Loss on Ignition
MS	Mean square
NREL	National Renewable Energy Laboratory
PAH	Polycyclic Aromatic Hydrocarbons
SLPM	Standard Litres Per Minute
T	Temperature
TAPPI	Technical Association of Pulp and Paper Industries
TAN	Total Acid Number
TG	Thermogravimetric
VGO	Vacuum Gas Oil

WGSR	Water-Gas Shift Reaction
XRF	X-Ray Fluorescence
Y_{CHAR}	Char Yield
Y_{CH4}	CH_4 Yield
Y_{CO}	CO Yield
Y_{CO2}	CO_2 Yield
Y_{C2-C4}	Yield of C_2-C_4 hydrocarbon gases
Y_{H2}	H_2 Yield
Y_{LIQUID}	Total Liquid Yield
$Y_{O-PHASE}$	Organic Phase Yield
$Y_{P-WATER}$	Pyrolytic Water Yield

1 Introduction

The paper and pulp industry has been working on reducing their carbon emissions for some time now. This has been achieved by using increased amounts of renewable energy sources such as biomass generated as by-products from pulp production processes, black liquor and sludge (PAMSA 2016). This energy has mostly been produced through combustion in stationary equipment such as turbines and boilers for electricity generation. However, a drawback of this is that the energy has to be used on-site and the overall efficiency to power typically ranges from 15 – 30 % (Bridgwater 2003).

In South Africa, forestry residues or wastes, which are lignocellulosic biomass have the largest potential to increase the use of biomass for energy production (Ackerman et al. 2013). The forestry wastes are comprised of residues which are left behind after thinning and clearfelling of trees. Tree tops and branches make up most of the forestry wastes. When left in the plantation, the residue poses a fire hazard likely to destroy unfelled trees. Currently, these residues have no economic value and are disposed of by burning, or simply left to decompose in the plantation. No energy is recovered from the above mentioned practices and they also harm the environment through gaseous emissions, and are therefore considered as unsustainable (Phillips 2017). Sometimes the residue is sold as firewood but for prices as low as R50 (approximately $3) per tonne.

The use of agriculture and forestry residues for transportation fuel production may improve the economics in these industries (Junginger, Goh, and Faaij 2014). Conversion of these wastes to fuels that could be used in substitution of fossil fuels will also reduce carbon emissions from forestry. Reducing the CO_2 emissions will enable the pulp and paper industry to lower its carbon tax exposure. Assuming a sustainable forest management, fuels obtained from biomass have the potential to be carbon neutral, because the CO_2 released during combustion corresponds to the amount absorbed when the plants or trees regrow. Thus, the use of biomass sources for fuel production will lead to a reduction in pollution as well as aiding the worldwide drive towards using renewable fuels.

Biomass residues can be converted to energy and fuels via bio-chemical and thermo-chemical methods. The common thermo-chemical conversion methods are combustion, gasification and pyrolysis. Combustion of biomass material produces heat (with limited efficiency), which must be used instantaneously because heat cannot be stored efficiently (Bridgwater 2003).

Gasification is used to produce combustible fuel gas from biomass and it is limited to on-site use because the large volume of gas is not convenient to transport. Pyrolysis appears as a suitable method to convert biomass to fuel, especially in liquid form. Pyrolysis is the thermal conversion of biomass material in the absence of oxygen to produce a solid residue (char) and volatiles comprised of a condensable fraction (bio-oil) and permanent gases.

The liquid bio-oil product from pyrolysis can be conveniently stored and transported to a central site for usage or further processing. Furthermore, in comparison to other processes in general, pyrolysis accepts a diverse range of lignocellulosic feedstock materials such as agricultural and forestry residue as well as industrial waste streams from food processing (Yildiz et al. 2016). Bio-oils are a complex mixture of over 300 compounds, mostly oxygenated, which include alcohols, aldehydes, furans, esters, ketones and phenolics (Huber, Sara, and Corma 2006). Typical physical properties of bio-oil from lignocellulosic biomass and heavy fuel oil are given in ***Table 1-1*** (Czernik and Bridgwater 2004). Compared to fossil fuel, the relatively high level of oxygenation gives the bio-oils undesirable qualities, which limit their use as a transportation fuel. The most significant of these properties are high water content, low energy content, poor volatility, corrosiveness, oxidative instability (aging) and high viscosity.

Table 1-1: Typical physical properties of bio-oil and heavy fuel oil, adapted from Czernik and Bridgwater (2004)

Property	Bio-oil	Heavy Fuel Oil
Moisture content (wt. %)	15 – 30	0.1
pH	2.5	-
Specific gravity	1.2	0.94
Elemental composition (wt. %)		
C	54 – 58	85
H	5.5 – 7.0	11
O	35 – 40	1.0
Ash	0 – 0.2	0.1
HHV (MJ/kg)	16 – 19	40
Viscosity (at 50 °C), cP	40 – 100	180

The high-water content in pyrolysis oils lowers their heating value and leads to difficult ignition in diesel engines, although providing benefits in terms of lower viscosity (Czernik and Bridgwater 2004). Some compounds with relatively high boiling points (> 380 °C) such as oligomeric phenols and sugars are present in bio-oils making them unusable in applications that require complete evaporation before combustion (Czernik and Bridgwater 2004). Bio-oils also contain substantial amounts of carboxylic acids which are mainly formic and acetic acids. As a result of this high acidity, bio-oils are corrosive to common construction material such as aluminium and carbon steel (Czernik and Bridgwater 2004). During storage, the oxygenated compounds in bio-oil can undergo reactions to form additional oligomers resulting in a higher viscosity and lower compatibility with fossil fuel. Aldehydes were found to be involved in the majority of the chemical reactions that lead to bio-oil degradation (Dielbold 2000). High viscosity makes bio-oils much more difficult to pump and therefore increases the costs to handle them.

Because of the above limitations, bio-oils must be upgraded before considering them for blending with fossil oil for transportation fuel applications. Among the methods for upgrading bio-oils to transportation fuels are hydrotreating, gasification, Fluid Catalytic Cracking (FCC) and steam reforming, which can all be done in a dedicated bio-refinery. Although a dedicated bio-refinery for bio-oil upgrading is an attractive option, its construction is expensive and carries high economic risks (Yildiz et al. 2016). These authors also reported that a more economic method would be to produce a higher quality bio-oil through an improved single pyrolysis step using catalysts mixed in the reactor. The upgraded bio-oil could then be co-processed with vacuum gas oil (VGO) in a standard crude oil refinery to produce fuels. Capital expenses to modify existing petroleum refineries for bio-oil co-processing are likely to be much less than those of setting up a dedicated bio-refinery as only the bio-oil feed line to the FCC will need to be added (Yildiz et al. 2016).

The main goal of this study will be to produce a bio-oil with improved properties via catalytic pyrolysis using forest residues as feedstock. The quality of the upgraded bio-oil should be high enough, such that the bio-oil can be co-processed with VGO in an FCC to produce transportation fuels, enabling the forestry industry to lower its carbon footprint.

The structure of the thesis is as follows; Chapter 2 gives a review of the literature relevant to this study. The scope covered as well as the methodology used are given in Chapter 3. Results from the biomass characterisation and catalyst screening are discussed in Chapter 4, while Chapters 5 and 6 discuss the results from the MgO and CaO optimisations respectively. Results from the pilot scale experiments are discussed in Chapter 7. Chapter 8 gives the conclusions and recommendations from the study. An Appendix section is also included at the end of the document to show the calculations done in the estimation of the amount of forest residues in South Africa, raw data and the regression models developed for various responses from the bench optimisation experiments, as well as the elemental analysis of the different oil fractions obtained from the pilot scale experiments.

2 Literature Review

The following sections discuss the literature concerning to this study. Section 2.1 gives a description of lignocellulosic biomass while a review on bio-oil co-processing is given in Section 2.2. Discussions on pyrolysis, its different types and the parameters affecting pyrolysis are given in Sections 2.3, 2.4 and 2.5. Catalytic pyrolysis is reviewed in Section 2.6. Section 2.7 gives the conclusions from the literature review.

2.1 Lignocellulosic Biomass

Biomass is any organic matter which is either living or produced by living organisms. It is divided into plant, animal, aquatic and other types of biomass. Most of the plant biomass in the world is agricultural and woody biomass, which together can be classified as lignocellulosic biomass (Tripathi, Sahu, and Ganesan 2016). Forestry residue falls under woody biomass, that is biomass produced from trees. It includes branches, leaves, bark and wood chips. Trees can be classified botanically as hardwoods or softwoods. Hardwoods are angiosperms (flowering plants) and softwoods are gymnosperms (seed producing plants) (Wiedenhoeft and Miller 2005). A variety of different biomasses have been considered for energy applications and the elemental compositions of some of them are detailed in ***Table 2-1***. The carbon content of woody biomass ranges from 45 – 53 wt.% while the oxygen content ranges from 40 – 50 wt. %. The nitrogen content is small (< 0.5 wt. %). Sulphur content of woody biomass is relatively very low (< 0.1 wt.%) compared to fossil fuel (> 2 wt.%) and is rarely measured (Nsaful, Collard, and Görgens 2018).

Table 2-1: Elemental analysis of different biomasses (dry and ash free basis)

Biomass	Elemental Composition (wt.%)				Reference
	C	H	O	N	
E. grandis	48.2	6.20	44.10	<0.5	(Joubert 2013)
Pine wood	49.9	5.95	44.05	0.1	
Beech wood	48.42	6.01	45.42	0.15	(Wang et al. 2005)
Bamboo wood	48.62	5.90	45.15	0.33	
Forest Residue	52.50	6.13	40.86	0.51	(Oasmaa and Kuoppala 2003)
Pine sawdust	50.35	6.01	43.54	0.10	

2.1.1 Structure and Chemical Composition

Since woody forest residue is the biomass of interest in this study, the structure and chemical composition of woody lignocellulosic biomass will be discussed. Lignocellulose is a three-dimensional bio-polymer composed of three major components: cellulose, hemicelluloses and lignin. Cellulose and hemicelluloses are sugar-based polymers (polysaccharides). Woody biomass also contains low molecular weight compounds called extractives as well as inorganics in minor amounts (Rowell et al. 2005). Typical chemical composition of woody biomass is given in ***Table 2-2***. The inorganics content of woody biomass is generally < 2 wt.% (Neves et al. 2011).

Table 2-2: Typical chemical composition of biomass

Biomass	Component (wt. %)				Reference
	Cellulose	Hemicelluloses	Lignin	Extractives	
Hardwood fibres	40.1	27.8	23.1	7.2	(Garcìa-Pérez et al. 2007)
E.grandis	±51	±20	±27	-	(Oasmaa et al. 2010)
Scots pine	40	28.5	27.7	3.5	(Sjöström 1993)
Spruce	39.5	30.6	27.5	2.1	

As seen from ***Table 2-2***, the proportions of structural components of biomass: cellulose, hemicelluloses and lignin differ according to biomass types. The ratio of these components in biomass have an effect on the product distributions during pyrolysis (Alves and Figueiredo 1989). This emphasises the need to characterise the biomass feed used in this study.

2.1.1.1 Cellulose

Cellulose is the major component of lignocellulosic biomass and typically accounts for 40 – 50 wt.% of the total biomass on a dry, ash and extractive free basis (Serrano-Ruiz and Dumesic 2012). It is a long chain linear polymer of glucose, connected by beta-1,4-glycosidic bonds. Each chain contains an average of 9000 – 10000 glucose molecules (Rowell et al. 2005). This linear arrangement results in the formation of strong hydrogen bonds between different cellulose chains, giving cellulose high crystallinity and a low surface area resulting in improved stability/resistance to chemical attack (Serrano-Ruiz and Dumesic 2012).

2.1.1.2 Hemicelluloses

Hemicelluloses are amorphous polysaccharides that surround the cellulose fibres and typically amount to 20 – 30 wt. % of the total biomass content on a dry, ash and extractive free basis (Serrano-Ruiz and Dumesic 2012). They have a heterogeneous composition and are named according to the type of sugars they contain. Hemicelluloses from hardwoods are mostly xylans, whereas those from softwoods are mostly glucomannans. Examples are glucuronoxylan and galactoglucomanan. Hemicelluloses with a xylan backbone contain acetyl groups. On average, seven acetyl groups can be found per ten xylose units in glucuronoxylan. The acetyl content in hardwoods ranges from 3.1 – 4.4 wt. % while in softwoods it is generally less than 1.7 wt. % (Rowell et al. 2005).

2.1.1.3 Lignin

Lignin gives the structural rigidity of wood by holding the cellulose and hemicellulose fibres together. It is made up of three-dimensional polymers of propyl-phenol groups that are linked by carbon-carbon and ether bonds (Serrano-Ruiz and Dumesic 2012). The monomer units for lignin; p-coumaryl alcohol, coniferyl alcohol and sinapyl alcohol are shown in **Figure 2-1**.

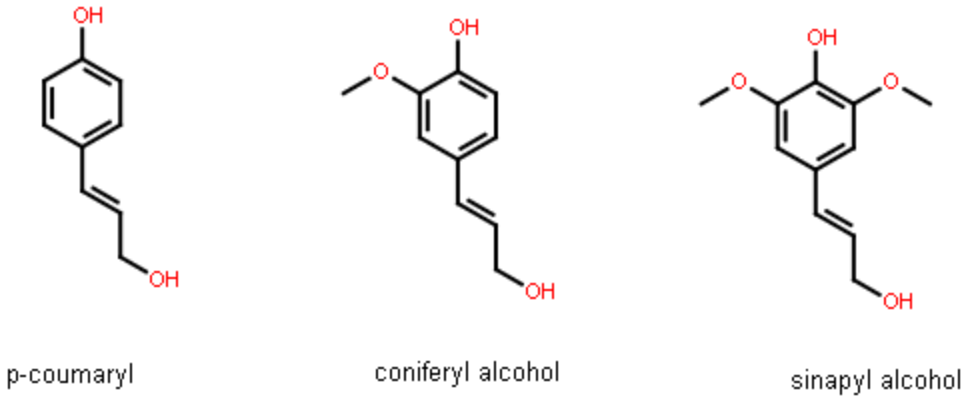

Figure 2-1: Chemical structures of lignin precursors p-coumaryl alcohol, coniferyl alcohol and sinapyl alcohol. Redrawn from Rowell et al. (2005)

Softwood lignin mainly consists of polymerisation products of coniferyl alcohol, while hardwood lignin is made up of copolymers of coniferyl and sinapyl alcohols. The typical lignin content for hardwoods ranges from 18 – 25 wt. %, whereas that of softwoods ranges from 25 – 35 wt. % (Rowell et al. 2005). However, higher lignin contents for hardwoods have been reported in literature, especially for eucalyptus. Park et al. (2012) and Inalbon et al. (2015) reported lignin contents of 30 and 29 wt. % respectively for *E. grandis*.

2.1.1.4 Extractives

Extractives are soluble chemicals which can be separated from wood using solvents (Rowell et al. 2005), and they are typically classified by the solvent used for their extraction. Extractives are responsible for giving the wood its colour and smell. Compounds that make up extractives are mainly fatty acids, phenols, terpenes and steroids (Rowell et al. 2005). It was reported by the same authors that the extractive content of hardwoods varies significantly (1.9 – 13.2 wt. %) depending on the tree species.

2.1.1.5 Inorganics

Wood fibre is also composed of inorganic elements absorbed in the form of mineral salts and other inorganic matter in the wood fibre. Hardwoods typically contain 0.5 wt. % inorganics whereas softwoods contain 0.3 wt. % inorganics. Around 80 wt.% (dry basis) of the inorganics in wood consists of Ca, Mg and K (Rowell et al. 2005). Most of the mineral cations present in lignocellulosic biomass are contained in hemicelluloses (Nowakowski and Jones 2008). These inorganics are also referred to as ash, which remains behind after lignocellulose combustion.

2.1.1.6 Bark

The bark is the outermost layer of the tree and it is made up of dead cells. Besides the other chemical components in wood, bark usually contains another compound, suberin which has a lignin-like aromatic matrix (Gellerstedt, Ek, and Henriksson 2009). The typical chemical composition of bark is shown in ***Table 2-3*** (Rowell et al. 2005).

Table 2-3: Typical hardwood and softwood bark chemical composition (Rowell et al. 2005)

Constituent	**Composition (wt. %)**	
	Hardwood	**Softwood**
Polysaccharides	19.9	41.7
Lignin	23.0	43.7
Suberin	39.4	1.5
Extractives	14.2	11.4

As seen from ***Table 2-3***, the polysaccharide (cellulose and hemicelluloses) content of bark is less than that of wood, especially for hardwood bark. In hardwood bark, suberin is the most abundant component whereas in softwood bark it accounts for only 1.5 wt. %. The extractive content of bark is much higher than that of wood. Rowell et al. (2005) also report that bark has a much higher inorganic content (around 13 wt.%) than associated wood.

2.2 Bio-oil Co-processing in Petroleum Refineries

As stated earlier, pyrolysis bio-oil cannot be used as it is in facilities using conventional fossil fuels. Recently, some studies have been carried out to investigate the possibility of blending (co-processing) pyrolysis bio-oil with Vacuum Gas Oil (VGO) in the Fluid Catalytic Cracking (FCC) unit of a conventional crude oil refinery, to produce gasoline (petrol) and diesel type fuels. VGO is a product from the vacuum distillation of crude oil and it is the standard feed into an FCC. An illustration of such bio-oil co-processing in conventional oil refineries, adapted from De Rezende Pinho et al. (2017), is shown in ***Figure 2-2***.

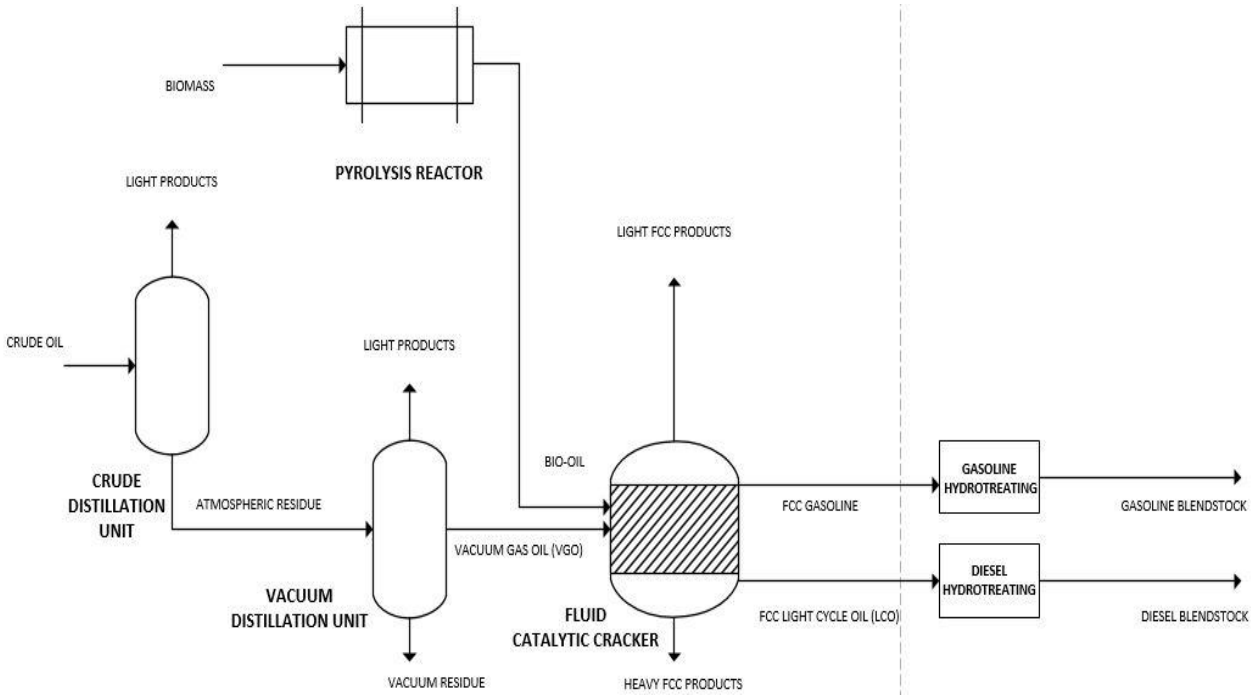

Figure 2-2: Illustration of bio-oil co-processing in standard oil refineries, adapted from De Rezende Pinho et al. (2017)

Some of the reports on bio-oil co-processing are presented in **Table 2-4**. The blending ratio is the mass fraction of bio-oil oil in the FCC feed. Crude bio-oil refers to bio-oil produced from direct pyrolysis without further upgrading, for example via the use of a catalyst or hydrodeoxygenation. Co-processing studies have been cried out on both lab and pilot scale. De Rezende Pinho et al. (2015; 2017) have demonstrated the co-processing of untreated pyrolysis oils on a pilot scale.

One of their studies showed that bio-oils with an oxygen content of up to 32.8 wt.% (dry basis) can be successfully co-processed at a 5 wt.% blending ratio with little impact on the product yield and quality (De Rezende Pinho et al. 2017). The water content of these bio-oils can be as high as 32 wt.%. On lab scale, it was shown that with upgraded bio-oils, with an oxygen content of less than 28 wt.% on a dry basis, blending ratios greater than 5 wt.% can be successfully co-processed (de Miguel Mercader et al. 2010; Fogassy et al. 2010; Thegarid et al. 2014).

Table 2-4: Co-processing of pyrolysis oils in crude oil petroleum refineries

Blending ratio (wt.%)	**Bio-oil O Content (wt. %, db)**		**Water content (wt. %)**	**Scale**	**Impact on product yield**	**Reference**
	Crude	**Upgraded**				
5	32.8	-	31.9	Pilot	Insignificant	De Rezende Pinho et al. (2017)
10	38.2	-	25.5	Pilot	Small	De Rezende Pinho et al. (2015)
20					Large	
10	-	18.9	3	Lab	Insignificant	Thegarid et al. (2014)
10		19.4	11		Insignificant	
20	-	21	-	Lab	Insignificant	Fogassy et al. (2010)
20	38.4	28	15.9	Lab	Small	De Miguel Mercader et al. (2010)
		24.4	10			
		22.6	5.7			
		16.9	2.1			
		15.5	3.2			

2.2.1 Advantages of Bio-oil Co-processing in FCC

One of the main advantages of co-processing bio-oil and vacuum gas oil is that liquid transportation fuels can be partially produced from lignocellulosic biomass in a conventional petroleum refinery. After co-processing, the presence of renewable carbon from biomass origin was confirmed in both light cycle oil (diesel range) and gasoline products (Thegarid et al. 2014; De Rezende Pinho et al. 2015; 2017).

Another advantage of co-processing is that it should not affect the water contents of the liquid effluents from the FCC. For bio-oils with water contents of less than 32 wt.%, the liquid effluents produced from bio-oil co-processing and those produced from pure VGO had practically the same amount of water, which was approximately 0.04 wt. % (De Rezende Pinho et al. 2015; 2017).

With relatively low blending ratios, co-processing bio-oil in refineries can produce liquid yields similar to those produced by processing pure vacuum gas oil. Fogassy et al. (2010) reported that yields of gasoline and Light Cycle Oil (LCO) obtained from bio-oil co-processing were similar to the yields obtained when only crude-oil-derived VGO was cracked at a 10 wt.% blending ratio. At a blending ratio of 20 wt.%, De Miguel Mercader et al. (2010) observed small differences in the liquid yields from co-processing and those from the use of pure VGO. However, at higher blending ratios, the liquid yields can be affected. De Rezende Pinho et al. (2017) observed that for a 5 wt. % blending ratio, the gasoline and LCO yields were comparable to those obtained with a pure VGO feed, while at 10 wt. %, a slight decrease in both yields was observed. A clear drop in gasoline yield (about 3 wt. %) was observed when the blending ratio was increased to 20 wt. % (De Rezende Pinho et al. 2015). The above suggests that to maximise gasoline and LCO production, bio-oil blending ratios greater than 20 wt.% should not be used. Other limitations of co-processing are discussed in Section 2.2.2.

2.2.2 Limitations of FCC co-processing

2.2.2.1 Acidity

The development of the use of pyrolysis oils in refineries is affected by the high acidity of the oil (Marinangeli et al. 2005). The acidity of the oil is most likely to cause corrosion in standard refinery units. The acidity of bio-oil is a problem but it is expected that the dilution effect when co-processing at low blending ratios, (5 – 15 wt. %) will have a minor effect on the FCC process (Mante and Agblevor 2014).

Acidity of bio-oils is linked to the oxygen content. Carboxylic acids are common oxygenated compounds in bio-oil and can account up to 10 % of the bio-oil (Aguado et al. 2000). This is one of the reasons to limit the oxygen content fed into the oil refinery as this also limits the amount of acids and hence corrosivity of the bio-oil in the feed. In addition, the use of basic catalysts like CaO and MgO during the pyrolysis process can be considered in order to convert carboxylic acids in the bio-oil, into less acidic compounds like ketones (Lin et al. 2010; Stefanidis et al. 2011).

2.2.2.2 Coke Formation

The presence of bio-oil in FCC units is known to promote coke (carbon deposits) formation (De Rezende Pinho et al. 2017). Coke formation is undesirable in these units, because it alters the activity of FCC catalysts. At 5 and 10 wt.% blending ratios, coke formation was found to be negligible. However, at 20 wt.%, the coke formation can be twice that produced from the processing of pure VGO (Fogassy et al. 2010; De Rezende Pinho et al. 2015). This suggests that with crude bio-oil the blending ratio should be limited to 10 wt.% to limit coke formation.

2.2.2.3 Phenolic Content

Products from bio-oil co-processing are characterised by an increase in the phenolic content. In particular, the phenolic content of the gasoline fraction was reported to increase with increasing blending ratio (De Rezende Pinho et al. 2017). At the lower blending ratio, the phenolic fraction was comparable to the one from pure VGO processing whereas at 20 wt. % blending, it was significantly higher and might have a negative impact on vehicle engines. Other refinery products are not significantly affected.

The typical concentration of phenols in gasoline obtained from pure VGO is around 0.3 wt.% and that obtained from a 5 wt. % blend is about 0.46 wt. % (De Rezende Pinho et al. 2017). The gasoline fraction from blending a crude bio-oil at 20 wt. % was reported to contain 1.6 wt. % phenolic content (De Rezende Pinho et al. 2015). Hui-Peng et al. (2009) reported that phenols decreased the stability of fuels, as they are likely to recombine to produce oligomers.

As mentioned in the Introduction (Chapter 1), high oxygen content is an undesirable property for bio-oils as it lowers their energy content. A discussion of the bio-oil oxygen content acceptable for co-processing in crude oil refineries follows in Section 2.2.2.4.

2.2.2.4 Oxygen Content

De Miguel Mercader et al. (2010) studied co-processing of different upgraded bio-oils with oxygen contents between 15.5 and 28.0 wt. % (dry basis) at a blending ratio of 20 wt. % (**Table 2-4**). They found out that the yields of liquid products (LCO and gasoline), from the bio-oils did not differ significantly from each other. Thegarid et al. (2014) co-processed upgraded bio-oils with oxygen contents of 18.9 and 19.4 wt. % (dry basis) respectively and made a similar observation at a blending ratio of 10 wt. %. Therefore, it seems that for blending ratios not exceeding 20 wt.%, complete deoxygenation is not required for co-processing, but partial deoxygenation could be sufficient. However, the oxygen mass fraction in bio-oil should be "low" to ensure a decent fraction of bio-based carbon in the eventual diesel/gasoline fuels. A lower oxygen content in bio-oil will therefore always be beneficial.

A rudimentary method to determine an oxygen content target for bio-oil intended for co-processing, is to assume that the oxygen content that is fed into the FCC at 5 wt. % blending of crude bio-oil is the total oxygen that the FCC can take. This reference was chosen because De Rezende Pinho et al. (2017) reported that blending 5 wt.% crude bio-oil results in gasoline and LCO yields similar to the processing of VGO while coke yields did not increase. In their work, crude bio-oil had an oxygen content of 32.8 wt.% (dry basis). Based on this estimation, the required oxygen contents (dry basis) at different blending ratios are shown in ***Figure 2-3***.

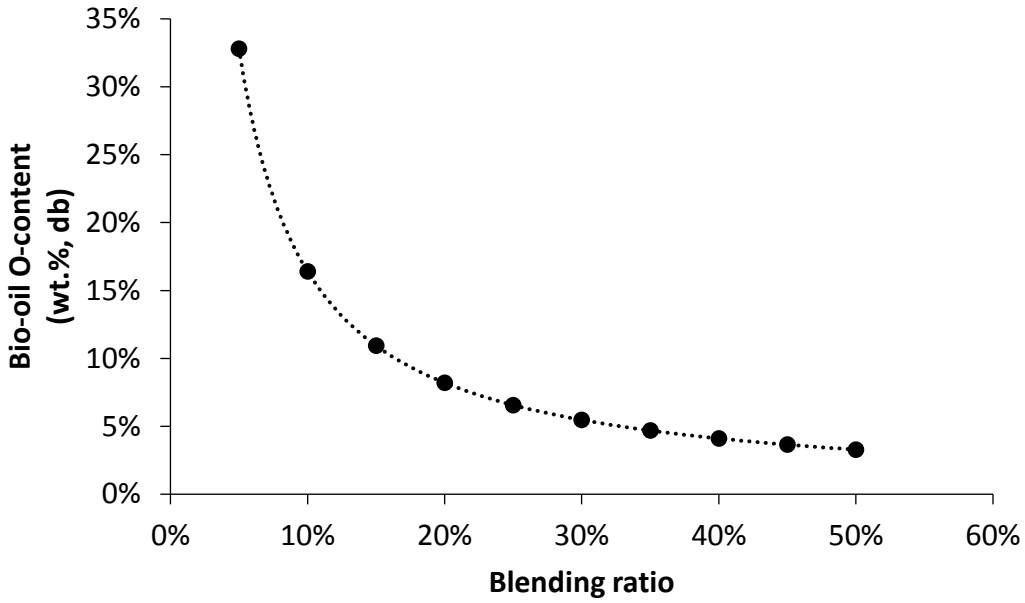

Figure 2-3: Estimation of the acceptable oxygen content in co-processed bio-oil, according to the intended blending ratio

At 10 wt. % blending, the bio-oil oxygen content should not be higher than 17 wt. % on a dry basis. According to Thegarid et al. (2014) at this blending ratio, bio-oils with oxygen contents up to 19.4 wt.% (dry basis)can be successfully co-processed with VGO in a fluid catalytic cracker. Therefore, a dry basis oxygen content target of 17 wt.% is conservative.

A review of the refinery capacity in South Africa as well as the potential biomass available (and hence bio-oil available) is given in the next section to estimate the blending ratios that could be achieved. This will assist us to define the bio-oil quality to be targeted in terms of the oxygen content.

2.2.3 Bio-Oil Blending Ratios According to Biomass Availability in South Africa

2.2.3.1 Forest Residue and Forestry Plantation Area in South Africa

Forest residue includes branches, tops, small trees and un-merchantable wood left in the forest after clear-felling and thinning operations (European Biomass Industry Association 2017). Residue from plantations also includes litter, which is smaller sized residue such as twigs and leaves. ***Figure 2-4*** shows forest residues from a eucalyptus plantation in KwaZulu Natal, South Africa.

Figure 2-4: Forestry residues from a eucalyptus plantation. Photo Credit: Ben Du Toit (Department of Forestry and Wood Science, SU)

Removal of litter from a plantation was reported to decrease the wood volume production on the same plantation in the next harvesting period. Litter left on a forest plantation after harvesting helps to conserve organic matter and nutrients which improve soil fertility. Therefore, its removal would stunt the growth of trees (Nambiar and Kallio 2008). The pulp and paper industry will be reluctant to remove litter from their plantations as it will reduce the wood products yield and ultimately affect their economics. This means that the available forest residue for energy conversion should only consist of stem tops, branches and bark to maintain sustainable operation of the pulp and paper industry.

Pulpwood production accounts for the largest portion (56 %) of the total forestry plantation area in South Africa (Forestry Economics Services 2015). Hardwoods are mainly grown for pulpwood and mining timber whereas softwoods are mainly grown for sawlogs as seen in ***Table 2-5***.

Table 2-5: Purpose for which hardwoods and softwoods are grown (Forestry Economics Services 2015)

Product	Softwood	Hardwood
Pulpwood	29.1 %	83.6 %
Sawlogs	70.5 %	2.9 %
Mining timber	0.0 %	8.6 %
Other	0.4 %	5.0 %

The dominant hardwood species in South Africa is *Eucalyptus grandis* which accounts for 47.9 % of the total hardwood area. The largest hardwood area is in KwaZulu-Natal and Mpumalanga South. Most of the softwoods grown in South Africa are pine species which are predominantly grown in the Western Cape region (Forestry Economics Services 2015).

2.2.3.2 Forest Residue Estimation

Forest residue availability was estimated using a model developed by Dovey (2009). The ratios used to convert timber mass to volume are shown in ***Table 2-6*** and the model parameters to convert timber volume to bark and branch mass are shown in ***Table 2-7***.

Data for timber products sold from plantations was obtained from forestry data compiled for the Department of Forestry and Fisheries (Forestry Economics Services 2015). Timber productions in tons were multiplied by the ratios in ***Table 2-6*** to get the cubic meter equivalent.

Table 2-6: Conversion ratios for commercial Roundwood (tons to m^3) (Ackerman et al. 2013)

Species	Ratio
Pine standing	1
E. grandis standing	1
Hardgums standing	0.8
Wattle standing	0.8

Table 2-7: Multipliers to convert timber volume to timber dry mass and then to bark and branch mass (Dovey 2009)

Species	Timber Dry Mass (t/m^3)	Bark Dry Mass (t/ha)	Branches Dry Mass (t/ha)
Pinus patula	0.387	0.09	0.26
Acacia mearnsii	0.654	0.13	0.26
Eucalyptus grandis	0.45	0.12	0.12
Eucalyptus dunni	0.536	0.16	0.12
Eucalyptus macarthurii	0.551	0.15	0.21
Eucalypts nitens	0.526	0.12	0.34
Eucalyptus smithii	0.581	0.1	0.21

The total forest residue in South Africa was estimated at 1.5 million tonnes and most of it is in the Mpumalanga South and KwaZulu-Natal regions. Excel tables used in the calculations are given in Appendix A. The following assumptions were made during the forest residue estimations:

- Biomass has a 10 wt. % moisture content.
- 80 % of the stem tops, branches and bark residues can be recovered from the forests.
- *Pinus patula* represents all softwoods.
- Conversion factors for the "Other gum" (see Appendix A) species weere averages of the conversion factors for *Eucalyptus dunni*, *Eucalyptus macarthurii*, *Eucalyptus nitens* and *Eucalyptus smithii*.
- Conversion factors for wattle and other hardwoods which are not gum species can be represented by those of *Acacia mearnsii.*
- The yield of upgraded bio-oil from catalytic pyrolysis, independent of the oxygen content, ranges from 15 – 35 wt. %. This is based on literature data shown in ***Figure 2-6*** .
- Density of crude oil is 947.2 kg/m^3 (De Rezende Pinho et al. 2015).
- The biomass processing points (pyrolysis centres) were chosen such that they are central within a 300 km distance from the biomass source in the region to minimise transport costs.

2.2.3.3 Refining Capacity

At present South Africa has 7 oil refineries. These comprise of 4 crude oil refineries, 2 CTL (Coal to Liquid) refineries and 1 GTL (Gas to Liquid) refinery. The crude oil refinery capacities and locations are shown in ***Table 2-8*** (South African Petroleum Industry Association 2014). The yield of VGO from crude oil in North America ranges from 22.7 – 25.1 % on a volume basis (Hill 2011). It will be assumed that a yield of 25.1 wt.% can be obtained in South Africa.

Table 2-8: Capacities of crude oil refineries in South Africa (South African Petroleum Industry Association 2014)

Refinery	Location	Type	Capacity m^3/day	VGO m^3/day
Sapref	Durban	Crude oil	28618	7183
Enref	Durban	Crude oil	19078	4789
Chevref	Cape Town	Crude oil	15 899	3991
Natref	Sasolburg	Crude oil	17171	4310

2.2.3.4 Blending ratios

The possible bio-oil blending ratios in South African crude oil refineries are given in ***Table 2-9***. In the table, A and B represents blending ratios obtained with pyrolysis bio-oil yields of 15 and 35 wt. % respectively. These values are within the typical range of catalytic pyrolysis oil yields which are reported in Section 2.6. The blending ratios were obtained using a VGO yield of 25.1 % and are rounded off to 1 decimal place. Blending ratios for a 22.7 % VGO yield are not more than 1 % higher than those reported in the table.

Table 2-9: Estimate of potential blending ratios of bio-oil in crude oil refineries in South Africa, depending on bio-oil yield obtained by pyrolysis (A: 15 wt.%; B: 35 wt.%)

Region	Biomass Processing Point	Closest Refinery	Blending Ratio	
			A	B
Limpopo, Mpumalanga North Gauteng, Free State North West	Lydenburg	Natref – 390 km	[a]3.3 wt. %	[a]7.5 wt. %
	Klerksdorp	Natref – 145 km		
Mpumalanga South KwaZulu-Natal	Bergville	Enref – 238 km	10.5 wt. %	21.4 wt. %
		Sapref – 242 km	7.2 wt. %	15.3 wt. %
Southern Cape, Western Cape	Swellendam	Chevref – 218 km	0.9 wt. %	2.1 wt. %

[a]Total of Lydenburg and Klerksdorp contributions

Under the given assumptions, blending ratios above 5 wt. % can be achieved in South Africa and values up to 21 wt. % can be reached as seen in ***Table 2-9***. However, as discussed in Section 2.2.2, blending ratios greater than 10 wt.% are not recommended because they result in decreased diesel and petrol yields, increased phenolic content in the petrol product and a significant increase in coke formation in the FCC. Therefore, a 10 wt.% blending will be the target and it can be achieved at the Enref and Sapref refineries in Durban, based on biomass availability within the specified 300km. It should also be noted that the highest blending ratios (≥ 10 wt.%) can be achieved in the Kwa Zulu Natal and Mpumalanga regions which are dominant hardwood areas. This motivates for the use of the most abundant hardwood species *E. grandis*, as the feedstock in this study.

The maximum acceptable bio-oil oxygen-content for 10 wt.% blending and co-processing is 17 wt.% (dry basis), according to the estimation shown in ***Figure 2-3***. Upgraded bio-oils with a similar oxygen content have been successfully co-processed at the same blending ratio (10 wt.%). Thegarid et al. (2014) successfully co-processed an upgraded bio-oil with an oxygen content in the range 18.9 – 19.4 wt.% (dry basis) at a 10 wt.% blending ratio.

Crude bio-oil cannot be used for 10 wt.% blending since its oxygen content typically ranges from 35 – 40 wt.% (Czernik and Bridgwater 2004). Thus, the use of catalyst is highly recommended to improve the deoxygenation of bio-oils to achieve an oxygen content < 17 wt.%, as will be discussed in Section 2.6.

De Rezende Pinho et al. (2015; 2017) reported that the water content of bio-oils fed into an oil refinery can be relatively high (25 – 32 wt.%). However, since water does not end up in the gasoline and diesel products, water contents less than this range are preferable as more renewable organics can then be recovered in gasoline and diesel. Therefore, the goal of the project is to maximise the bio-oil yield (> 15 wt.%) and achieve an acceptable oxygen content of < 17 wt. % (dry basis) while attaining a bio-oil water content acceptable in a crude oil refinery (< 32 wt.%).

A detailed review of pyrolysis follows in Sections 2.3 – 2.6.

2.3 Pyrolysis

Pyrolysis is a thermochemical process in which a material is heated in an inert environment to give a solid product (char) and volatiles. Part of the volatiles can be condensed at room temperature to give a liquid product called pyrolysis oil. In the case of biomass pyrolysis, the liquid product can also be called bio-oil. The incondensable part of the volatiles exists as permanent gases. Biomass pyrolysis processes are often described as occurring via two mechanisms, i.e. primary and secondary mechanisms, which occur simultaneously. The primary mechanisms which affect the main matrix (initial biomass and char in formation) include char formation, depolymerisation and fragmentation (F.-X. Collard and Blin 2014). The secondary mechanisms are associated with further reactions of the volatile compounds.

2.3.1 Primary Mechanisms

2.3.1.1 Char Formation

Char has a polycyclic aromatic structure, which results from the formation of benzene rings and the subsequent combination of these rings to form polycyclic structures. Reactions which cause char formation generally result in the release of compounds with relatively low molecular weights such as water and/or incondensable gas (F.-X. Collard and Blin 2014).

2.3.1.2 Depolymerisation

During depolymerisation, bonds between monomer units of the polymers are broken. The two new chain ends are likely to undergo further reactions. As bond breaking continues, the size of the polymer chains decreases until the produced molecules become volatile. The volatiles produced from lignocellulose depolymerisation are condensable at ambient temperature and are found in the liquid fraction (F.-X. Collard and Blin 2014).

2.3.1.3 Fragmentation

In fragmentation, many covalent bonds of the polymer break up, resulting in the formation of incondensable vapours and a variety of low molecular weight condensable organics (F.-X. Collard and Blin 2014).

2.3.2 Secondary Mechanisms

If the released volatile compounds are not stable, they can undergo secondary reactions such as cracking or recombination before leaving the reactor. During cracking reactions, chemical bonds within the volatile components are broken, resulting in lower molecular weight products being formed. As the same chemical bonds can be broken within the polymer, there are similarities between fragmentation and cracking reactions. Recombination consists of the association of two volatile compounds to produce a new compound with higher molecular weight, which can be involatile at the reactor temperature. Secondary char can be formed when recombination reactions occur within the polymer matrix (F.-X. Collard and Blin 2014). The surfaces of the reactor, char or of an added catalyst can also catalyse secondary mechanisms, resulting in the formation of secondary char at the surface of the catalyst material (Morf, Hasler, and Nussbaumer 2002).

2.4 Types of Pyrolysis

Pyrolysis processes can be classified based on the operating conditions. The most common classes are slow, fast, vacuum and intermediate pyrolysis. In the following section, the main attributes and operating conditions of the different pyrolysis processes will be discussed.

2.4.1 Slow Pyrolysis

This type of pyrolysis is characterised by low heating rates and long volatile residence time in the reactor. Biomass is pyrolysed at heating rates lower than 1 °C/s (60 °C/min) to temperatures in the range 400 – 500 °C (Tripathi, Sahu, and Ganesan 2016). These authors also reported that vapour residence times for slow pyrolysis typically range between 300 and 550 s. These relatively long vapour residence time allows for the completion of secondary reactions. Char is the main targeted product of slow pyrolysis. Relatively large biomass particle sizes in the range 5 – 50 mm are required (Tripathi, Sahu, and Ganesan 2016). Liquid yields in slow pyrolysis are typically around 30 wt. % while the char and permanent gas yields are around 35 wt.% (Bridgwater 2003).

2.4.2 Fast Pyrolysis

Fast pyrolysis is characterised by very short volatile residence times and high heating rates in the range 10 – 200 °C/s (Tripathi, Sahu, and Ganesan 2016). This type of pyrolysis is typically used for the conversion of the biomass to volatiles before char is produced. The short vapour residence times of approximately 1 second avoid the secondary reactions likely to convert some condensable compounds into permanent gases (Bridgwater 2012). Therefore, fast pyrolysis is primarily used to produce pyrolysis oil as the liquid product yield is greater than both the solid and gaseous product yields. The typical fast pyrolysis product yields are: 60 – 75 wt. % liquid, 15 – 25 wt.% char and 10 – 20 wt. % incondensable gas. A biomass particle size of < 1 mm is generally required for fast pyrolysis (Tripathi, Sahu, and Ganesan 2016). The typical reaction temperature to maximise liquid yields during fast pyrolysis of biomass is around 500 °C (Neves et al. 2011; Bridgwater 2012).

2.4.3 Intermediate Pyrolysis

Pyrolysis processes operating between the reaction conditions of fast and slow pyrolysis are termed intermediate pyrolysis processes. They operate at heating rates between 1 – 10 °C/s to a final temperature ranging from 500 – 650 °C. A biomass particle size in the range 1 – 5 mm is typical for intermediate pyrolysis processes (Tripathi, Sahu, and Ganesan 2016) while vapour residence times are less than 30 s (Bridgwater 2012).

Hornung, Apfelbacher, and Sagi (2011) reported that typical yields for intermediate pyrolysis are 40 – 60 wt.% liquid, 15 – 25 wt.% char and 20 – 30 wt.% permanent gases. Although intermediate pyrolysis processes result in lower liquid yields than fast pyrolysis, this type of technology is more and more considered due to less complexity. Moreover, it does not require the very small particle sizes that fast pyrolysis technologies require to achieve extreme heating rate (Hornung, Apfelbacher, and Sagi 2011). Particle size reduction affects the energy efficiency of the process as a lot of energy is required to mill the particles to a smaller size.

2.4.4 Vacuum Pyrolysis

Vacuum pyrolysis is sometimes considered as a type of intermediate pyrolysis, and occurs under low pressure, typically 15 kPa (absolute) or less (Roy et al. 1998; Garcìa-Pérez et al. 2007; Carrier et al. 2011). The heating rates in vacuum pyrolysis are similar to those used in slow or intermediate pyrolysis, while the final pyrolysis temperature ranges between 350 – 600 °C (Tripathi, Sahu, and Ganesan 2016). The low or vacuum pressure applied helps removing the pyrolysis vapours, thus resulting in a relatively short vapour residence time. This limits the secondary reactions, resulting in a higher liquid product yield and a bio-oil with more primary products than from slow pyrolysis (Benallal et al. 1995). In case of slow heating rate with vacuum, liquid yields in the order 35 – 50 wt. % have been reported (Bridgwater 2003).

2.4.5 Pyrolysis Reactors

The most common pyrolysis reactors are batch, fluidised bed and rotary kiln/auger-type reactors. They are all typically cylindrical in shape.

A carrier gas such as nitrogen is usually purged in these reactors to provide an inert environment prior conversion and sometimes during pyrolysis in order to influence the volatile residence time in the reactor. In the case of vacuum pyrolysis, no carrier gas is used, and a vacuum pump is connected to the outlet of the reactor.

Typically, in batch reactors, the feed material is placed inside the reactor before being heated to the desired temperature and kept there for a specific amount of time (Pütün 2010; Stefanidis et al. 2011; Aysu 2015). In auger and fluidised bed reactors, the feed material is introduced in a feed hopper and then pushed by a mechanical screw or piston into an already hot reactor (Veses et al. 2014; Kim, Weaver, and Labbé 2016; Funke et al. 2017).

For auger reactors, the feed is pushed into a horizontal rotating reactor whereas in fluidised bed reactors the feed is pushed into a fluidised bed of hot material (typically sand). The contact between the hot sand and the feed material results in very high heating rates in fluidised bed reactors (Bridgwater 2003). Examples of the different of reactors used in literature for biomass are shown in ***Table 2-10***. Batch reactors are typically for slow pyrolysis processes, auger reactors for intermediate pyrolysis and fluidised bed reactors for fast pyrolysis.

Table 2-10: Pyrolysis reactor types

Reactor Type	Heating Rate (°C/min) / Pyrolysis Type	Feed Throughput	Reference
Batch	10 / Slow	50 g	Ertaş and Hakki Alma (2010)
	10 – 50 / Slow	20 g	Aysu (2015)
	70 / Intermediate	5 g	Pütün (2010)
Rotary kiln / Auger	Intermediate	2 kg/hr	Veses et al. (2014)
	Intermediate	8 kg/hr	Kim, Weaver, and Labbé (2016)
	Intermediate	3 kg/hr	Funke et al. (2017)
Fluidised Bed	Fast	20 kg/hr	Oasmaa et al. (2003)
	Fast	0.3 – 0.43 kg/hr	Shen et al. (2009)
	Fast	100 g/hr	Funke et al. (2017)

Batch reactors are limited in terms of production due to the need of filling and emptying the reactor between two processes. In fluidised bed and auger reactors the feed material can be input continuously, with throughput up to 3100 kg/hr (Dhyani and Bhaskar 2018).

The operating parameters at which the pyrolysis processes above take place influence the quality and yield of pyrolysis products. The influence of these conditions is discussed in Section 2.5.

2.5 Effect of Operating Parameters

2.5.1 Temperature

It is widely accepted that of all the operating parameters, temperature has the highest effect on pyrolysis mechanisms and product distribution (Neves et al. 2011; Yildiz et al. 2016; Russell et al. 2017). Lower temperatures (< 300 °C) favour the formation of char due to limited feedstock conversion, which restricts the production of volatiles (Balat et al. 2009). At higher temperatures (> 300 °C), more chemical groups are unstable and react to produce volatiles. Initially, as temperature increases, the bio-oil yield increases up to a maximum and then decreases with further increases in temperature while gas production increases. This is because as the temperatures increase, secondary cracking reactions and further decomposition of char are promoted, resulting in increased gas yields (Pütün 2010; Aysu 2015). Maximum bio-oil yield at intermediate heating rates of biomass ranges from 40 – 60 wt.% and is obtained between 500 °C – 600 °C (Neves et al. 2011).

2.5.2 Heating Rate

Higher heating rates favour the formation of volatiles products, while lower heating rates favour char yields. Higher heating rates favour depolymerisation and fragmentation reactions, thereby increasing the yield of liquid and gaseous products (Tripathi, Sahu, and Ganesan 2016). At around 500 °C, the liquid yield from biomass pyrolysis at low heating rates (< 10 °C/s) ranges from 35 – 55 wt. % whereas at higher heating rates (> 10 °C/s) it ranges from 60 – 85 wt. % (Neves et al. 2011).

2.5.3 Volatile Residence Time

Volatile residence times corresponds to the time that volatiles remain in the hot part of the reactor where further reactions (secondary) are likely to happen; therefore, increasing the vapour residence time leads to more secondary reactions. Reactor pressure (as in vacuum pyrolysis) or sweeping gas flow rate can be set to control volatile residence time. Generally, decreasing the sweeping/carrier gas flow rate and hence increasing the volatile residence time, decreases the liquid yields, while the char and gas yields increase (Pütün 2010; Auta, Ern, and Hameed 2014; Aysu 2015).

Long volatile residence times typically used in slow pyrolysis (300 – 550 s) sometimes promote undesirable secondary reactions such as over cracking or repolymerisation of the desired volatile compounds (Tripathi, Sahu, and Ganesan 2016). However, short residence times of < 30 s typically used in intermediate and fast pyrolysis (Bridgwater 2012) may reduce the time available for the completion of some desired reactions, for instance when a catalyst is used. Therefore the residence time should be optimised to achieve a balance between limitation of undesirable secondary reactions and allowing enough time for the completion of the catalysed reactions (Yildiz et al. 2016). It is likely that when a catalyst is used, volatile residence times in the intermediate pyrolysis range will give a compromise for the above (Veses et al. 2014).

2.5.4 Particle Size

The particle size is a key factor during pyrolysis because it controls the heat transfer rate to the input biomass. It is particularly critical in fast pyrolysis where high heating and heat transfer rates are required (Bridgwater 2003). Increase in particle size generally results in a decrease in bio-oil yields while the char and gas yields increase. When the biomass particle size increases, heat transfer limitations from the particle surface to the inner core also increase, meaning that the actual biomass heating rates of the inner core are lower than at the surface and thus char yields are favoured (Encinar, Gonzalez, and Gonzalez 2000). As biomass particle size increases volatiles remain longer in the particle as well and are more subject to secondary reactions leading to an increase in the char and gas yield. It is reported that to achieve high heating rates in fast pyrolysis (> 10 °C/s), biomass particles < 1 mm are required (Tripathi, Sahu, and Ganesan 2016).

As energy is required to reduce the size of biomass feedstock, when possible it would be desirable to use relatively large particle sizes (> 1 mm) during pyrolysis. However, when using a catalyst mixed with biomass, particle sizes should be adapted to improve contact between the two and promote catalysed reactions (refer to Section 2.6.2).

Pyrolysis involving the use of catalyst to enhance the quality of products is called catalytic pyrolysis (CP) and it is discussed next in Section 2.6.

2.6 Catalytic Pyrolysis

Different methods have been used to upgrade bio-oil and thereby enhance its fuel properties. The most common methods are catalytic pyrolysis (CP) and hydro-treating. Catalysts can aid in the removal of oxygen through the release of oxygenated compounds such as carbon monoxide (decarbonylation), carbon dioxide (decarboxylation) and water (dehydration), thereby improving the bio-oil properties in the process. In hydro-treating, bio-oil produced by thermal pyrolysis is exposed to large quantities of hydrogen to remove oxygen in the presence of catalysts. Although this method is effective in deoxygenating pyrolysis oils, this technology is not mature enough and it is capital intensive due to high pressures required and hydrogen cost (Marinangeli et al. 2005; Thegarid et al. 2014).

In this study, it is proposed to use catalysts with deoxygenation capabilities during pyrolysis to improve the bio-oil properties and make it more compatible with petroleum refinery feedstock. Deoxygenating the bio-oil will also lead to an increase in its calorific value (HHV). Although catalysts enhance the bio-oil quality, they generally have the disadvantages of reduced bio-oil yield, due to conversion of a fraction of bio-oil into permanent gases by cracking reactions, and organic deposit at the catalyst surface (Thegarid et al. 2014). This organic deposit is commonly referred to as coke. The ideal catalyst should be stable and robust, regenerable, inexpensive and effective at deoxygenation and increasing HHV. Catalysts can be configured in two different ways in a pyrolysis process and these configurations are described in Section 2.6.1.

2.6.1 Catalyst Configurations

The two catalyst configurations are *in situ* and *ex situ* as reported in the review by Yildiz et al. (2016). Regarding *in situ* configuration, the biomass and catalyst are physically mixed in the pyrolysis reactor. The catalyst will be reactive at the pyrolysis reactor temperature and will instantly convert the produced volatiles that come into contact with their surface. In an *ex situ* setup, the biomass is placed in a primary reactor where pyrolysis takes place. Volatiles from the primary reactor then pass through a catalyst bed (secondary reactor) where upgrading takes place (Yildiz et al. 2016). The primary and secondary reactors can be operated at different temperatures, optimised for each type of conversion. However, the energy required for the second reactor will affect the energy efficiency and *ex situ* configurations typically have a higher capital cost (Yildiz et al. 2016).

The configuration also impacts the possibility of catalyst recycling (Yildiz et al. 2016). In *ex situ* configurations, as the char is separated from the catalyst, recycling only requires the removal of the organics condensed at the catalyst surface (and eventual reactivation). Separation of the catalyst from the char presents a technical challenge for *in situ* configurations. An option is to combust the char in order to recover the inorganic catalyst. The purity of the recovered catalyst will depend on the ash content of the biomass. Another option would be to use the catalyst/char mixture for soil amendment of agricultural soils, depending on the nature of the catalyst (Samac and Tesfaye 2003; Zimdahl 2015). The catalysts may be beneficial in that they may add nutritional value to the soil and/or neutralise it.

In a study comparing the two approaches, similar results were obtained, suggesting that the use of a second reactor could be avoided if there is sufficient mixing and contact time during the conversion (Imran et al. 2014). The mixing and contact time is probably not enough for the bench test but it is sufficient on auger reactors (Veses et al. 2014). For the *in situ* set up, the catalyst can be mixed in two ways. The discussion of these follows below.

2.6.2 Catalyst Mixing for *in situ* Pyrolysis

From literature, feedstock and catalyst are commonly mixed by two ways; impregnating the biomass with the catalyst or dry mixing the two. Dry mixing involves mechanical mixing of the biomass and catalyst particles. Typically for impregnation, the catalyst particles are dissolved in water to form a catalyst solution. The biomass sample is then put in the catalyst solution and the resultant mixture is stirred to get a homogeneous slurry, which will be dried to obtain the impregnated feedstock (Patwardhan et al. 2010).

Impregnation has been used mostly in studies using water soluble metal salts as catalysts. It was suggested that the metal cations are mostly impregnated in interaction with some oxygenated groups of the hemicelluloses (F. X. Collard et al. 2012). These metals are well dispersed and are in intimate contact with the biomass (Richardson et al. 2010). Together with the catalytic cracking of volatiles, the intimate contact could also influence some primary reactions within the biomass matrix (Patwardhan et al. 2010). However, impregnation requires energy for drying which affects the energy efficiency of the process. Also, when the catalyst is not soluble, similar contact has not been evidenced and the advantage of impregnation is unsure. The ratio in which the catalyst and the biomass are mixed has an influence on pyrolysis. Its effects are discussed in the next section.

2.6.3 Catalyst to Biomass Ratio

Pyrolysis product yields are partly dependent on the catalyst to biomass ratio (C/B). Using catalysts at very high catalyst to biomass ratios of greater than 1/1 i.e. more than 50 wt.% catalyst, poor bio-oil yields were observed as well as increases in the gas and char yields (Veses et al. 2015; Chen et al. 2017; Russell et al. 2017). However, the bio-oil quality in terms of deoxygenation and energy content increased.

The presence of large amounts of catalyst in the feedstock is believed to enhance the cracking of vapours resulting in an increased incondensable gas fraction (Yildiz et al. 2016). Also, some secondary reactions of the volatiles leading to the formation of high molecular weight compounds (recombination) are promoted. These compounds generate carbonaceous deposits and hence increase the char yield.

It was observed that changing the C/B from 1/3 to 3/1 resulted in an increase in the char yield from 27 wt. % to 44 wt. % on a catalyst free basis (Veses et al. 2015). A lower catalyst concentration means that the available active catalyst surface area is limited, thereby allowing some of the volatiles to exit the reactor unreformed and leading to limited deoxygenation. Therefore, the C/B must be optimised in the range 0/1 – 1/1 i.e. 0 – 50 wt.% catalyst for an efficient and economic CP process.

2.6.4 Catalyst Selection

Different types of catalysts can promote different pyrolysis mechanisms, resulting in different effects on the pyrolysis product yields and qualities (Shadangi and Mohanty 2014b). Catalysts are selective towards specific bonds and different compounds; therefore, the type of catalyst affects both the bio-oil yield and composition.

Lignocellulosic biomass has been pyrolysed using different catalysts in the *in situ* configuration. A review of these catalysts is given in this section. Of interest will be the bio-oil deoxygenation capabilities of the catalysts, typically through decarboxylation, decarbonylation, dehydration and associated with an increase in the HHV of the bio-oil. The improvement in bio-oil quality will come at the expense of the yield of the organic fraction due to the formation of CO_2, CO and H_2O in the deoxygenation process.

2.6.4.1 Zeolites

Zeolites are microporous, solid-acid aluminosilicate catalysts, which have been studied extensively to upgrade bio-oil because of their similar use in the petroleum cracking industry. There have been numerous studies on the upgrading of biomass pyrolysis vapours using various zeolite catalysts like ZSM-5, HZSM-5, H-Y and H-mordenite (Adjaye and Bakhshi 1995; Lappas et al. 2002; Zhang et al. 2014). Adjaye and Bakhshi (1995) observed the best results with HZSM-5 during the upgrading of a fast pyrolysis bio-oil. However, only 33.6 % of the original bio-oil was recovered as organics. Additionally, coke formation was a problem; up to 16 % of the original bio-oil ended up as coke deposits on the catalyst surface. Small pore zeolites result in the increase of water and gaseous products, therefore reducing organic liquid yield (Pattiya, Titiloye, and Bridgwater 2008).

Acidic zeolite sites favour aromatisation reactions and form the aromatics benzene, toluene and xylene (BTX). These aromatisation reactions further lead to the formation of polycyclic aromatic hydrocarbons (PAH), which are precursors of catalytic coke (Stefanidis et al. 2016). Coke formation results in catalyst deactivation and a reduction in the desirable liquid products (Du, Valla, and Bollas 2010; Stefanidis et al. 2016). Moreover, due to their stability, the presence of aromatics in significant amounts decreases the efficiency of bio-oil combustion.

Another major disadvantage of zeolite structures is that they undergo irreversible deactivation when the structures are de-aluminated by the water produced by pyrolysis and catalytic dehydration reactions (Serrano-Ruiz and Dumesic 2012). Paasikallio et al. (2014) also reported that alkali and alkaline earth metals (AAEMs) found in biomass irreversibly deactivated the HZSM-5 catalyst by substituting the proton of the catalyst acid site. This makes zeolites not appropriate for the *in situ* catalyst configuration wherein the biomass is in contact with the catalyst.

2.6.4.2 Metal Oxides

Metal oxides are known to improve bio-oil quality by deoxygenating it and increasing its HHV. Catalytic pyrolysis using Al_2O_3, CaO and MgO in particular, has been studied because they have been reported to be relatively inexpensive (Veses et al. 2014). The deoxygenating capabilities of metal oxides during the catalytic pyrolysis of seeds has been publicised (Pütün 2010; Shadangi and Mohanty 2014a; Shadangi and Mohanty 2014b). Very high bio-oil HHVs (40 – 43 MJ/kg), comparable to fossil derived fuels are obtained when seeds were pyrolysed. However, it is worth noting that the high HHVs were also due to the low oxygen content of seeds and relatively high amounts of extractives and fats in seeds, in comparison with lignocellulose. Since the HHVs of the seed derived bio-oils is relatively high, these bio-oils are not comparable to lignocellulosic biomass derived bio-oils. However, the same oxides: Al_2O_3, CaO and MgO have also been reported to improve the quality of lignocellulosic biomass derived bio-oils by decreasing their oxygen content and increasing their HHV. A summary of the metal oxides used in the *in situ* CP of lignocellulosic biomass is given in **Table 2-11**.

In some of the reviewed literature (Veses et al. 2014), the pyrolysis liquid was obtained in 2 phases, which were separated by decanting. The phases were: an organic phase containing mostly organics and an aqueous phase containing mostly water. The organic phase is what is referred to as bio-oil in **Table 2-11**. In the instances when a 2-phase liquid was not obtained, water content analysis of the liquid was done to determine the pyrolytic water yield. Pyrolytic water is water that is produced from the dehydration reactions that occur during pyrolysis and does not include the initial moisture bound to the biomass. The total yield of organic compounds in the bio-oil (organics yield) was then determined as the difference between the total liquid yield and the water yield. In **Table 2-11**,

Table 2-11: Metal oxides used in the *in situ* CP of lignocellulosic biomass

Reference	Feedstock	Reactor	Catalyst	C/B ratio	Temp (°C)	Bio-oil Yield (wt.%)		Bio-oil Oxygen Content (wt.%)		Bio-oil HHV (MJ/kg)		Total Organics Yield (wt.%)		Pyrolytic Water Yield (wt.%)	
						Non-Cat	Cat	Non-Cat	Cat	Non-Cat	Cat	Non-Cat	Cat	Non-Cat	Cat
(Lin et al. 2010)	White Pine	Fluidised Bed	CaO	5/1	520	-	-	39	31	20.2[a]	29.9[a]	39.1	34.1	16.5	28.1
(Stefanidis et al. 2011)	Beech	Fixed Bed	Al_2O_3	1/2	500	-	-	41.68	24.00 21.94	19.4[a]	29.8[a] 31.2[a]	37.37	16.62 15.02	21.38	29.08 29.22
(Li et al. 2012)	Rice Husk	Spout Fluidised Bed	[c]CaO [d]CaO CaO.MgO	-	460	-	-	48.30	41.09 41.78 42.35	16.98	20.47 20.14 19.71	32.59	11.61 13.08 21.13	15.61	19.56 19.38 16.60
(Veses et al. 2014)	Forest Pine	Auger	CaO CaO.MgO	1/3	450	27	34 31	31.5	24.2 25.4	22.4 [b]	30.2[b] 29.6[b]	- -	- -	- -	- -
(Chen et al. 2017)	Cotton Stalk	Fixed Bed	CaO	1/1	600	-	-	-	-	-	-	21	12	28	32

[a]Estimated using Dulong Formula (Mason and Gandhi 1983) [b]Lower Heating Value (LHV) [c,d]Calcined from calcite/limestone. "Cat" means the bio-oil/organics from CP, "Non-Cat" means bio-oil/organics from non-catalytic pyrolysis

CaO

CaO has been reported to promote deoxygenation of bio-oils and increase its heating value as shown in **Table 2-11**. Lin et al. (2010) reported that bio-oil oxygen content decreased from 39 to 31 wt.% with the use of CaO catalyst while Veses et al. (2014) reported an oxygen content decrease from 31.5 to 24.2 wt.%. Both research groups as well as Chen et al. (2017) concluded that the deoxygenation occurred mainly via dehydration reactions. When CaO was used as a catalyst, an increase in pyrolytic water yield or an increase in the bio-oil water content was reported while the total organics yield decreased.

A range of temperatures and C/B ratios have been used for catalytic pyrolysis using CaO. In the catalytic pyrolysis of white pine in a fluidised bed reactor at 520 °C, Lin et al. (2010) attributed the low contact efficiency between the biomass and catalyst to be the cause of the need to use of a high C/B ratio (5/1). A lower C/B ratio of (1/3) was used in pine catalytic pyrolysis in an auger reactor at 450 °C (Veses et al. 2014). The authors reported that from their preliminary experiments, they found that higher catalyst concentrations resulted in very low organic yields. They attributed this to the promotion of secondary reactions because of the higher volatile residence times in an auger reactor. A corresponding increase in the pyrolytic water yield from 28 to 32 wt.% was observed. While catalytic effect was generally found to decrease total organic yield, Veses et al. (2014) reported that the bio-oil (organic phase) yield increased with the use of catalyst. It increased from 27 wt.% to 34 and 31 wt.% with CaO and CaO.MgO respectively, while the water content of the organic phase decreased slightly from 13 to 12 and 11 wt.%. This is possibly a consequence of the oil collection method used. When a catalyst is used, there is better separation between the aqueous and organic phases due to the increased moisture content of the aqueous phase and hydrophobicity of deoxygenated organic compounds. The above shows the variations of bio-oil quality and yield with temperature and catalyst concentration.

Lin et al. (2010) also did an analysis of the incondensable gas product. The gas analysis showed a decrease in the CO_2 yield from 9.5 to 3.2 wt.%, while the CO yield decreased from 6.8 to 4.3 wt.% and the H_2 yield increased from 0.3 to 0.8 wt.% in the presence of catalysts. However, this trend is not sufficient to conclude about the effect of the catalyst on the primary mechanisms.

This change in gas composition was probably due to the combined effect of CO_2 absorption by CaO and the water-gas shift reaction (WGSR) taking place. The WGSR has been reported to occur in the presence of CaO at temperatures below 700 °C under pyrolysis conditions (Widyawati et al. 2011; Chen et al. 2017). CaO absorbs CO_2 forming $CaCO_3$ according to the following equation.

$$CaO + CO_2 \rightarrow CaCO_3$$

The depletion of CO_2 as well as the increase in water formation due to the pyrolytic dehydration reactions, drives the WGSR forward led to an increase in the H_2 yield.

$$CO + H_2O \rightarrow CO_2 + H_2 \qquad \text{(WGSR)}$$

Similar observations were made by other researchers. Veses et al. (2014) reported a decrease in CO_2 fraction from 42.9 vol.% to 34.4 vol.%, while the H_2 fraction increased from 2.9 vol.% to 8.0 vol.% with the addition of catalyst. The CO fraction increased slightly from 39.3 to 41.0 vol.%. Chen et al. (2017) observed a decrease in the CO_2 fraction from 40 to 8 vol.% while the H_2 fraction increased from 17 to 50 vol.%. The CO fraction decreased from about 33 to 29 vol.%. The CO_2 absorption capabilities of CaO makes it an interesting catalyst since the absorption of CO_2 means that a gas with higher calorific value can be produced.

Li et al. (2012) performed the catalytic pyrolysis of rice husks in a fixed bed reactor at 460 °C at an unspecified C/B ratio using Ca and Mg based minerals: calcite, limestone and dolomite which were calcined before use. After calcining the catalysts had the following composition; calcite (52.9 wt.% CaO), limestone (50.2 wt.% CaO) and dolomite (30.8 wt.% CaO and 20.6 wt.% MgO). As seen in **Table 2-11**, the observed trends are similar to those when the pure CaO was used. The bio-oil oxygen content decreased, while the bio-oil HHV increased with the use of a catalyst and the pyrolytic water yield increased. An interesting observation can be made from the comparison of results between Veses et al. (2014) and Li et al. (2012) who both used a catalyst containing both MgO and CaO. In both studies, the “mixed” catalyst resulted in a bio-oil with a lower heating value and a higher oxygen content compared to the bio-oil produced using a pure CaO catalyst, suggesting that CaO is a better performing catalyst than MgO in terms of deoxygenation of the organic compounds.

Al_2O_3 and MgO

Stefanidis et al. (2011) carried out *in situ* catalyst screening experiments with beech wood in a fixed bed reactor at 500 °C using various metal oxides (MgO, Al_2O_3, NiO, TiO_2 and ZrO_2) and a traditional zeolite catalyst (ZSM-5) at a C/B ratio of 1/2. MgO and alumina (Al_2O_3) resulted in the most significant deoxygenation. The oxygen content of the bio-oil decreased from 41.68 wt.% to 21.94 and 24.00 wt.% with MgO and Al_2O_3 respectively, while the organics yield decreased from 37.37 wt.% to 15.02 and 16.62 wt.%. The pyrolytic water yield increased from 21.38 to 29.22 and 29.08 wt.% for MgO and Al_2O_3 respectively showing that dehydration reactions are responsible for improved deoxygenation.

Gas product analysis was also done in this catalyst screening. An increase in the CO_2 yield from 10.02 wt.% to 14.79 and 11.18 wt.% for MgO and Al_2O_3 was observed, while the CO yield increased from 6.54 to 9.64 and 10.17 wt.% for MgO and Al_2O_3. A slight increase in CH_4 yield from 0.88 wt.% to 1.61 and 1.26 wt.% for MgO and Al_2O_3 was observed. The above gas data shows that MgO and Al_2O_3 also promote decarboxylation and decarbonylation reactions. It was concluded that with the use of acidic catalysts like Al_2O_3, formation of carbon oxides through deoxygenation occurred mostly via decarbonylation, whilst base catalysts like MgO promote deoxygenation via decarboxylation reactions (Stefanidis et al. 2011). The increase in CH_4 yield with catalyst addition suggests that MgO and Al_2O_3 catalysts also enhanced cracking of the organic volatiles via demethylation.

The same researchers Stefanidis et al. (2016) conducted catalytic pyrolysis of beech wood sawdust using various natural MgO catalysts. MgO promoted oxygen removal by formation of CO_2. MgO performance was also compared to that of industrial standard zeolite, ZSM-5. It was reported that MgO catalysts produced either a lower oxygen content at the similar organic fraction yields or a higher organic fraction yield at a similar oxygen content compared to the zeolite catalyst. The use of most of the MgO catalysts resulted in an organic fraction yield in the range 17 – 22 wt. % and a bio-oil oxygen content between 28 and 30 wt. % (Stefanidis et al. 2016).

Char yield in *in situ* catalytic pyrolysis

The char yield was not reported to be significantly affected by catalyst addition during *in situ* catalytic pyrolysis, since the biomass and catalyst are not in intimate contact and hence the primary reactions are not expected to be affected. Lin et al. (2010) and Veses et al. (2014) observed slight increases in the char yield of 25.3 to 27.9 wt.% and 25 to 27 wt.% respectively when CaO was added. On the other hand, Chen et al. (2017) observed a slight decrease in char yield of 27 to 25 wt.% after catalyst addition. Stefanidis et al. (2011) reported a significant increase in char yield from 22.89 wt. % to 27.50 and 29.55 wt.% with MgO and Al_2O_3 addition. They concluded that coke formation on the catalyst was the cause of the increase in char yield when a catalyst was added. It is not clear whether the same basis or method (including or excluding catalyst) to determine char yield was used by all the researchers mentioned above. However, it is seen that there is generally no substantial change in the char yield for *in situ* catalytic pyrolysis.

2.6.4.3 Catalyst Comparison

A plot of the bio-oil oxygen content and organics yield obtained using the catalysts mentioned in **Table 2-11** is shown in ***Figure 2-5***. The figure includes results of the catalytic screening performed by Stefanidis et al. (2011) using different metal oxides and a traditional zeolite catalyst ZSM-5. It can be seen that low oxygen contents (< 25 wt.%) can be achieved using catalysts like CaO, MgO, Al_2O_3. CaO has the potential to give higher organics yield; this is more evident in ***Figure 2-6***.

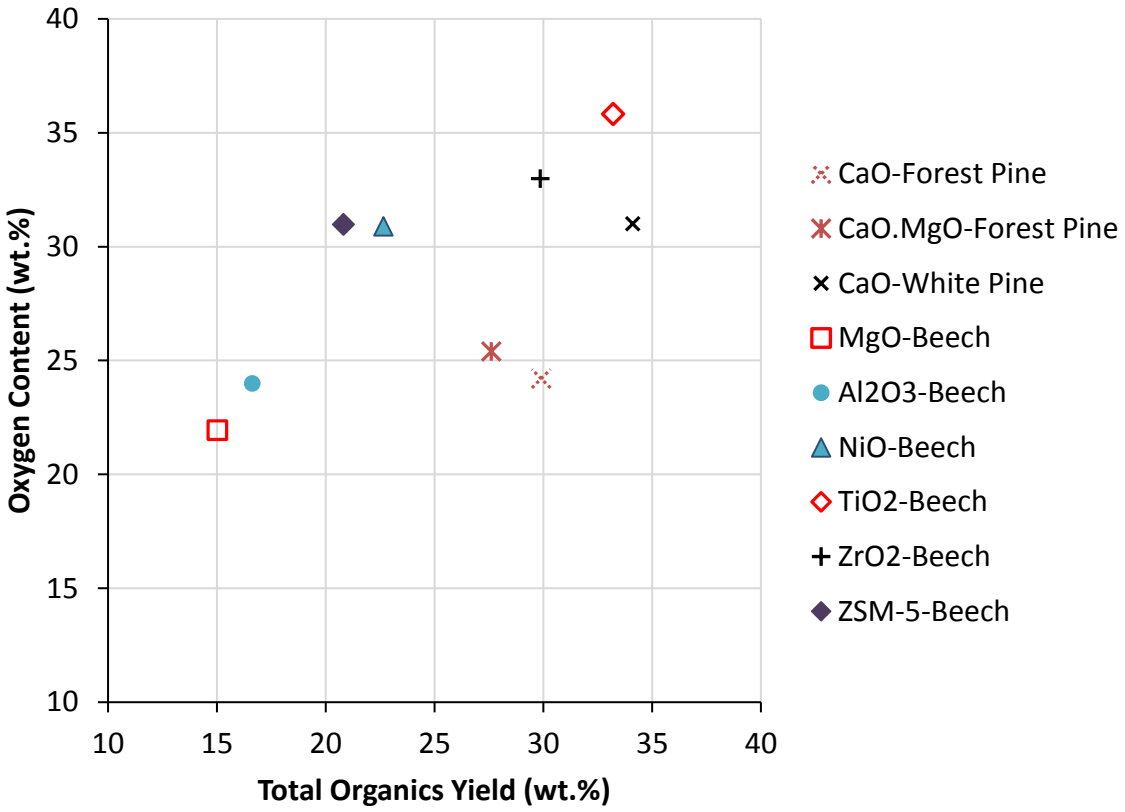

Figure 2-5: Oxygen content vs total organics yield from various literature sources

Figure 2-6 shows a plot of the organics yield reduction and the corresponding oxygen content decrease as a result of the effects of the catalysts listed in **Table 2-11**. The oxygen content decrease and the organic yield reduction were calculated according to the equations below.

$$O\ Content\ decrease = \frac{O\ in\ non\ catalytic\ bio\ oil\ - O\ in\ catalytic\ bio\ oil}{O\ Content\ in\ noncatalytic\ bio\ oil}\ \%$$

$$Organics\ yield\ reduction = \frac{noncatalytic\ organic\ yield\ - catalytic\ organic\ yield}{non\ catalytic\ organic\ yield}\ \%$$

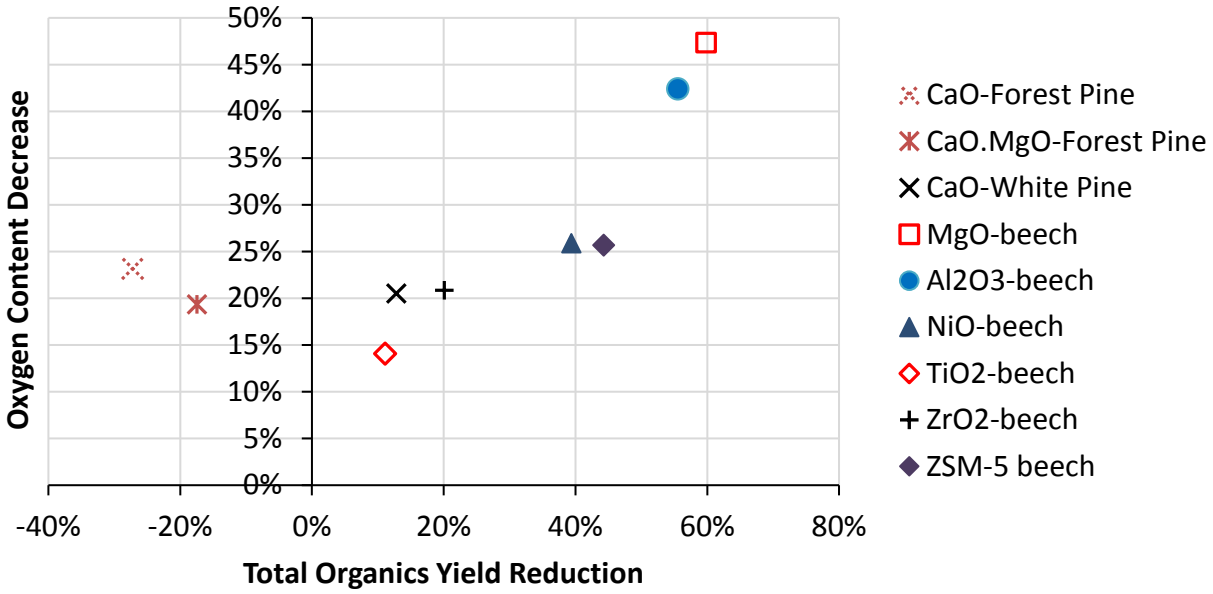

Figure 2-6: Oxygen content decrease vs total organics yield reduction (% decrease in bio-oil O-content from non-catalytic pyrolysis to CP vs % reduction in the organics yield from non-catalytic pyrolysis to CP)

It can be seen from ***Figure 2-6*** that CaO can achieve significant deoxygenation (around 20 % deoxygenation) with a minimal reduction in oil yield (< 15 %). MgO and Al_2O_3 showed very significant deoxygenation (> 40%) albeit at high organic yields reduction (> 50 %). The industrial zeolite catalyst showed medium performance i.e. significant deoxygenation at slightly increased organics yield reduction, compared to CaO.

Figure 2-7 below shows the HHV increase and the corresponding organics yield reduction. A similar trend to that seen in ***Figure 2-6*** is observed. CaO can achieve an HHV increase of around 30 % at low organics yield reduction while Al_2O_3 and MgO can increase HHV by over 50 % but at high organics yield reduction.

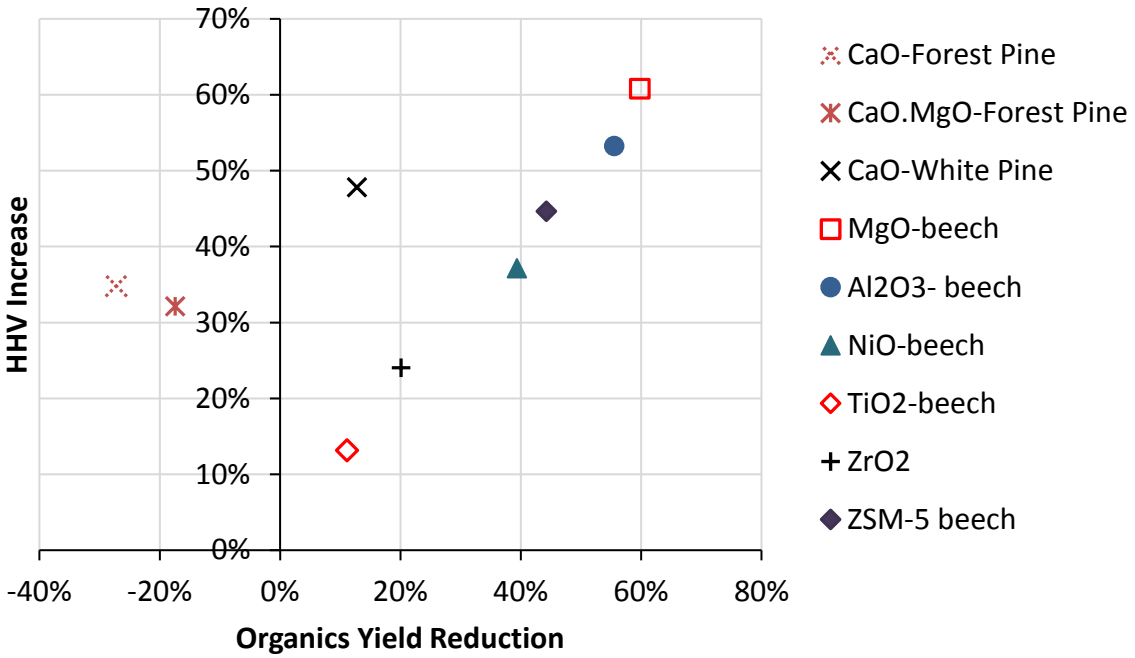

Figure 2-7: HHV increase vs organics yield reduction (% increase in HHV from non-catalytic pyrolysis to CP vs % reduction in the organics yield from non-catalytic pyrolysis to CP)

Conclusions from the studied literature are given next in Section 2.7.

2.7 Conclusions

The studied literature shows that pyrolysis has the potential to produce a bio-oil that can be co-processed with VGO in a standard refinery to produce gasoline (petrol) and diesel products. Although fast pyrolysis is associated with production of the highest liquid yields, it is a complicated technology, with high operational costs associated with reducing the biomass particle to sizes < 1mm required for this process, as well as costs to maintain the very high heating rates (> 10 °C/s). Intermediate pyrolysis offers reasonably high liquid yields and larger biomass particle sizes (> 1mm) can be processed at lower heating rates, resulting in cheaper costs and will thus be investigated in this study.

The bio-oil will need to be upgraded if it is to be co-processed at blending ratios > 5 wt.%. A maximum blending ratio of 10 wt.% is recommended to avoid an impact on product yield and quality, as well as to avoid operational problems in FCC units.

In South Africa, 10 wt.% blending can be achieved at the Enref refinery in Durban. To achieve this blending ratio, a bio-oil produced at a yield > 15 wt.%, with an oxygen content of < 17 wt.% (dry basis) and a water content < 32 wt.% and is required.

E. grandis is the most used tree species in the pulp and paper industry, and it also the most abundant tree species around the Durban region, hence it was selected as the biomass feedstock to be used in this study.

The use of catalysts physically mixed with biomass during the pyrolysis process (*in situ*) was chosen to upgrade the bio-oils due to the higher capital costs associated with *ex situ* setups. Furthermore impregnation, as a method to mix biomass and catalyst was not considered due to impracticability at larger scale.

From the reviewed literature, it can be seen that Al_2O_3, CaO and MgO are promising catalysts for the *in situ* pyrolysis of lignocellulosic biomass. CaO can result in significant oxygen decrease with limited impact on organics yield while Al_2O_3 and MgO can achieve very high bio-oil deoxygenation. These catalysts were reported to promote deoxygenation via decarboxylation, decarbonyation and dehydration. Decarboxylation is more preferable over decarbonylation because for every carbon atom removed, 2 oxygen atoms are removed instead of 1.

As bio-oil quality increases (decrease in bio-oil oxygen content and increase in bio-oil HHV) the bio-oil yield generally decreases due to release of oxygenated compounds: H_2O, CO and CO_2. Temperature and C/B ratio play a critical role in determining the bio-oil yield and quality. It is probable that the catalyst will have limited deoxygenation abilities at lower temperatures, while at higher temperatures and C/B ratio, volatile cracking reactions producing C_xH_y gases are likely to be favoured, resulting in low oil yields. Therefore, an optimisation of these two parameters is needed to produce a bio-oil with the highest possible quality at the acceptable yield (> 15 wt.%).

The water content is a problem in most catalytic experiments as it results in one homogeneous mixture with high water content. When the organic phase is retrieved by decanting, some of the organics are left in the aqueous phase. Therefore, it would be desirable to design a condensation system that allows for efficient recovery of organics, with a low water content.

3 Project Scope and Methodology

3.1 Project Scope

3.1.1 Research Questions

The research question that this study will answer is; is it possible through catalytic pyrolysis of forestry residue, using CaO, MgO or Al_2O_3 catalyst, to produce a bio-oil of sufficient quality to be co-processed with vacuum gas oil at a 10 wt.% blending ratio in an oil refinery? The following specific questions hope to be answered in the study to address the main question above:

1) How do the 3 catalysts, CaO, MgO and Al_2O_3 differ in terms of the chemical reactions of deoxygenation they favour, and how does this impact the relationship between oxygen content and bio-oil yield?
2) What are the optimal process conditions on bench scale which maximise bio-oil quality (< 17 wt.% oxygen, dry basis) while achieving sufficient bio-oil yields (> 15 wt.%)?
3) Can these optimal conditions be transferred from a fixed bed, gram-scale batch reactor, to an auger-type, kg-scale continuous reactor to obtain similar bio-oil yield and quality?

3.1.2 Aims/ Objectives

The main objective of this study is to produce an upgraded bio-oil from forest residues using intermediate pyrolysis, for co-processing in a conventional oil refinery. To answer the research questions, the specific objectives below need to be met:

1) Characterise the biomass feedstock: chemical composition, HHV, proximate, ultimate and thermal analysis.
2) Compare the performance of the catalysts determined from literature at bench scale under an appropriate range of process conditions and select the one which best meets the main objective at an acceptable yield.
3) Optimise the quality of bio-oil at bench scale using intermediate pyrolysis conditions via the investigation of the influence of pyrolysis parameters and catalyst content.

4) Adapt the optimised conditions found at bed scale in a batch reactor, to obtain similar or improved bio-oil quality on a pilot scale with a continuous reactor.

The details of these objectives and how they will be realised are given in the applied methodology (Section 3.2).

3.1.3 Limitations/ Scope

Only *Eucalyptus grandis* forest residue (tops and branches) was considered for this study based on this tree species being the most grown for the pulp and paper industry. It is also the dominant species in the regions with the largest forest residue amounts (KwaZulu Natal and Mpumalanga).

While 3 most promising catalysts (CaO, MgO and Al_2O_3) were selected from literature and confirmed via screening tests, only two of these catalysts, CaO and MgO were selected from the screening tests for further optimisation because they showed a similar performance in the initial tests.

Only intermediate pyrolysis technology was investigated. Although fast pyrolysis processes are associated with high liquid product yields, sufficient deoxygenation could be achieved via technologies easier to implement such as intermediate pyrolysis. *In situ* catalytic pyrolysis was chosen to further decomplicate the technology by avoiding the use of a second reactor. Additionally, intermediate pyrolysis yields more char than fast pyrolysis, which could be used for CO_2 sequestration and soil amendment in forests.

Investigating co-processing in an FCC was not in the scope of the study. Literature was used to estimate the required bio-oil quality in terms of oxygen and water content.

3.2 Materials and Methodology

3.2.1 Biomass Supply and Pre-treatment

3.2.1.1 Biomass Supply

The *E. grandis* biomass used in this study was sourced from Backsberg Estate Cellars; a wine farm located close to the town of Klapmuts in the Cape Winelands District of the Western Cape province of South Africa. The trees are grown as part of the Estate's efforts to counterbalance the carbon emissions related to their wine processing operations. The trees are grown on a short rotation of 6 – 8 years, which is the typical rotation period for eucalyptus trees grown for pulpwood in South Africa.

The residue consisted of mainly dry branches picked up from the ground in the *E. grandis* plots. Twigs and leaves were not picked, so as not to disturb the soil fertility. The biomass was personally sampled by the author of the thesis with careful attention to take samples from various parts of the plots. Most of these branches are a product of thinning of the trees. The branches were packed in polypropylene bags and were transported to Stellenbosch University's Department of Forestry and Wood Science where part of the pre-treatment and analysis was done.

3.2.1.2 Biomass Chipping and Milling

The branches were mechanically chipped to smaller pieces using a wood chipper. The chipped biomass was sampled by the cone and quartering technique (Alakangas and Impola 2015) before being transported to the Department of Process Engineering where it was milled through a 5 mm sieve using a hammer mill. The milled samples were put through a pilot shaker to separate it into different particle size distributions. Particles with a diameter size of < 2 mm were used for bench and pilot scale experiments. The chosen particle size was sufficient to enable high heating rates of the particle as well as allow reasonable contact between the biomass and catalyst as discussed in Section 2.5.4. Particles with a size > 2mm where re-milled and sieved again until the particle size was < 2 mm.

A lab scale ZM500 mill supplied by Retsch was used to mill the biomass to a particle size of < 425 µm which was suitable for the diverse types of analytical activities done on it (lignocellulosic characterisation, ultimate and thermogravimetric analysis).

3.2.2 Thermogravimetric Analysis

Thermogravimetric (TG) analysis of *E. grandis* was carried out on a, TGA/DSC Star Systems thermogravimetric analyser supplied by Mettler Toledo, to determine the active pyrolytic zone. TG data is also important because it gives an indication of the different lignocellulosic components making up a feedstock. Nitrogen at a flowrate of 100 ml/min was used as the inert gas in the TG experiments. For each experiment, a 20 mg biomass sample was heated from 30 to 900 °C at a heating rate of 20 °C /min. It is reported that to accurately define the active pyrolytic zone using TG analysis, heating rates of 20 °C/min and below should be used (F.-X. Collard and Blin 2014).

3.2.3 Biomass Characterisation

The biomass was characterised in terms of chemical composition, proximate and ultimate analyses as well as energy content (HHV).

3.2.3.1 Chemical Composition

Lignocellulosic and Extractive Composition

A common method for quantifying and characterising woody biomass chemical composition is according to the TAPPI standards, which do not prioritise closing the mass balance and determination of the separate biomass constituents (Burkhardt et al. 2013). However, constituent proportion is important because it is known to significantly influence pyrolysis product yields and composition. An alternative is the National Renewable Energy Laboratory (NREL), Laboratory Analytical Procedures (LAP), which has been cited extensively in recent literature (Burkhardt et al. 2013). These methods were used to determine the lignocellulosic and extractive composition of the biomass in this study. The lignin and structural carbohydrate (cellulose and hemicelluloses) composition of the biomass was determined by the NREL method described by Sluiter et al. (2012).

The acetyl content of the biomass was also determined using the same method described above. A two-solvent extraction method using ethanol and water as described by Sluiter, Ruiz, et al. (2008) was used to determine the extractive content of the biomass.

Moisture and Inorganic Content

To determine its moisture content, the biomass was dried in an oven at 105 ± 3 °C in accordance to the NREL method described by Sluiter, Hames, Hyman, et al. (2008). The inorganic content of the biomass was then determined by combusting the sample in a muffle furnace at 575 ± 25 °C in accordance to the NREL method described by Sluiter, Hames, Ruiz, et al. (2008). The chemical composition of these inorganics was then determined by X-Ray Fluorescence (XRF) analysis using a PANalytical Axios wavelength dispersive spectrometer at Central Analytical Facilities (Stellenbosch University).

3.2.3.2 Proximate Analysis

Proximate analysis was carried out on the thermogravimetric analyser to determine the inorganic, fixed carbon and volatiles matter content of the sample. The standard ASTM E1131 test method was used for this analysis.

3.2.3.3 Ultimate Analysis

Ultimate analysis gives the elemental composition of the organic fraction (C, H, N and S elements) of a substance. The oxygen is generally determined by difference. This analysis was done using a Elementar Vario EL Cube elemental analyser at Central Analytical Facilities (Stellenbosch University).

3.2.3.4 Higher Heating Value

The HHV of the feedstock was determined by bomb calorimetry using a Cal2K Eco Calorimeter supplied by DDS Instruments. The standard ASTM D5865-11a method was used for this analysis.

3.2.4 Bench Scale Pyrolysis

3.2.4.1 Experimental Setup

The fixed-bed, bench scale pyrolysis setup used in this study is illustrated by ***Figure 3-1***. A stainless-steel tubular reactor, internal diameter 100 mm and length 450 mm was used. Nitrogen was used as the sweeping gas and it was controlled to a flow rate of 5 standard litres per minute (SLPM) by an Alicat MC Series mass flow controller.

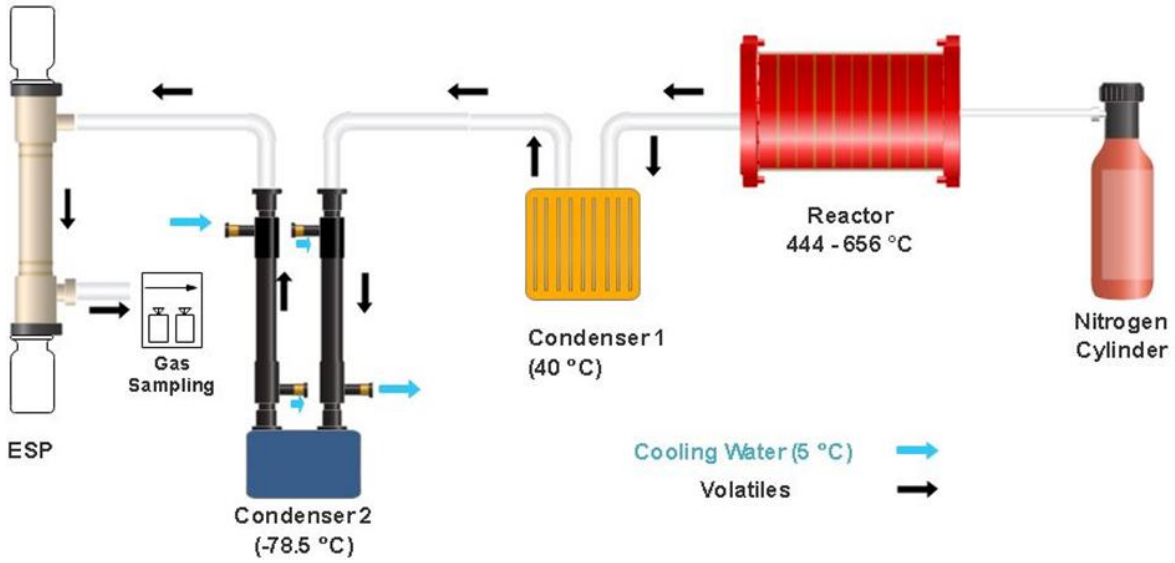

Figure 3-1: Bench scale pyrolysis setup

For each experiment, the biomass sample mass was 30 g. The catalyst/biomass mixture was put in a cylindrical, quartz sample boat, which was then placed in the middle of the reactor. The volatile residence time in the reactor, calculated from the middle of the reactor was approximately 24 s which corresponds to intermediate pyrolysis conditions (Bridgwater 2012). For the catalytic runs, the biomass and catalyst were premixed in a glass beaker and then transferred to the sample boat by a spatula. For each run, the reactor was heated by induction heating to the required pyrolysis temperature at around 300 °C/min and held at that temperature for 30 minutes. A heating rate of 300 °C/min is within the reported range for intermediate pyrolysis (Tripathi, Sahu, and Ganesan 2016).

The mass of char produced was taken as the mass of the residue, $m_{residue}$ left in the sample boat after an experiment was completed. In the case of catalytic pyrolysis, the mass of catalyst, m_{cat} used was subtracted from the mass of residue to give the char product yield, Y_{CHAR} on a catalyst free basis as given by the following equation.

$$Y_{CHAR} = \frac{m_{residue} - m_{cat}}{mass_{sample}(catalyst\ free)}.$$

From the reactor, the volatiles went through a series of condensers to extract the condensable volatiles. Due to the known problem of a high bio-oil water content (Czernik and Bridgwater 2004), a fractionation condensation system was designed to separate the bio-oil into different fractions based on boiling point; a desirable fraction containing mostly organics and an undesirable fraction containing mostly water. This condensation system is described next.

Condensation System

The hot volatiles from the reactor passed through a 3-part condensation system consisting of Condenser 1, Condenser 2 and an electrostatic precipitator (ESP) as shown in ***Figure 3-1***. Condenser 1 was made of stainless steel (internal diameter 125 mm, length 115 mm) and was heated to 40 °C by a 1500 W mica band heater. Preliminary pyrolysis tests at 550 °C were carried out to determine the Condenser 1 operating temperature and 40 °C was preferred. Lower temperatures resulted in an organic phase with a high water content, while at higher temperatures, minimal to zero condensation occurred in Condenser 1. Condenser 2 consisted of two shell and tube type condensers (internal diameter 23 mm, length 88 mm), which were connected to a stainless-steel pot. The pot (internal diameter 125 mm, length 100 mm) was immersed in a dry ice bath at -78.5 °C, while the tubular condensers were cooled down by water at 5 °C. The ESP, also made of stainless steel (internal diameter 50 mm, length 500 mm) was kept at 10 kV during experiments. The products from Condenser 1 and the ESP were viscous and dark brown. They contained mostly organics and were collectively termed the organic phase. The Condenser 2 product was a light brown liquid containing mostly water and was termed the aqueous phase. The mass of the condensers was measured on a micro balance to the nearest centigram, before and after each experiment to determine the mass of product by difference.

The mass of product in Condenser 1, Condenser 2, and the ESP were termed m_{C1}, m_{C2} and m_{ESP} respectively. The organic phase and aqueous phase yields, $Y_{O\text{-}PHASE}$ and $Y_{A\text{-}PHASE}$ were calculated according to the equations below.

$$Y_{O-PHASE} = \frac{m_{C\,1} + m_{ESP}}{mass_{sample}(catalyst\ free)}.$$

$$Y_{A-PHASE} = \frac{m_{C2}}{mass_{sample}(catalyst\ free)}.$$

Gas Collection System

The gas exiting from the ESP was collected every two minutes in 10 L Tedlar bags. This was done for the duration of the hold time after the final pyrolysis temperature had been reached (30 minutes). Gas from the Tedlar bags was then analysed by gas chromatography using a Compact GC 4.0 supplied by Global Analyser Solutions. The instrument had 3 columns; a Flame Ionisation Detector (FID) to analyse C_3 – C_6 hydrocarbons, a Thermal Conductivity Detector (TCD) to analyse CO_2 and C_2 hydrocarbons and another TCD to analyse H_2, O_2, N_2, CH_4 and CO.

Gas analysis gave the volume/mole composition of each compound in the sampled gas. The mass of a compound X produced at each sampling time was calculated based on the nitrogen volume composition (sweeping gas not produced during pyrolysis) and flow rate according the following equation:

$$\text{Mass X} = \frac{\text{Vol \% X}}{\text{Vol \% N}_2} . \frac{\text{N}_2\text{ flow rate[SLPM]}}{\text{Standard gas volume[L/mol]}} . \text{MM}_\text{X}\text{[g/mol]}. \text{Sampling time[min]}$$

where $\mathbf{MM_x}$ is the molecular mass of compound **X**

A standard gas volume value of 22.4 L/mol was used. The total mass of a compound produced in an experiment, m_X was calculated as the sum of its individual masses in all the gas samples taken during that experiment and its yield, Y_x was then calculated using the following equation.

$$\text{Y}_\text{X} = \frac{\text{m}_\text{X}}{\text{mass}_{\text{sample}}(\text{catalyst free})}.$$

Before the start of each experiment, a vacuum pump was used to check the system for leaks. A reading -100 kPa or less, on a pressure gauge attached to Condenser 2, indicated that the system was well sealed. Once sealing was confirmed, the system was purged with nitrogen. Gas samples were then collected and analysed. The experiment would only start when the oxygen concentration was below 0.5 %.

3.2.4.2 Design of Experiments

Catalyst Screening

Three catalysts: CaO, MgO and Al_2O_3 were selected based on literature review, with the goal to select the best performing catalyst in terms of deoxygenation, bio-oil energy content and bio-oil yield, for further optimisation. Non-catalytic runs were also carried out to set a benchmark for the catalytic experiments. A temperature of 550 °C was used for the screening experiments as it lies in the temperature range for maximum bio-oil yield (Section 2.5.1). The catalyst concentration, C_{cat} was set at 30 wt.%. C_{cat} is calculated as follows:

$$C_{cat} = \frac{mass\ catalyst}{mass\ catalyst + mass\ biomass}$$

The chosen C_{cat} is similar to the C/B reported in literature. Veses et al. (2014) used a C/B ratio of 1/3 and Stefanidis et al. (2011) used a C/B ratio of 1/2 which correspond to a C_{cat} of 25 and 33 wt.% respectively. All the pyrolysis experiments were done in duplicates to check the repeatability of the tests. All the catalysts were used as received from suppliers. MgO and CaO were supplied by Lasec SA (Pty) Ltd and the Al_2O_3 by Fizmerck India Chemicals.

Optimisation Experiments

A response surface design was used in the design of experiments (DoE) for the catalyst optimisation. It was chosen because it enables the entire process spectrum to be investigated and allows for the different responses to be modelled using quadratic models ("NIST/SEMATECH e-Handbook of Statistical Methods" 2012). The response surface design used was the circumscribed central composite design (CCD) because it is rotatable and covers the greatest process space.

It is desirable for response surface responses to be rotatable because you have better-behaved error bars in the response variable, as the uncertainty is similar in any direction you go from the design centre point ("NIST/SEMATECH e-Handbook of Statistical Methods" 2012). The centre point of the CCD corresponded to the catalyst screening conditions: 550 °C and 30 wt.% C_{cat}. 2 factors, temperature and C_{cat} were varied. The low and high values for temperature were 475 and 625 °C, while extra points 444 °C and 656 °C were generated due to the rotatability of the CCD. The catalyst concentration was varied between 10 wt.% (low value) and 50 wt.% (high value) and extra points, 1.7 wt.% and 58.3 wt.% were also investigated to make the response surface design rotatable. The temperature range was chosen based on the reported temperature range for maximum liquid product yield from biomass pyrolysis (Neves et al. 2011). The catalyst concentration range was chosen to cover both low and high catalyst concentrations as reported in literature (Veses et al. 2014; Chen et al. 2017). The random experimental design was generated using the software, Statistica 13®. The combinations of factors for each run are displayed in ***Table 3-1***. Each run was duplicated for purposes of repeatability assessment.

Table 3-1: Design of experiments for the catalyst optimisation (C: centre point)

Run	Temperature (°C)	C_{cat} (wt.%)
1	475	10
2	475	50
3	625	10
4	625	50
5	444	30
6	656	30
7	550	1.7
8	550	58.3
9 (C)	550	30
10 (C)	550	30

Since a statistical design was used in this study, a brief description of the statistical analysis used is given in Section 3.2.4.3.

3.2.4.3 Statistical Analysis

A regression model is an equation that describes the response variable as a function of the independent factors/variables. Regression models are a helpful way to understand the interdependence of variables. They are particularly useful in the prediction of data and in the optimisation of responses. Quadratic regression models of the form given by the equation below, were developed for various response variables in the optimisation experiments.

$$Y = \beta_0 + \beta_1 T + \beta_2 T^2 + \beta_3 T * C_{cat} + \beta_4 C_{cat} + \beta_5 {C_{cat}}^2$$

where **Y** is the response variable in question

β_0, β_1, β_2, β_3, β_4 and β_5 are the regression model coefficients

T is final pyrolysis temperature (°C)

C_{cat}, the catalyst concentration (wt.%)

A regression model is gauged using the following criteria (Stillwell and Webber 2016):

- Whether the factors/coefficients used in the model are significant?
- Is the overall model significant?
- Does the model exhibit heteroscedasticity?
- Does the model exhibit autocorrelation?

A good model contains only significant factors, i.e. those whose p-values are < 0.05, which corresponds to a 95 % confidence interval. This interval is the typical significance level used in statistical analysis (Stillwell and Webber 2016) and was therefore used in this study. The overall model significance is measured by the R^2 statistic, which gives an indication of how much the model can account for the total variability in the response variable. An R^2 equal to 1 means that the model accounts for all the variability in the response. The adjusted R^2 is similar to R^2 but considers the number of factors in the model. Addition of non-significant terms to the model will decrease adjusted R^2 value while addition of significant terms will increase the adjusted R^2 value. During the regression model development, in some cases, certain terms were removed from the model as they were statistically insignificant and resulted in an inaccurate model which was observed by a decrease in the adjusted R^2 value.

Model validation via the use of residuals was also used to validate the regression models. The residual value is the difference between the experimental (observed) value and the value predicted by the model. The mean square residual (MS residual) is the average of the squared residuals. The closer the MS residual to zero, the better the model. A statistical model with pronounced heteroscedasticity and autocorrelation is ill-suited to describe a relationship between variables (Stillwell and Webber 2016). Heteroscedastic data does not have constant variance, while homoscedastic data varies constantly. A plot of the residual values and the predicted values can be used to determine if the data is homoscedastic. If the data is heteroscedastic, the residual values would be scattered evenly across the predicted value distribution. If the data is heteroscedastic, the residuals scatter unevenly, typically with a smaller variation at the lower values of the predicted variable and then larger variation at the higher values. Autocorrelation is when a general trend between the residuals is observed. A scatter plot in which the data does not show a definite pattern, means that the regression model is a good fit to the data ("NIST/SEMATECH e-Handbook of Statistical Methods" 2012).

The adequacy of the regression model was also assessed by checking if the residuals fit a normal distribution. This is because in practical applications, the normal distribution accurately describes the distribution of random errors. Whether or not the residuals follow a normal distribution can be checked by plotting a normal probability plot. If the residuals are normally distributed, the plotted points will lie on a straight line while the presence of a curvature or scattered points indicates a non-normal distribution ("NIST/SEMATECH e-Handbook of Statistical Methods" 2012).

3.2.5 Pilot Scale Pyrolysis

After the bench scale experiments, the optimal conditions of the preferred catalyst were adopted for conversion with the pilot scale reactor. The pilot reactor is an auger-type, continuous reactor and has a 1 kg/hr capacity. 1.5 kg of catalyst free material was used per experiment. The experiments were done in duplicate for repeatability purposes.

3.2.5.1 Experimental Setup

An illustration of the pilot scale reactor is given in ***Figure 3-2***.

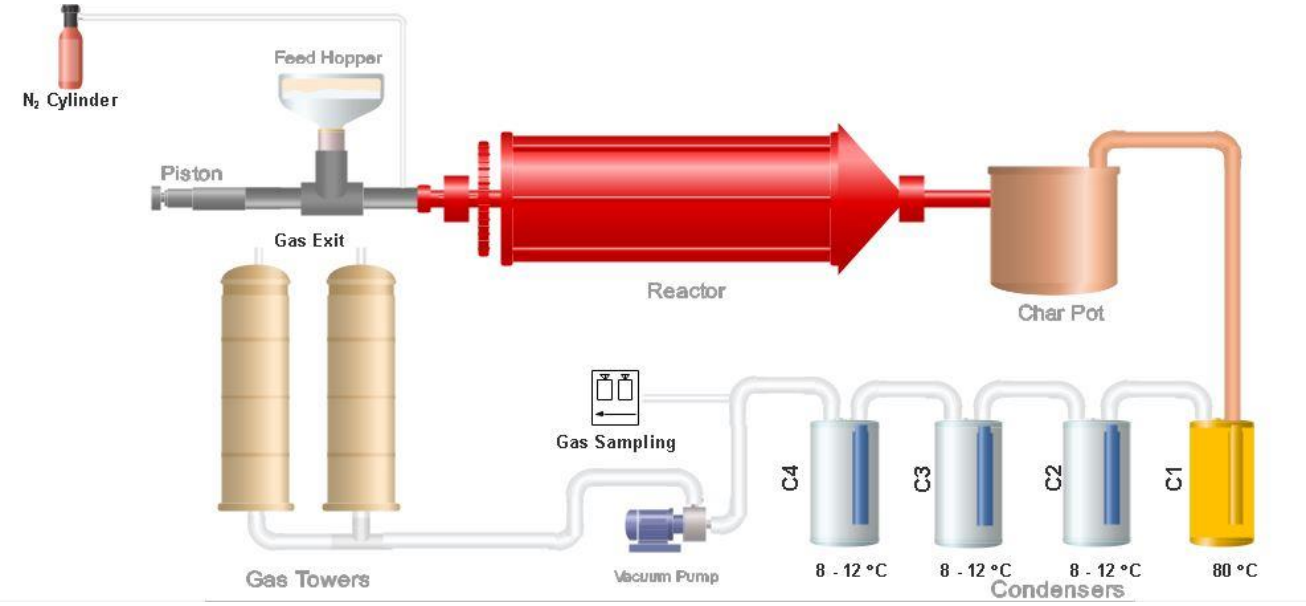

Figure 3-2: Pilot scale reactor illustration (Not drawn to scale)

The catalyst/biomass mixture was put in through the feed hopper. A piston feeder system pushed the feedstock into a heated rotary drum where the pyrolysis reactions took place. The drum had an effective internal diameter of 102 mm and a length of 742 mm. It had a baffle design to help push the material across it. Rotation speed of the reactor was set at 25 Hz. Feeding of material only started once the reactor reached the required pyrolysis temperature. The pyrolysis products (solid and volatiles) were conveyed from the reactor to a char pot where the solid product (char and catalyst) was collected. This chamber was maintained at 300 °C using electrical heating to limit the condensation of heavy volatiles (tars) in the pot.

The volatiles were then passed from the char pot to the condensation system through an arm which was also heated to 300 °C to minimise tar condensation. The condensation system consisted of four, 5L glass jars which were housed in metal containers connected in series. All the containers were filled with water. The first condenser, C1 was heated to 80 °C to minimise water condensation and obtain a liquid phase rich in organics and with low water content.

This condensation system design was similar to the heated pot used on the bench scale setup (***Figure 3-1***). Ice was added to containers 2 – 4, to maintain the water temperature between 8 and 12 °C.

Gas exiting condenser C4 was passed through water-containing gas towers (scrubbers), were the volume of gas produced was measured using the water displacement method. Gas was collected in each tower for a time between 7 – 10 minutes, depending on how quickly it took to fill the tower. During gas collection, samples of gas were taken just before the gas towers using 10 L Tedlar bags and the gas composition was measured using gas chromatography. The towers were used alternatingly; as one tower collected the gas, the other was being filled with makeup water. A portion of the gas exiting the condensation system went through an online oxygen analyser which monitored the oxygen content throughout the process. The oxygen content was maintained at < 3 mol. % O_2. Nitrogen was used as the carrier gas at 0.6 ± 0.1 L/min while a vacuum pump was used to help remove the volatiles quickly achieve volatile residence times in the reactor comparable to those of intermediate pyrolysis processes. In addition, the piston helped to push volatiles in the reactor as it pushed the feedstock in. The pilot plant operating pressure was controlled between -0.2 and +0.2 kPa gauge (close to atmospheric conditions) and therefore pressure had a limited effect on product yields.

Quantification of Products

The mass of the residues, $m_{residue}$ left in the char pot after the reaction was determined as the solid product and the char yield, Y_{CHAR} was calculated in the same way as for the bench scale experiment (Section 3.2.4).

The distribution of the different liquid product phases, organic and aqueous, resembled the one on the bench scale setup. C1 contained mostly organics due to the fractionation, while C2 contained a mostly aqueous phase. However, an organic phase was obtained at the bottom of C2 and was easily separated by decanting off the aqueous phase. The last 2 condensers, C3 and C4 contained mostly organics, similar to what was collected in the ESP on the bench scale. Therefore, the liquid product was composed of two phases; an aqueous phase from C2 and organic phase composed of C1, C3, C4 and part of C2.

3.2.6 Product Characterisation

3.2.6.1 Liquid Product

HHV tests were performed on the pyrolysis liquid products using the same equipment and method described for biomass characterisation. The water content of the liquid products was determined via Karl Fischer titration as reported in most literature (Lappas et al. 2002; Yildiz et al. 2016). A 701 KF Titrino titrator supplied by Metrohm was used for all the Karl Fischer titrations. A Honeywell/ Fluka Hydranal KetoSolver reagent supplied by Capital Research Distributors (Pty) Ltd was used for the titrations. Ultimate analysis of the pilot scale liquid products was carried out using a ThermoScientific Flash 2000 Elemental Analyser at the University of KwaZulu Natal.

3.2.6.2 Gas

Gas chromatography (GC) was used to analyse the incondensable gases from the pyrolysis experiments using the same configuration as described in Section 3.2.4.1. Gas analysis helped to close the overall pyrolysis mass balance and to detect changes in the gas product evolution due to the catalytic effect.

3.2.6.3 Char

An altered ASTM E1131 method previously used in our research group by Ridout et al. (2016) was used for the proximate analysis of chars when CaO was used. This method enabled the estimation of CO_2 absorbed by the catalyst during the reaction. The altered method included an isothermal step at 650 °C for 5 minutes to drive of volatiles. After this isothermal step, the sample was then heated to 900 °C and kept at that temperature for 5 minutes, before combustion of fixed carbon as per the standard ASTM E1131 method. Most volatiles are released from the char below 650 °C (Ridout et al. 2016). The volatiles released above 650 °C were taken to be CO_2. This value was then corrected for the volatiles released above 650 °C by a char produced without catalyst at the same conditions. The proximate analysis was carried out on a TGA 5500 Thermogravimetric Analyser supplied by TA Instruments.

The results and discussion of the biomass characterisation as well as the catalyst screening results are discussed next in Chapter 4.

4 Biomass Characterisation and Catalyst Screening Results

4.1 Biomass Characterisation

Characterisation results of the biomass are given below. They include thermal behaviour, chemical composition, proximate analysis, ultimate analysis and higher heating value (HHV) analysis.

4.1.1 Thermogravimetric Analysis

The TG and derivative thermogravimetric (DTG) curves of the *E. grandis* sample are shown in ***Figure 4-1***. The DTG shows the mass loss rate of the sample.

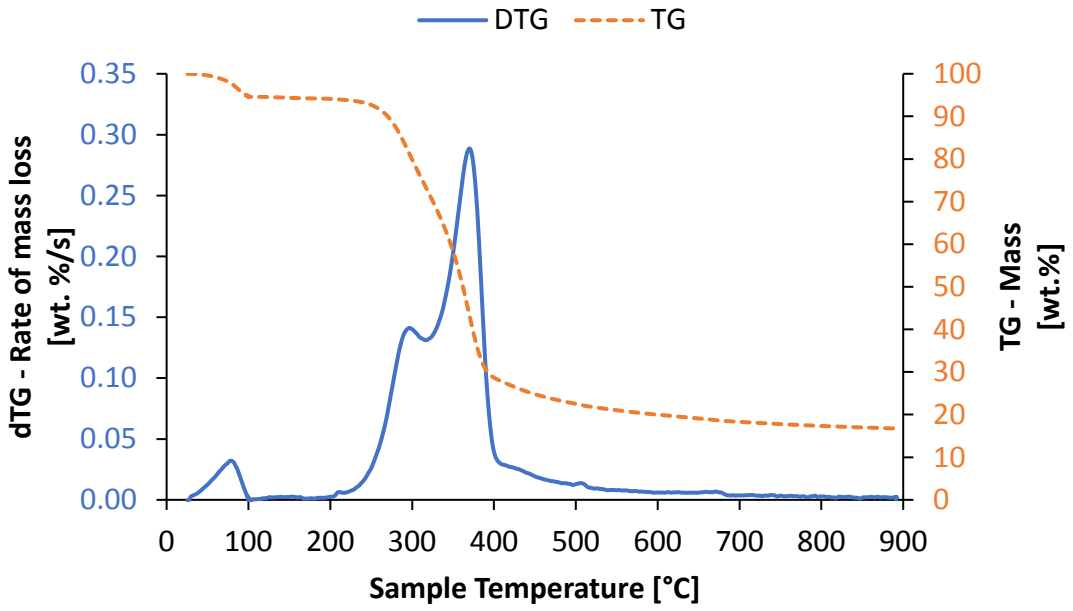

Figure 4-1: TG and DTG curves of *E. grandis*

The initial peak on the DTG at temperatures < 100 °C is a result of the loss of the moisture bound to the biomass. Two other major peaks were observed; one between 200 and 320 °C and the other between 320 and 400 °C. The first peak is characteristic of xylan degradation which is the main hemicellulose in hardwood, while in the range 320 – 400 °C, a peak characteristic of cellulose conversion was observed (F.-X. Collard and Blin 2014). The same authors reported that degradation of lignin occurs over a wide range of temperature from around 200 °C to about 600 °C.

This is consistent with the results from this study, as the DTG curve rises upwards from 200 °C and tapers off between 600 and 700 °C. The peak temperatures discussed above are consistent with lignocellulosic feedstock and confirm the need for temperature ≥ 400 °C for significant conversion and oil production.

4.1.2 Chemical Composition

4.1.2.1 Moisture and Inorganic Content

The moisture and inorganic content of the biomass is given in **Table 4-1**. Generally, inorganic content for wood species is lower than 0.8 wt.% but in this study, the biomass inorganic content of > 1 wt.% was likely due to the relatively high proportion of bark in the forest residues. Typically the inorganic content of bark is greater than 5 wt.% (Rowell et al. 2005).

Table 4-1: Moisture and inorganic content of biomass

Component	Amount (wt.%)
Moisture	8.28 ± 0.01
Inorganics	1.12 ±0.01

4.1.2.2 Lignocellulosic and Extractive Composition

The lignocellulosic and extractive composition of the biomass is given in ***Table 4-2***. The hemicelluloses were measured based on xylans and acetyl content; most acetyl is part of the hemicelluloses (Rowell et al. 2005). 12.5 wt.% of the sample was unidentified.

Table 4-2: Chemical composition of *E. grandis* (dry, ash free basis)

Component	Amount (wt.%)
Extractives	7.8 ± 0.3
Lignin	28.8 ± 0.1
Cellulose (glucose)	37.1 ± 0.5
Hemicelluloses (xylose + acetyl)	13.8 ± 0.3
Others	12.5

The extractives, cellulose and lignin compositions are consistent with the studied literature in Section 2.1.1. The relatively high lignin content, > 25 wt.%) is consistent with previous reported values for eucalyptus (Park et al. 2012; Inalbon et al. 2015). Although hemicelluloses content is typically 20 – 30 wt. % for wood (Section 2.1.1.2), low hemicelluloses content similar to what was found in ***Table 4-2***, has been reported in literature for *E. grandis*. Emmel et al. (2003), Joubert (2013), Yu et al. (2010) and Park et al. (2012) reported hemicelluloses contents (dry ash free basis) of 15.3 wt.%, 11.5 wt.%, 11.4 wt.% and 13.3 wt.% respectively. The same authors reported that 11.0 – 14.8 wt.% of the biomass was unidentified. The unidentified compounds could be 4-O-methyl-glucuronic acid found in heteroxylans (Emmel et al. 2003). Glucomannan, a hemicelluloses polymer (usually found in significantly lower amount than xylan in hardwood) was not determined in the method used in this study and could also account for part of the missing composition.

Hemicelluloses and extractives are known to react at temperatures below 320 °C (Melzer et al. 2013). According to ***Figure 4-1***, the TG mass loss around 320 °C, degradation is 23.4 wt.%. This was more than the total of measured hemicelluloses and extractives (21.6 wt.%), which is consistent with probable underestimation of the hemicelluloses content.

4.1.2.3 Inorganic Composition

The composition of the inorganics in the biomass was determined using XRF analysis. The results are shown in ***Table 4-3***. The LOI (Loss on Ignition) represents the total volatile content of the ash which also includes the water bounded to the lattice of silicate compounds.

Table 4-3: Composition of the inorganics from *E. grandis*

Inorganic	Al_2O_3	CaO	Fe_2O_3	K_2O	MgO	MnO	Na_2O	P_2O_5	SiO_2	TiO_2	L.O.I
Amount (wt.%)	0.63	39.93	0.33	0.66	13.38	1.29	2.79	5.85	2.73	0.15	31.34

Among the 3 major components of biomass inorganics mentioned in Section 2.1.1.5, Ca and Mg were found to be in largest content in the *E. grandis* used in this study.

4.1.3 Proximate Analysis

Results of the proximate analysis of the *E. grandis* feedstock are shown in ***Table 4-4***.

Table 4-4: Proximate analysis of *E. grandis*

Component	Moisture	Inorganics	Volatile Matter	Fixed Carbon
Composition (wt.%)	5.0	1.0	78.4	15.6

The inorganic content found by proximate analysis on the TGA was consistent with the one found using the NREL methods (Section 4.1.1), while the moisture content was different between the 2 methods. The difference in moisture content could be because the sample used on the TGA dried during pre-treatment, as it was being milled to particle size of < 425 µm. Although the inorganic content of hardwoods is typically around 0.5 wt.% as discussed in Section 2.1.1, the feedstock used in this study contains bark, which compared to wood, contains relatively higher inorganic content resulting in an inorganic content of 1.0 wt. %. The amount of volatiles is consistent with values found in literature for wood (Oasmaa et al. 2010; Lin et al. 2010). The fixed carbon content is within the range 14.3 – 19.5 wt. % reported in literature for woody biomass (Garcia-Perez et al. 2008; Lin et al. 2010).

4.1.4 Ultimate Analysis

Table 4-5 gives the elemental composition of the feedstock on a dry, ash free basis (daf). These results were consistent with those in the literature mentioned in Section 2.1.1.

Table 4-5: Ultimate analysis of *E. grandis* (dry ash free basis)

Element	C	H	N	S	O[a]
Composition (wt.%)	48.01	6.36	0.12	0.06	44.36

[a] Determined by difference

4.1.5 Higher Heating Value

The calorific value of *E. grandis* is shown in ***Table 4-6***. Although the measured HHV in this study is lower than that reported in literature, it becomes comparable when a correction is made to estimate the value on dry basis.

Table 4-6: *E. grandis* HHV (dry ash free basis)

	This Study	Oasmaa et al.(2010)
Measured value (MJ/kg)	17.7	19.9
Moisture content (wt.%)	8.28	dry
Moisture corrected value (MJ/kg)	19.3	19.9

4.2 Catalyst Screening

4.2.1 Overall Product Yields

This section details the results obtained from the catalytic pyrolysis tests at bench scale using the three catalysts selected from literature: Al_2O_3, CaO, and MgO. A summary of the overall product yields obtained from the catalytic screening runs is shown in ***Figure 4-2***. All the yields are expressed on catalyst free basis and are also based on a feed with an initial moisture content of 8.28 wt.%. This means that no correction was done to get results on a moisture free basis. 8.28 wt.% of the condensable product is water due to moisture. The rest of the water is pyrolytic water, produced by thermochemical reactions. “Non Cat” refers to non-catalytic pyrolysis experiments. The values reported on the figures are the means of 2 experiments while the error bars indicate the standard deviation from the mean. The experiments were found to be repeatable with a standard deviation of < 1 wt. % achieved for all the yields. The total mass balance ranged from 89 – 92 wt. %. The missing 8 – 11 wt. % can be attributed to incomplete condensation of the volatiles due to the relatively high flow rate of the carrier gas (5 SLPM). This was consistent with the presence of some oily residues condensed on the Tedlar bags during the gas collection.

Some coke was also likely to be condensed at the surface of the reactor wall. However, due to the relatively large mass of the reactor (3.3 kg), it was not possible to estimate accurately the amount (< 1g) condensed on a scale accurate to 1 g. The unmeasured mass of the coke introduced an error representing up to 3.3 wt.% (worst case scenario) in the mass balance.

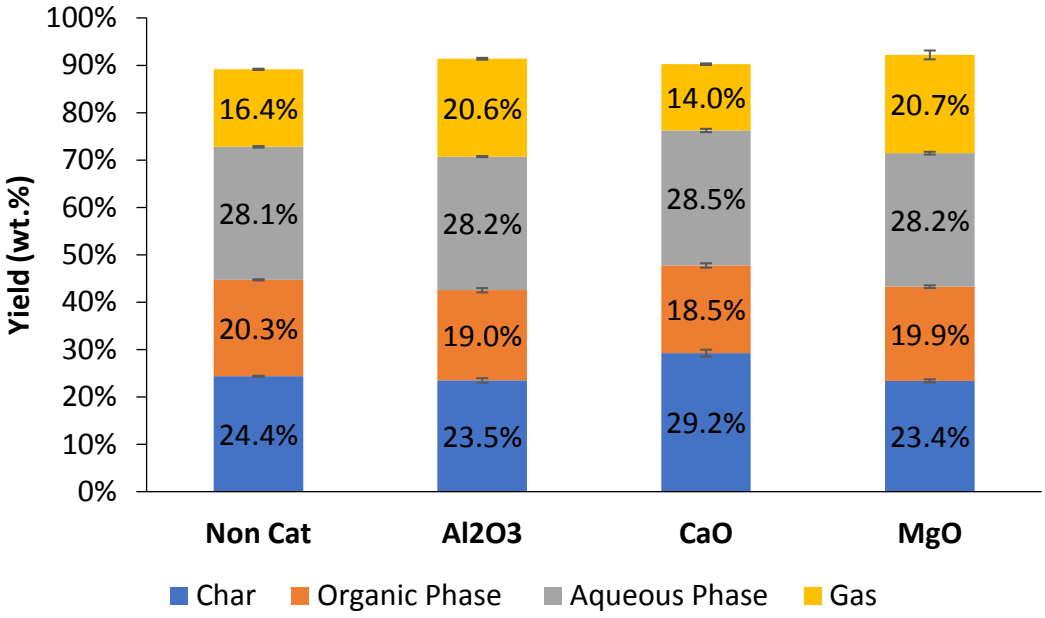

Figure 4-2: Overall product yields from catalyst screening (550 °C and 30 wt.% C_{cat})

4.2.2 Char

4.2.2.1 Yield

The char yield for non-catalytic pyrolysis is consistent with the yields reported by Neves et al. (2011) for biomass pyrolysis at 550 °C . An ANOVA was done on the char yields and the results are shown ***Table 4-7***.

Table 4-7: ANOVA results for char yields from catalyst screening

	p-value	Conclusion
Non-Cat/Al_2O_3	0.2233	insignificant
Non-Cat/MgO	0.1695	insignificant
Non-Cat/CaO	0.0207	significant

The above results show that char yields were not significantly modified with catalyst addition except for when CaO was used. This is because when the biomass and catalyst are physically mixed, they are not in intimate contact and therefore the catalyst does not influence the primary reactions which are related to the breakdown of the biomass matrix (Stefanidis et al. 2011).

Some articles report no change in the char yield (Veses et al. 2014) and some report an increase (Lin et al. 2010; Stefanidis et al. 2011). For those reporting an increase, most assume it is due to the formation of secondary char at the catalyst surface and char yield increase is generally < 3 wt.%. The differences in char yield observed in this study when CaO was used were significantly higher. When CaO is the catalyst, the formation of $CaCO_3$ through the absorption of CO_2 produced by pyrolysis, has been reported by Lin et al. (2010) and Chen et al. (2017) (equation below). This reaction is likely to be the reason of the substantial increase in the char yield.

$$CaO + CO_2 \rightarrow CaCO_3$$

4.2.2.2 Inorganic Content and Char Application

The solid product from catalytic pyrolysis is likely to have a high inorganic content due to the presence of the catalyst, which makes the use of char for fuel purposes undesirable because the inorganics lower the overall calorific value of the char significantly. Proximate analysis results of the non-catalytic char and that produced using CaO in the catalyst screening are detailed in ***Table 4-8*** below.

Table 4-8: Proximate analysis results (dry basis) of non-catalytic char and CaO pyrolysis char from catalyst screening (550 °C)

	Non-Cat		**30 wt.% CaO**
	Standard Prox	Altered Prox	Altered Prox
Volatiles < 650 °C, (wt.%)	-	15.4	14.0
Volatiles > 650 °C, (wt.%)	-	6.2	18.9
Total Volatiles at 900 °C (wt.%)	20.5	21.6	32.9
Fixed Carbon, (wt.%)	76.8	75.6	19.9
Inorganics (wt.%)	2.7	2.8	47.1

The proximate results in ***Table 4-8*** confirmed that CO_2 was absorbed during CaO catalysed pyrolysis, as much more volatiles at temperatures > 650 °C (18.9 wt.%), were released from the CaO pyrolysis char than the non-catalytic char (6.2 wt.%). When corrected for the volatiles released at temperatures > 650 °C in the non-catalytic char, the CO_2 released from the CaO pyrolysis char was estimated to be 16.6 wt.%. The high inorganics content (> 45 wt.%) confirmed that the char from catalytic pyrolysis is unsuitable for combustion purposes.

It is more desirable to use the solid product for agricultural purposes, specifically in soil amendment. Bio-char applied to soil is known to aid in improving the water holding capacity of sandy soils, carbon sequestration and soil pH alteration (Sohi et al. 2010). The use of "ammonium based, inorganic nitrogen fertilisers" as well as acid rain are the main cause of soil acidification which results in reduced activity of microbes and the release of ions toxic to plants. To neutralise this acidity, agricultural lime, typically composed of $CaCO_3$ and sometimes $MgCO_3$ is applied to the soil (Zimdahl 2015). The neutralising ability of char derived from wood was found to be less than that of char derived from feedstocks with higher ash content (Kookana et al. 2011). Therefore, it is expected that the char produced from the process considered in this study could have a significant liming effect. The char from catalytic pyrolysis using CaO is therefore very suitable for this purpose since it contains $CaCO_3$, the main component of agricultural lime in large amounts. MgO can be used as a fertilizer to counteract magnesium deficiency in plants (Van Mannekus & Co. B.V. 2013). This is most likely possible in acidic soils were the MgO can be dissolved by the acids to form soluble magnesium ions which can then be absorbed by the plant. Therefore, there is potential to use char from catalytic pyrolysis using MgO to neutralise acidic soils as well as to improve magnesium concentrations in that soil.

Aluminium ions are highly toxic to plants especially in acidic soils (Samac and Tesfaye 2003). This means that adding char containing Al_2O_3 to the soil can potentially increase the toxicity of the soil leading to poor plant growth.

4.2.3 Gas

4.2.3.1 Overall Yield

An overall gas yield of 16.2 wt.% was obtained in this study for non-catalytic pyrolysis, as shown in ***Figure 4-2***. A collection of data on the pyrolysis yields from different biomass types was made by Neves et al. (2011). Overall gas yields as low as 15 wt. % were reported for a pyrolysis temperature of 550 °C, which is consistent with the results from this study. From the same review article, it was found out that the main permanent gas products of biomass pyrolysis are CO_2 and CO. CH_4 and H_2 as well as some C_2-C_4 hydrocarbon gases such as ethane, ethene, propane and butane are also produced but in smaller quantities.

4.2.3.2 Gas Product Yields

The yields of the different gases produced in this study are shown in ***Figure 4-3***. The individual gas product yields for non-catalytic pyrolysis were consistent with the literature (Neves et al. 2011). When a catalyst was added, there was a general increase in all the gas products except when CO_2 yield decreased when CaO was used. A detailed discussion of the yield of each individual gas product is provided below.

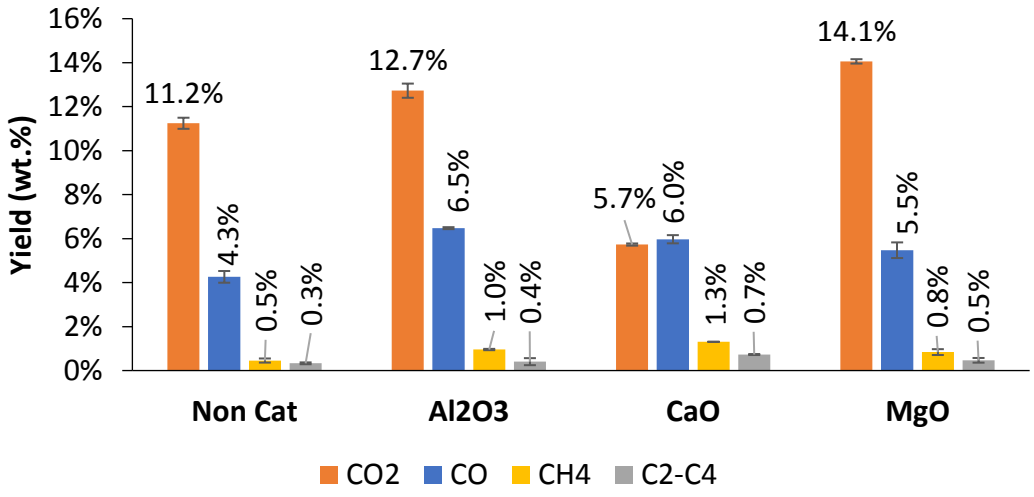

Figure 4-3: Gas product yields from catalyst screening

CO_2

As seen from ***Figure 4-3***, the use of a catalyst results in the increase of the CO_2 yield except when CaO is used as a catalyst. Catalytic effect promoting deoxygenation through decarboxylation reaction was previously reported by Stefanidis et al. (2011) and Stefanidis et al. (2016). The decrease in the CO_2 yield could be explained by the absorption of CO_2 by CaO to form $CaCO_3$ as mentioned earlier in Section 4.2.2.1. In support of this is previous research by Lin et al. (2010), Veses et al. (2014) and Chen et al. (2017) which reported a similar observation. The results of the ANOVA of the CO_2 yield are shown in ***Table 4-9*** below.

Table 4-9: ANOVA for CO_2 yield from catalyst screening

	p-value	**Conclusion**
Non-Cat/Al_2O_3	0.0362	significant
Non-Cat/CaO	0.0011	significant
Non-Cat/MgO	0.0046	significant

From ***Table 4-9*** it can be concluded that the presence of both Al_2O_3 and MgO resulted in a statistically significant increase in the CO_2 yield whereas the use of CaO resulted in a significant decrease in the CO_2 yield. MgO is a much greater decarboxylation catalyst compared to Al_2O_3 as the increase in CO_2 yield due to MgO (25.9 %) is almost twice the increase due to Al_2O_3 (13.4 %). Due to the absorption of CO_2 by CaO, it is difficult to determine the extent of decarboxylation resulting from the use of CaO.

In comparison to the results in this study, Stefanidis et al. (2011) found that MgO increased the CO_2 yield from 10.02 to 14.79 wt.% (47.6 % increase) and Al_2O_3 from 10.02 to an average of 12.31 wt.% (22.8 % increase). In the experimental setup used by Stefanidis et al. (2011), the biomass and catalyst were not physically mixed and the volatiles passed through a catalyst bed in a single reactor system. The C_{cat} used by these researchers was approximately 32 wt.%, similar to the catalyst concentration used for catalyst screening test in this work.

With the use of a catalyst bed, there is a greater contact between the volatiles and catalyst resulting in a greater catalytic effect and a larger CO_2 yield increase when compared to this study where the biomass and catalyst were physically mixed. Regarding CaO catalyst, Lin et al. (2010) reported a 66.3 % decrease in CO_2 yield in a fluidised bed reactor, from 9.5 to 3.2 wt.% compared to a 49.1 % decrease (from 11.2 to 5.7 wt.%) in this study. The lower catalyst concentration used in this study could result in less CO_2 being absorbed by CaO, thus the lower decrease in CO_2 yield.

It was reported that the catalysed CO_2 production is due to ketonisation reactions which are promoted by metal oxide catalysts (Gliński, Kijeński, and Jakubowski 1995; Deng, Fu, and Guo 2009). Organic acids can account for up to 9 wt.% of the bio-oil (Yildiz et al. 2013), and these are converted to ketones leading to release of CO_2 according to the equation below. This was confirmed by Lin et al. (2010) and Stefanidis et al. (2011) who saw a decrease in acid composition, while the composition of ketones increased when CaO and MgO catalyst were used respectively. Water is also produced in the ketonisation reactions reaction.

$$R_1COOH + R_2COOH \rightarrow R_1COR_2 + CO_2 + H_2O$$

As seen from the above reaction, ketonisation produces longer chain molecules with a higher calorific value. Some of these higher molecular compounds from ketonisation can be converted by aldol condensation to produce gasoline/ diesel range molecules in an oil refinery (Pham et al. 2013). Gliński, Kijeński, and Jakubowski (1995) found that Al_2O_3 had a lower effect on ketonisation compared to MgO which agrees with what was observed in this study. CaO is reported to promote ketonisation reactions as well (Chen et al. 2017).

According to Davidian et al. (2008) and Li et al. (2012), organic acids may be cracked to produce CO_2 in the presence of CaO and MgO according to the equation below. This is another possible mechanism by which CO_2 was produced when MgO catalyst was used in this study.

$$RCOOH \rightarrow RH + CO_2$$

CO

The use of catalyst resulted in an increase in CO yield as illustrated by ***Figure 4-3***. The CO yield increased by 51.2 % with Al_2O_3, 39.5 % with CaO and 27.9 % with MgO. An ANOVA test (***Table 4-10***), showed that all the increases in the CO yield are statistically significant.

Table 4-10: ANOVA for CO yield from catalyst screening

	p-value	Conclusion
Non-Cat/Al_2O_3	0.0073	significant
Non-Cat/CaO	0.0175	significant
Non-Cat/MgO	0.0351	significant

It is known that CO is a major product of the secondary cracking of organic volatiles (Neves et al. 2011). A possible mechanism is that the catalysts used in this study promoted secondary volatile cracking, resulting in the production of CO. Acidic catalysts like ZSM-5 and Al_2O_3 are reported to favour decarbonylation reactions (Stefanidis et al. 2011). A possible mechanism by which this can happen is the cracking of carboxylic acids to produce CO and a hydrocarbon via the production of a ketene intermediate. This happens according to the reaction steps below, which are given for the example of acetic acid (Yan et al. 2017).

$$2CH_3COOH \rightarrow 2H_2O + 2C_2OH_2$$

$$2C_2OH_2 \rightarrow 2CO + C_2H_4$$

Overall $$2CH_3COOH \rightarrow 2H_2O + 2C0 + C_2H_4$$

Compared to ketonisation which produces CO_2 and higher molecular compounds which stay in the liquid phase, the above reaction scheme is not favourable since it promotes cracking reactions which form lower molecular weight compounds only, thereby inevitably reducing the bio-oil yield.

CaO was reported to catalyse decarbonylation reactions which result in CO formation during pyrolysis (Chen et al. 2017). This supports the increase in CO yield with the use of CaO reported in this study.

Similarly, Veses et al. (2014) reported an increase in CO yield from 8.9 to 10.2 wt.% when CaO catalyst was used in an auger reactor. However, Lin et al. (2010) reported a decrease in CO yield from 6.8 to 4.3 wt.% which is different to what was observed in this study. In the fast pyrolysis setup used by Lin et al. (2010) the volatile residence times in the reactor were very low (< 1 s) and thereby secondary reactions were limited and consequently the production of CO. This coupled with the water-gas shift reaction (WGSR), which consumes CO, might have resulted in an overall decrease in CO yield. In this study, although the WGSR was also likely to consume CO, it is probable that there was significant cracking of volatiles taking place due to the considerably higher volatile residence time (> 20 s), leading to an overall increase in CO yield.

The results of Stefanidis et al. (2011) showed a similar trend to what was observed in this study. Their research found that the use of Al_2O_3 and MgO resulted in CO yield increases by 55.5 and 47.4 % respectively. The higher percentage increases obtained by Stefanidis et al. (2011) can be attributed to the experimental setup they used, which enhanced the catalytic effect as discussed earlier in this section. With a greater contact between the volatiles and catalyst, catalytic cracking was enhanced resulting in higher CO yields.

C_xH_y

The use of all the catalysts resulted in an increase in the yields of hydrocarbon gases, C_xH_y (CH_4 and C_2-C_4) as presented in ***Figure 4-3***. CaO gave the largest increase in the hydrocarbon gases yield, followed by Al_2O_3 and MgO respectively. An ANOVA of the C_xH_y yields showed that only the increase due to the use of CaO was statistically significant, although the increase was not far from being significant for the other catalysts (***Table 4-11***).

Table 4-11: ANOVA for C_xH_y yield from catalyst screening

	p-value	Conclusion
Non-Cat/Al_2O_3	0.0731	insignificant
Non-Cat/CaO	0.0061	significant
Non-Cat/MgO	0.1160	insignificant

After the major gas product of volatile cracking CO and CH_4, the C_2-C_4 hydrocarbon gases are the other products of secondary cracking of volatiles (Neves et al. 2011).This supports the conclusion presented in the CO results above that the oxides used in this study also promote volatile cracking, with CaO being the strongest cracking agent. These results are consistent with those of Stefanidis et al. (2011) who observed increases in the C_xH_y yield when Al_2O_3 and MgO catalysts were used in biomass pyrolysis. Contrary to what was observed in this study, Lin et al.(2010) observed a decrease in CH_4 yield from 2.2 – 1.6 wt.% when CaO catalyst was used in a fast pyrolysis process. Widyawati et al. (2011) postulated that CaO could promote the steam reforming reactions of CH_4 which could explain the decrease in the methane yield.

H_2

The H_2 yields are shown in ***Figure 4-4***.

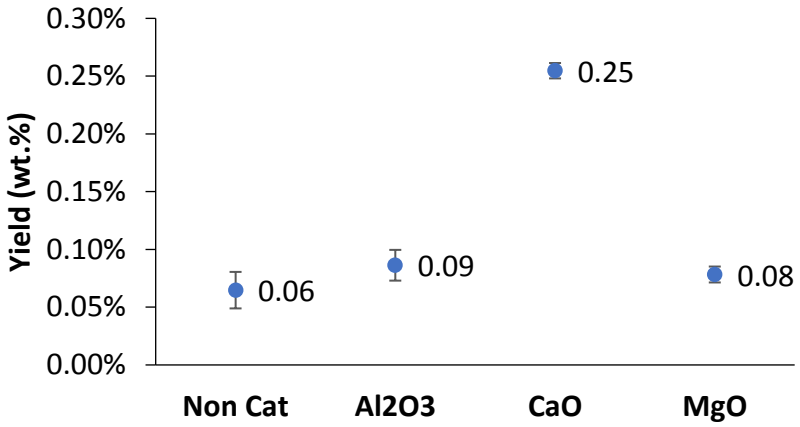

Figure 4-4: H_2 yields from catalyst screening

The ANOVA for H_2 yield (***Table 4-12***) showed that there was no significant increase in the H_2 yield in the presence of Al_2O_3 and MgO, while a significant increase was seen when CaO is used.

Table 4-12: ANOVA for H_2 yield from catalyst screening

	p-value	Conclusion
Non-Cat/Al_2O_3	0.2779	insignificant
Non-Cat/CaO	0.0040	significant
Non-Cat/MgO	0.3374	insignificant

The results from the above are consistent with Stefanidis et al. (2011) who found that the use of Al_2O_3 and MgO did not influence the H_2 yield. In the study by Lin et al. (2010), the use of CaO increased the H_2 yield by 2.5 times whereas it increased by 4 times in this study. It has been reported in literature (Lin et al. 2010; Chen et al. 2017), that the increase in H_2 yield when CaO catalyst is used, is due to the occurrence of the WGSR. It is therefore likely that the absorption of CO_2, coupled with the increased production of pyrolytic water, drove the WGSR forward, resulting in an increase in the H_2 yield. With the short volatile residence times in fast pyrolysis, the WGSR is minimised compared to an intermediate pyrolysis process used in this study, where the volatile residence times are much higher. As a result, more H_2 was produced in this study than in the fast pyrolysis process used by Lin et al. (2010).

4.2.3.3 Calorific Value

The volumetric/ molar composition of the gas products is shown in ***Figure 4-5***. When CaO was used as a catalyst, the absorptions of CO_2 led to a large decrease in the CO_2 mole fraction as seen in ***Figure 4-5***. This is congruous with the observations made by Veses et al. (2014) and Chen et al. (2017). The CO_2 mole fraction decreased when Al_2O_3 was used because the increase in the CO_2 yield was less than the increase in the other gas compounds (C_xH_y and CO) which were produced through catalytic cracking. On the other hand, due to the strong decarboxylation effect of MgO, the increase in CO_2 yield was almost the same as the increase in the other gas products, resulting in a CO_2 mole fraction similar to that from non-catalytic pyrolysis. The hydrocarbons mole fractions for all the catalysts increased with the use of catalyst due to the increase in the C_xH_y yield which was a result of the cracking effect of the catalysts.

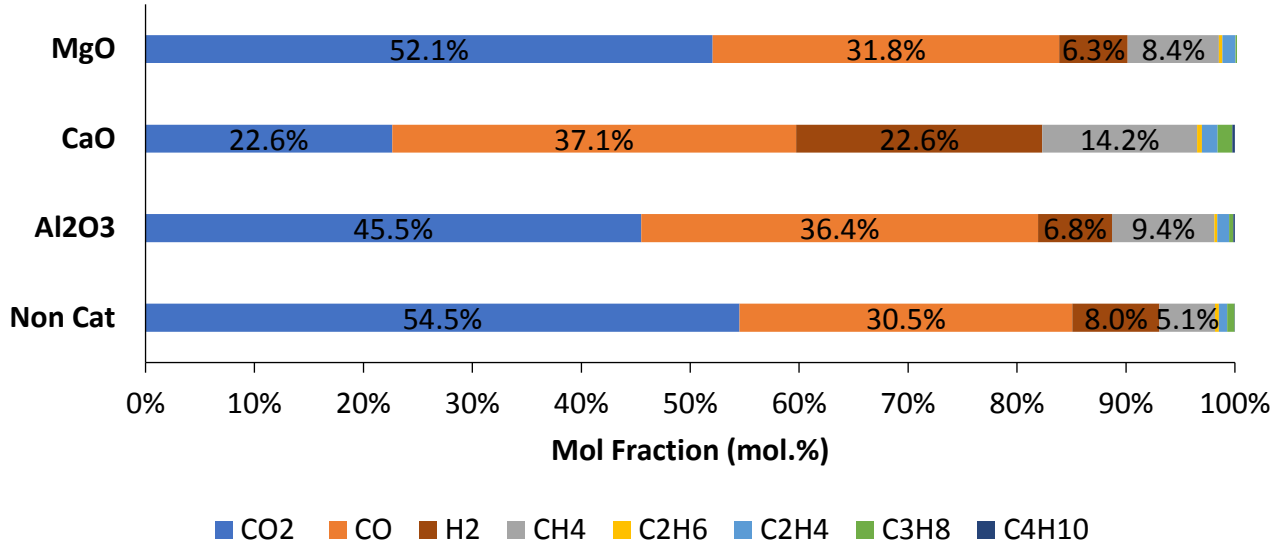

Figure 4-5: Mole composition of pyrolysis gas products from catalyst screening

In the presence of CaO and Al_2O_3, the CO mole fraction increased significantly as these catalysts promoted decarbonylation reactions. A huge increase in the H_2 fraction was observed with CaO due to the increased hydrogen yield brought about by the WGSR shifting towards H_2 production.

The lower heating value (LHV) of the pyrolysis gas (***Table 4-13***) was calculated using the molar composition in ***Figure 4-5*** as well as the enthalpy of combustion data from Green and Perry (2007).

Table 4-13: Calorific value of pyrolysis gas product from catalyst screening

Catalyst	None	Al_2O_3	CaO	MgO
LHV (MJ/kg)	5.2	6.9	13.7	6.2

The LHV obtained for non-catalytic pyrolysis gas is within the range of gas LHVs reported by Neves et al. (2011) at a pyrolysis temperature 550 °C. All catalysts increased the LHV of the gas due to the increased production of the gaseous hydrocarbons. The effect was more pronounced when CaO was used, as the LHV doubled with this catalyst. The huge rise when CaO was used was mostly due to the low concentration of CO_2 (absorption by CaO in char), which does not contribute to the calorific value of the gas, as well as the increased production of H_2.

4.2.4 Liquid

4.2.4.1 Yields

The total liquid yield (organic and aqueous phases) for non-catalytic pyrolysis was 48.4 wt.% and it is consistent with the typical liquid yield range of 40 – 60 wt.% reported for biomass intermediate pyrolysis (Hornung, Apfelbacher, and Sagi 2011). As seen in ***Figure 4-2***, the use of a catalyst only reduced the total liquid yields slightly to about 47.0 – 48.0 wt.%. The ANOVA results of the organic and aqueous phase yields are shown in ***Table 4-14***.

Table 4-14: ANOVA for organic and aqueous phase yields from catalyst screening

		p-value	Conclusion
Organic Phase	Non-Cat/Al_2O_3	0.0625	insignificant
	Non-Cat/CaO	0.0346	significant
	Non-Cat/MgO	0.1979	insignificant
Aqueous Phase	Non-Cat/Al_2O_3	0.4789	insignificant
	Non-Cat/CaO	0.2743	insignificant
	Non-Cat/MgO	0.7168	insignificant

Table 4-14 shows that, the p-values of the organic phase yields are lower than the p-values of the aqueous phase yields, showing that the decrease in organic phase yields is generally more significant than the changes in the aqueous phase yield. The similar yields between non-catalytic and catalytic pyrolysis seem to suggest that catalytic effect had a limited influence on the oil production. However, significant differences in oil composition and properties are possible and product characterisation is important.

4.2.4.2 Water Content

The water content of the organic and aqueous phases is displayed in ***Figure 4-6***. The organic phase water content ranged from 7.8 – 12.6 wt.% and the aqueous phase water content from 72.7 – 84.8 wt.%. The water content achieved for the organic phase was lower than the typical bio-oil moisture content range of 15 – 30 wt.% (***Table 1-1***). It was < 10 wt.% for all the experiments except for the MgO run where it was 12.6 wt.%.

This shows that a fractionation technique in the bio-oil condensation can be used to obtain a product concentrated in organic compound and energy. An increase in the water content of the aqueous phase was observed for all the catalysts.

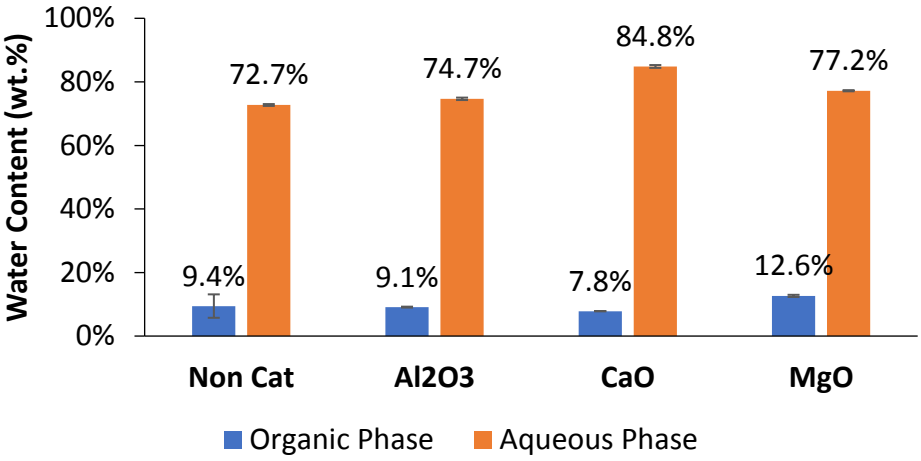

Figure 4-6: Water content of the different liquid product phases from catalyst screening

The water content of the different liquid phases is important in determining the pyrolytic water and organics yields which are discussed in Section 4.2.4.3.

4.2.4.3 Pyrolytic Water and Organics

Pyrolytic water is the water that is produced as a result of the dehydration reactions during breakdown of biomass structure (Neves et al. 2011). The inherent moisture bound to the biomass found in the liquid product is not considered to be pyrolytic water. Using the water content analysis in Section 4.2.4.2, the total water yield was calculated. Pyrolytic water was then calculated as the difference between the total water yield and the initial biomass moisture content. The organics yield is the difference between the total liquid product and the total water yield. ***Figure 4-7*** shows the pyrolytic water and organic yield from the catalytic screening. The pyrolytic water yield of 14.9 wt.% for non-catalytic pyrolysis at 550 °C, is consistent with the pyrolytic water yields reported from various literature by Neves et al. (2011) (10 – 16 wt.%). The use of catalysts results in an increase in the pyrolytic water yield as shown in ***Figure 4-7***. Based on an ANOVA test, the results showed that the increase in pyrolytic water yield with each catalyst was statistically significant (***Table 4-15***).

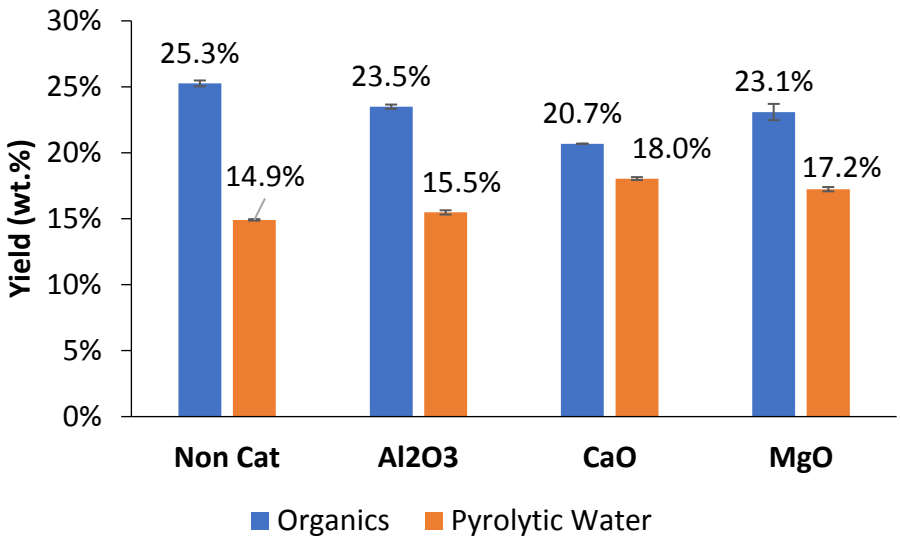

Figure 4-7: Organics and pyrolytic water yield from catalyst screening

Table 4-15: ANOVA for pyrolytic water yield from catalyst screening

	p-value	Conclusion
Non-Cat/Al_2O_3	0.0441	significant
Non-Cat/CaO	0.0007	significant
Non-Cat/MgO	0.0025	significant

The presence of CaO resulted in the greatest increase in pyrolytic water yield followed by MgO and Al_2O_3 respectively. Therefore, the dehydration ability of the catalysts is in the order CaO > MgO > Al_2O_3.

As seen in ***Figure 4-7***, the organic yield decreases when catalysts are used. This is because of the deoxygenation process, wherein oxygen is removed from the organics in the form of CO_2, CO and H_2O leading to a mass reduction of the affected compounds. An ANOVA test showed that the decreases in the organics yields were statistically significant (***Table 4-16***).

Table 4-16: ANOVA for the organics yield from catalyst screening

	p-value	Conclusion
Non-Cat/Al_2O_3	0.0044	significant
Non-Cat/CaO	3.61E-06	significant
Non-Cat/MgO	0.0382	significant

Contrary to this study, some authors have reported a significant increase in total liquid yield (55.9 to 62.2 wt.%) with the use of catalyst (Lin et al. 2010), while others reported a significant decrease in the total liquid yield (58.8 to 44.2 wt.%) when similar catalysts were used (Stefanidis et al. 2011). The findings of this study are more consistent with Veses et al. (2014) and Chen et al. (2017) who did not see a significant change in the liquid yield between catalytic and non-catalytic pyrolysis. The total liquid yields reported by these researchers for both catalytic and non-catalytic pyrolysis ranged from 48 – 50 wt.%. The increase in total liquid yield observed by Lin et al. (2010) using CaO catalyst was a result of the increase in pyrolytic water yield from 16.5 to 28.1 wt.%, which was much higher than the decrease in organics yield from 39.1 to 34.1 wt.%. In comparison, the pyrolytic water yield increase observed by Chen et al. (2017) in intermediate pyrolysis was much smaller (28 to 32 wt.%) and comparable to the increase in this study (14.9 to 18.0 wt.%). This difference in pyrolytic water increases can be attributed to the differences in the pyrolysis processes taking place. It is possible that at the very short volatile residence times in fast pyrolysis used by Lin et al. (2010), the time for secondary reactions such as WGSR is limited. As a result, the conversion of water was less than in intermediate pyrolysis where the volatile residence times are much longer.

Stefanidis et al. (2011) observed a significant, decrease in organics yield from 37.37 wt.% to 15.02 and 16.62 wt.% for MgO and Al_2O_3 respectively which led to a significant decrease in the total liquid yield, even though the pyrolytic water yield had increased from 21.38 to 29.22 and 29.08 wt.% respectively. The significant decrease in the organics yield compared to the results from this study is likely to be a result of the greater contact between the catalyst and volatiles in the experimental setup used by Stefanidis et al. (2011).

In this setup, the volatiles passed through a catalyst bed, leading to greater volatile cracking and catalytic effect, resulting in low organics yields, high pyrolytic water yields and enhanced gas yields.

Potential mechanisms explaining water formation

The increase in pyrolytic water when MgO and CaO are used can be partly attributed to the water producing ketonisation reactions which are promoted by these catalysts (Deng, Fu, and Guo2009; Stefanidis et al. 2011; Li et al. 2012). MgO is also reported to catalyse different condensation reactions which are likely to result in an increase in the pyrolytic water yield (AlGhamdi, Hargreaves, and Jackson 2009). These reactions include self-condensation of propanol (Ndou and Coville 2004), aldol condensation of ketones and aldehydes (Díez, Apesteguía, and Di Cosimo 2006) and self-condensation of ketones (Di Cosimo and Apesteguía 1998). Since CaO and MgO are in the same group on the periodic table and are expected to have a similar reactivity, it is possible that CaO is promoting similar condensation reactions. The general equation of a condensation reaction is shown below.

$$2R_1COCH_3 \rightarrow (R_1)_2C = CH(CO)CH_3 + H_2O$$

As seen in the reaction above, condensation reactions involve alkyl (R_1) chain molecular compounds being combined to give longer chain compounds. During catalytic pyrolysis, it is expected that as deoxygenation of organic compounds occurs, a decrease in the molecular weights of the affected compounds and of the organic phase yield would be observed. However, it is possible that some small molecule ketones and aldehydes which would have otherwise gone into the aqueous phase in the non-catalytic experiments are converted to larger and heavier molecules (via condensation reactions) which are then more likely to be collected as part of the organic phase.

Another possible dehydration mechanism, is detailed for the example of the deoxygenation of guaiacol, (a major product of lignin pyrolysis) which was reported to be promoted by CaO (Lin et al. 2010). These researchers found that the yield of guaiacol decreased while that of phenol increased as the catalyst concentration was increased.

From the literature (Xiao and Varma 2015), it has been suggested that guaiacol could be reduced to phenol under pyrolysis conditions in the presence of H_2, producing water in the process. The reaction schemes are shown by ***Figure 4-8***.

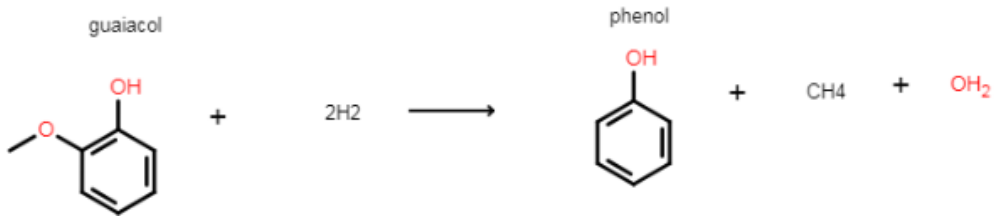

Figure 4-8: Possible mechanism for the reduction of guaiacol to phenol (Xiao and Varma 2015)

The same researchers, Lin et al. (2010), also observed a decrease in levoglucosan as the CaO concentration increased. Levoglucosan is the main product of cellulose pyrolysis (F.-X. Collard and Blin 2014) and has a high oxygen content of 49.38 wt.%. It was proposed by Mihalcik, Mullen, and Boateng (2011) that levoglucosan could be dehydrated to furanic compounds which have lower oxygen contents such as furfural (33.3 3 wt.% oxygen) and furfuryl alcohol (32.65 wt.% oxygen). The research by Lin et al. (2010) supports this, as the amount of furans was seen to increase when the amount of CaO used in the reaction was increased. Therefore, part of the increase in pyrolytic water when CaO is used could have been produced via this mechanism.

4.2.4.4 Higher Heating Value

The increase in CO_2, CO and H_2O yield using the different catalyst as discussed in the preceding sections, have alluded that deoxygenation was occurring during catalytic pyrolysis. Deoxygenation should result in increased bio-oil HHV, which is the goal of this study; the greater the deoxygenation, the higher the HHV. The HHV of the organic phases from the catalytic screening are given in ***Figure 4-9***. The HHV is reported on a water-free (dry) basis to make comparison with literature easier since the water content of the bio-oils differ from process to process. A general increase in the bio-oil HHV with the use of catalysts was observed.

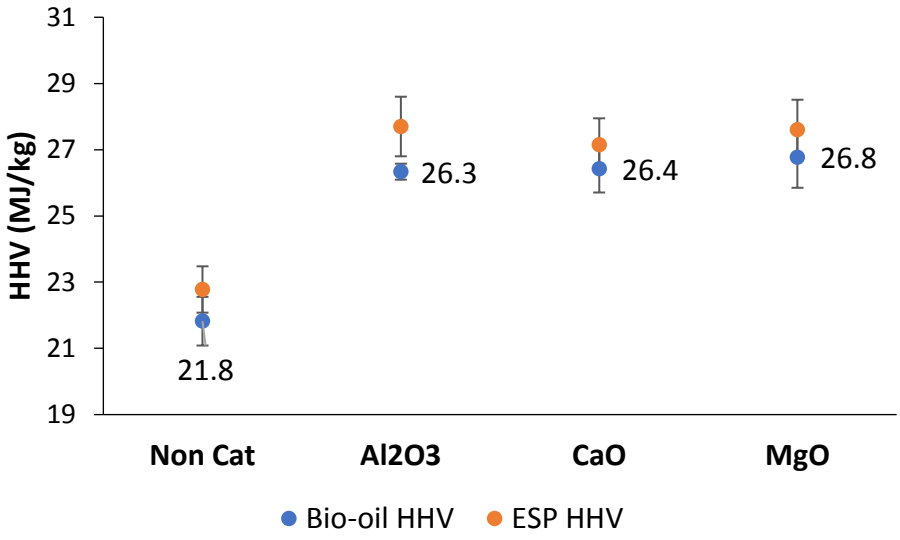

Figure 4-9: HHV of bio-oil products collected in the first condenser and in the electrostatic precipitator (ESP) from catalyst screening

As seen in ***Figure 4-9***, the HHV of the bio-oil obtained in Condenser 1 (Bio-oil HHV) was comparable to the HHV of the bio-oil obtained in the ESP. The ESP HHV lies within the range of bio-oil HHV ± bio-oil HHV standard deviation, except for when Al_2O_3 was used. This justifies considering the Condenser 1 and ESP products as one organic phase. The bio-oil HHV increased from 21.8 MJ/kg for non-catalytic bio-oil to 26.3, 26.4 and 26.8 MJ/kg for Al_2O_3, CaO and MgO catalysed pyrolysis respectively. An ANOVA test was done on the bio-oil HHV and the results are shown in ***Table 4-17***.

Table 4-17: ANOVA for bio-oil HHV from catalyst pyrolysis

	p-value	**Conclusion**
Non-Cat/Al_2O_3	0.0144	significant
Non-Cat/CaO	0.0240	significant
Non-Cat/MgO	0.0272	significant
Al_2O_3/CaO/MgO	0.8117	insignificant

Table 4-17 shows that all the catalysts significantly increased the HHV of the bio-oil. However, there is no significant difference between the HHVs of the catalytic bio-oils. This showed that under the tested conditions, CaO, MgO and Al_2O_3 had similar effects in terms of HHV improvement despite different deoxygenation mechanisms. The HHV of the non-catalytic bio-oil was comparable to the 22.7 MJ/kg (dry basis) heating value reported for fast pyrolysis bio-oil (Bridgwater 2003). It is also comparable with the other HHVs from the reviewed literature for non-catalytic bio-oils (**Table 2-11**). This shows that the cheaper and easier to implement intermediate pyrolysis technologies can produce bio-oil with a quality similar to fast pyrolysis derived bio-oil albeit at lower organic phase yields.

Lin et al. (2010) and Veses et al. (2014) reported calorific values higher than those obtained in this study for catalytic pyrolysis of woody biomass using CaO. They obtained 29.9 and 30.2 MJ/kg respectively using fluidised bed and auger reactors respectively. The differences can be attributed to better mixing and contact between the biomass and catalyst in a fluidised bed and auger reactors than in a batch reactor. The better mixing resulted in a greater catalytic effect and hence a higher bio-oil HHV. HHVs of up to 31.2 MJ/kg were also obtained by Stefanidis et al. (2011). This difference between the results is most likely because of the experimental setup used by these researchers as discussed in Section 4.2.3.2, which resulted in a greater catalytic effect and hence higher bio-oil HHV.

4.2.5 Conclusions

Compared to the other catalysts considered in this study, CaO was observed to promote dehydration over decarboxylation and decarbonylation reactions. It was also observed to catalyse volatile cracking reactions which resulted in a gas with highest calorific value (also due to CO_2 absorption by CaO) but the lowest yield of the organic phase (18.5 wt.%) and total organics (20.7 wt.%). Dehydration reactions can be seen as undesirable because they result in bio-oils with a higher water content. However, in the case where there is greater contact between volatiles and catalyst like in auger-type or rotary kiln reactors, a significant portion of the H_2O maybe converted to H_2 via the WGSR. Decarboxylation appeared to be the dominant deoxygenation mechanism during MgO catalysed pyrolysis, although significant dehydration occurred as well.

Al_2O_3 was seen to promote mostly decarbonylation reactions, but it catalysed decarboxylation reactions as well. Decarboxylation is preferred over decarbonylation because less atoms of carbon are lost per atom of O removed.

The 3 catalysts showed similar effects in HHV improvement despite promoting different deoxygenation mechanisms. The organic phase yields for all the catalysts were comparable to the non-catalytic organic phase yield at the screening conditions. This showed that significant deoxygenation could occur with minimal impact on the organic phase yield.

The selection of best performing catalyst was not obvious since all catalysts resulted in a similar bio-oil improvement. Two catalysts were selected for further optimisation. Al_2O_3 was not selected because char containing aluminium is not recommended for soil amendment applications since it can potentially increase the soil toxicity. Both MgO and CaO can be useful for soil amendment. However, char containing CaO is most suitable for soil amendment applications because of its similarities to agricultural lime. Additionally, CaO produces a gas with a higher calorific value which can be used to power up the pyrolysis plant.

The fractionation condensation system used in this study, was found to be effective in separating the bio-oil into an organic and aqueous phase. The organic fraction had a lower water content (< 12.6 wt.%) compared to typical bio-oil water contents (15 – 30 wt.%).

The MgO optimisation results are discussed in Chapter 5 and those for CaO in Chapter 6.

5 MgO Optimisation Results

Chapter 5 describes the results of the optimisation experiments for MgO catalyst. The statistical optimisation was based on a circumscribed central composite design (CCD) of 2 factors; temperature and catalyst concentration, C_{cat}. The goal was to maximise the bio-oil quality in terms of oxygen content while achieving a sufficient bio-oil yield (> 15 wt.%). The studied temperature range was 444 – 656 °C, while that for C_{cat} was 1.7 – 58.3 wt.%. In all the optimisation experiments, the heating rate was kept constant at around 300 °C/min and the carrier gas flow rate at 5 SLPM similar to the conditions used for catalyst screening experiments.

The overall mass balance for the MgO optimisation experiments was 90 – 93 wt.% which was consistent with the mass balance closure from the catalyst screening experiments. The MgO optimisation experiments were found to be repeatable, with a standard deviation of less than 2 wt. % achieved for the yields of the main products (char, bio-oil, gas). The influence of the studied factors on the yields of the different products is discussed below. Regression models describing various response variables from the MgO optimisation experiments are given in Appendix B.

5.1 Char

5.1.1 Yield

The 3D surface plot of the char yield, Y_{CHAR} as a function of temperature and C_{cat} is shown in ***Figure 5-1***. Y_{CHAR} was reported on a catalyst free basis. From ***Figure 5-1*** it was seen that there was a general decrease in char yield with temperature while the effect of catalyst concentration on Y_{CHAR} was less pronounced. An ANOVA for the char yield was done and the results are shown in ***Table 5-1***. In the ANOVA table, “L” represents a linear effect and “Q” a quadratic effect. A linear effect means that there is a directly proportional relationship between the response and dependent variables while a quadratic effect means that the response variable varies parabolically with the dependent variable.

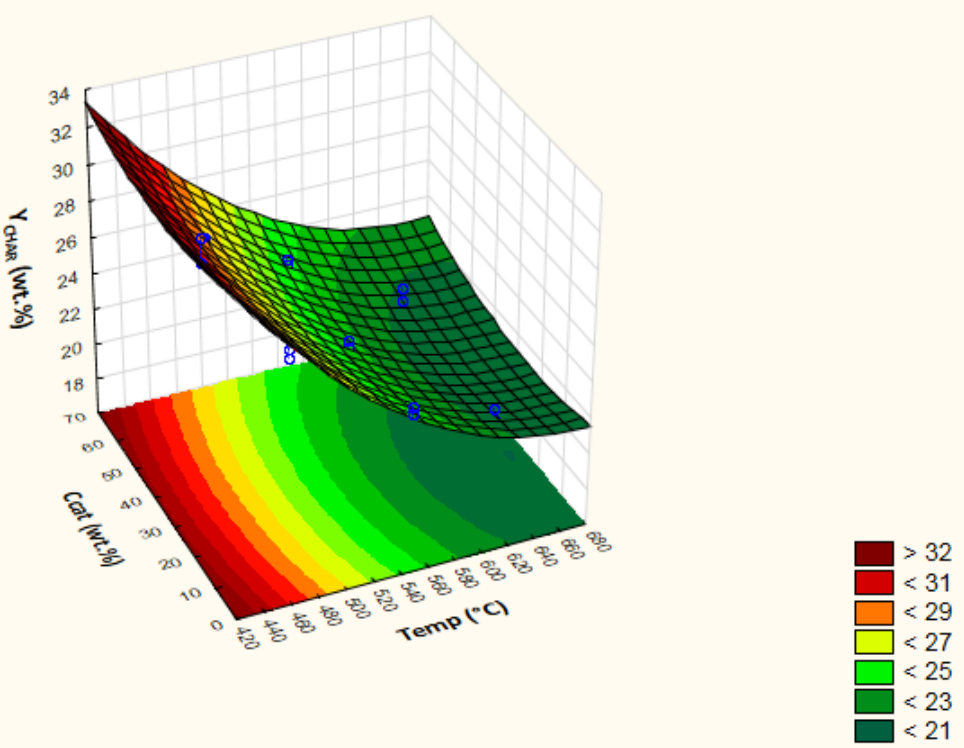

Figure 5-1: 3D surface plot of Y_{CHAR} from MgO optimisation

Table 5-1: ANOVA for Y_{CHAR} from MgO optimisation

	Factor	F value	p-value	Conclusion
	(1) Temperature (L)	542.4205	5.5165E-12	significant
R^2 = 0.97769	Temperature (Q)	25.7861	2.1176E-4	significant
adjusted R^2 = 0.9691	(2) C_{cat} (L)	0.0001	0.9913	insignificant
MS Residual = 0.310	C_{cat} (Q)	3.1123	0.1012	Insignificant
	1L by 2L	0.3118	0.5861	insignificant

The high R^2 value and the low MS residual value shows that the regression model fits the data well. ***Table 5-1*** shows that only temperature had a significant effect on Y_{CHAR} and that both linear and quadratic effects are significant. As observed from the screening test at 30 wt.%, the catalyst concentration had no significant effect on the char yield. For instance, at 550 °C, Y_{CHAR} was 23.4 wt.% with 30 wt.% MgO catalyst compared to 24.4 wt.% without catalyst (Section 4.2.2). Since there is no intimate contact between the biomass and catalyst when the two are physically mixed, the catalyst has minimal influence on the breakdown of the biomass matrix and therefore the char formation is not significantly affected (Stefanidis et al. 2011).

As the temperature increased from around 420 °C to about 520 °C there was a sharp decrease in Y_{CHAR} (linear effect). As temperature increased further, Y_{CHAR} decreased slowly and plateaued around 600 °C as the quadratic effect cancelled the linear effect at higher temperature. The observed trend was very similar to that observed by Neves et al. (2011) who compiled char yield data from the pyrolysis of various biomasses. Their model showed that above 600 °C, Y_{CHAR} became almost constant. According to literature, most of the primary reactions releasing volatiles are taking place at the lower temperatures (< 500 °C) (F.-X. Collard and Blin 2014). At higher temperatures, only char rearrangement reactions releasing permanent gases with relatively low molecular weight occur and the change of the char mass is limited.

5.2 Liquid

5.2.1 Total Yield

A 3D Surface plot of the total liquid yield, Y_{LIQUID} from the MgO optimisation is shown in ***Figure 5-2***.

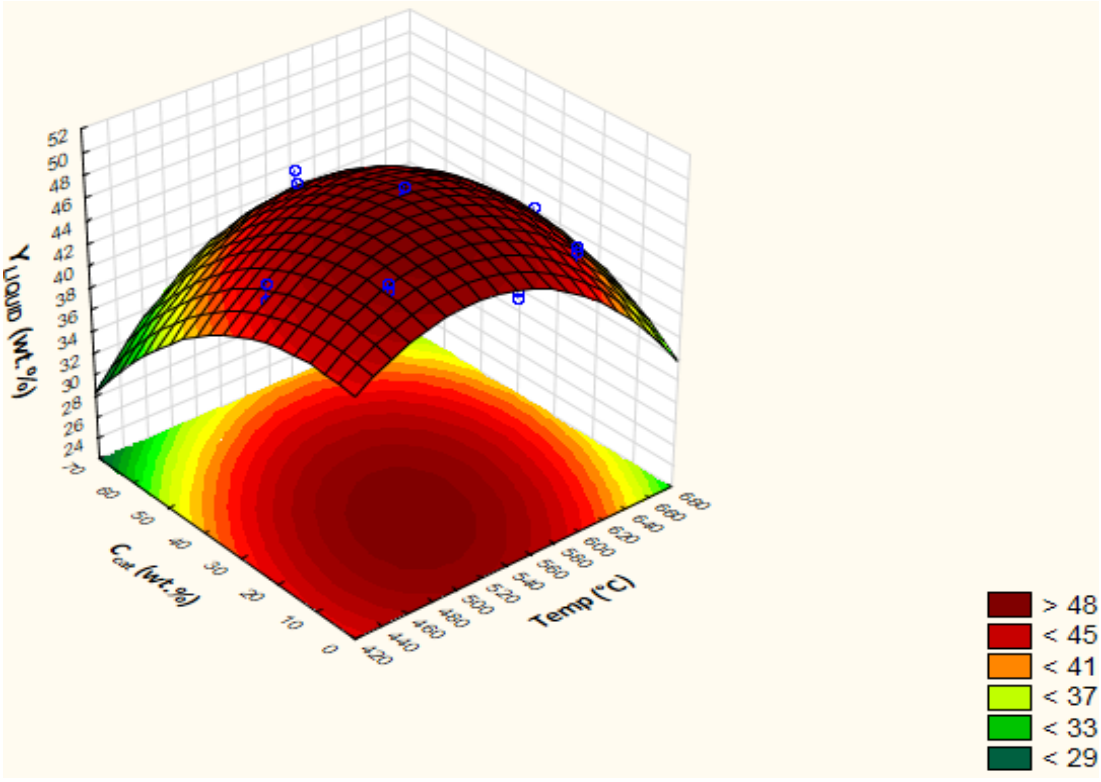

Figure 5-2: 3D surface of Y_{LIQUID} from MgO optimisation

A maximum total liquid yield of 48.9 wt.% at 530 °C and 21.3 wt.% catalyst concentration is obtained using the developed regression model for Y_{LIQUID}. This total liquid yield is consistent with the maximum liquid yield for intermediate pyrolysis (Bridgwater 2012). However, Y_{LIQUID} includes both the pyrolytic water and organics. Since the aqueous phase, containing mostly water is not desirable for co-processing in crude oil refineries, it is more relevant to consider the optimisation of the organic phase yield ($Y_{O\text{-}PHASE}$). The organic phase, containing mostly organic compounds, is the desirable bio-oil fraction and can be co-processed with VGO in crude oil refineries. $Y_{O\text{-}PHASE}$ variation with temperature and C_{cat} is discussed next.

5.2.2 Organic Phase

The 3D surface plot of $Y_{O\text{-}PHASE}$ is shown in ***Figure 5-3***. ***Table 5-2*** shows the ANOVA results for $Y_{O\text{-}PHASE}$.

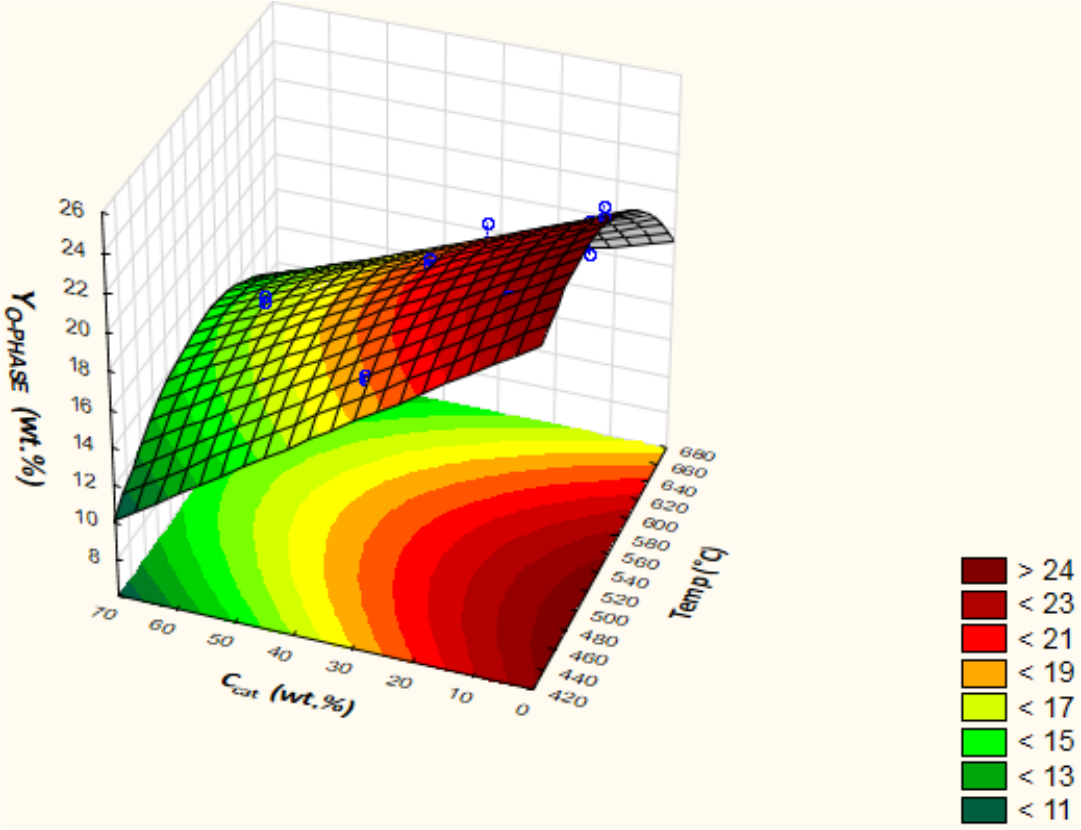

Figure 5-3: 3D surface plot of $Y_{O\text{-}PHASE}$ from CaO optimisation

Table 5-2: ANOVA for $Y_{O\text{-}PHASE}$ from MgO optimisation

	Factor	F value	p-value	Conclusion
	(1) Temperature (L)	23.0246	3.478E-4	significant
R^2 = 0.95361	Temperature (Q)	19.4391	7.059E-4	significant
adjusted R^2 = 0.9358	(2) C_{cat} (L)	212.9272	1.939E-9	significant
MS Residual = 0.597	C_{cat} (Q)	0.0052	0.9346	insignificant
	1L by 2L	5.1130	0.0415	significant

Table 5-2 shows that all the factors except the quadratic effect of C_{cat} were statistically significant. The linear effect of C_{cat} was the most significant factor when determining $Y_{O\text{-}PHASE}$. As seen in ***Figure 5-3***, as the catalyst concentration increased, $Y_{O\text{-}PHASE}$ decreased in the studied C_{cat} range. This was expected because from the catalytic screening, (Section 4.2.3) it was noted that MgO promoted some deoxygenation and cracking reactions which led to a decrease in $Y_{O\text{-}PHASE}$. Indeed, it is known that MgO catalyses the cracking of large oxygenated molecules into smaller ones (Pütün 2010; Zhang et al. 2014).

Figure 5-3 shows that the variation of $Y_{O\text{-}PHASE}$ with temperature was similar to that of Y_{LIQUID} with the presence of an optimum. As temperature increased up to 520 – 550 °C (depending on catalyst content), the organic phase yield increased. Above this temperature, $Y_{O\text{-}PHASE}$ began to decrease. The increase in $Y_{O\text{-}PHASE}$ was due to the increased release of volatiles from the biomass matrix as temperature increased (F.-X. Collard and Blin 2014). At higher temperatures, more extensive cracking of organic volatiles into smaller molecules, some of them being permanent gases, leads to a decrease in the liquid yield. Further evidence of the volatile cracking was the increases in the production of CO and C_xH_y gases with temperature as discussed in Section 5.3.

A discussion on the pyrolytic water yield, $Y_{P\text{-}WATER}$ follows in the section below. This aids in understanding the reactions/ mechanisms taking place during the catalytic pyrolysis.

5.2.3 Pyrolytic Water

Figure 5-4 shows the 3D surface plot of $Y_{P\text{-}WATER}$ while ***Figure 5-5*** shows the 2D surface plot. The results from the ANOVA analysis for $Y_{P\text{-}WATER}$ are shown in ***Table 5-3***.

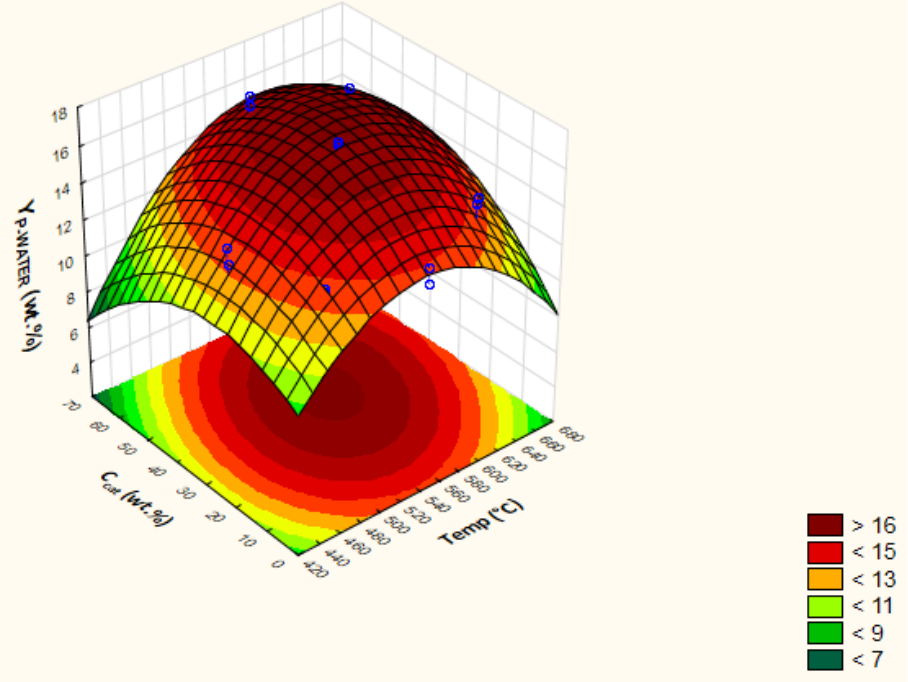

Figure 5-4: 3D surface plot of $Y_{P\text{-}WATER}$ for MgO optimisation

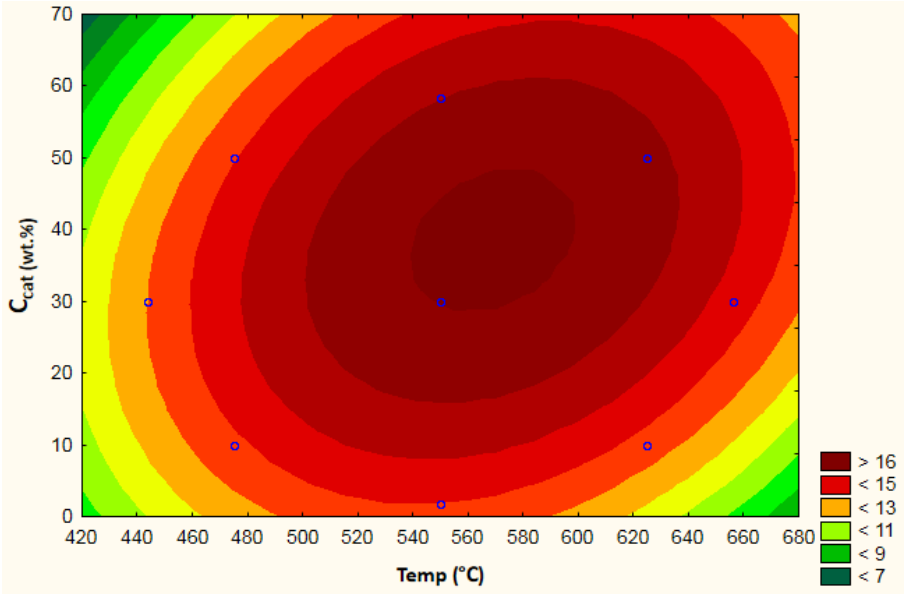

Figure 5-5: 2D surface plot of $Y_{P\text{-}WATER}$ for MgO optimisation

All the factors were found to be statistically significant except for 1L by 2L (***Table 5-3***). However, removing this factor resulted in an inaccurate model as seen by a decrease in the adjusted R^2 value hence it was included in the regression model to describe $Y_{P\text{-}WATER}$. An R^2 of 0.6838 and MS residual of 0.828 show that the model can be used to fit the data.

Table 5-3: ANOVA for $Y_{P\text{-}WATER}$ from MgO optimisation

	Factor	F value	p-value	Conclusion
	(1) Temperature (L)	5.745	0.0323	significant
R^2 = 0.7716	Temperature (Q)	24.122	2.843E-4	significant
adjusted R^2 = 0.6838	(2) C_{cat} (L)	9.704	8.205E-3	significant
MS Residual = 0.828	C_{cat} (Q)	9.678	8.271E-3	significant
	1L by 2L	3.926	0.0691	insignificant

As temperature increased, $Y_{P\text{-}WATER}$ increased up to a maximum of approximately 16 wt.% and then decreased at higher temperatures (***Figure 5-4*** and ***Figure 5-5***). Similarly, as C_{cat} increased from 0 to around 35 wt.%, $Y_{P\text{-}WATER}$ increased and then decreased linearly at higher catalyst concentrations. The increase in $Y_{P\text{-}WATER}$ could be linked to the deoxygenation mechanism taking place. MgO is known to catalyse deoxygenation via ketonisation of carboxylic acids, releasing water and CO_2 (Section 4.2.3). At higher temperature and C_{cat}, it is likely that the ketonisation reactions were minimised.

5.2.4 Higher Heating Value

The Higher heating value (HHV) is the parameter of interest in this study as it was used to assess the extent of deoxygenation of the organic compounds that will be used for co-processing in crude oil refineries. The HHV of the organic phase was studied on a water free basis for comparison purposes since the water content of the organic phase changes with the different operating conditions used in the design of experiments. The organic phase water content varied between 6 and 25 wt.% in the optimisation experiments. ***Figure 5-6*** and ***Figure 5-7*** show the 3D and 2D surface plots of the organic phase HHV. The ANOVA results for the organic phase HHV are given in ***Table 5-4***. The ANOVA table above shows that the linear effect of temperature as well as the interactions between temperature and catalyst were statistically insignificant. The influence of C_{cat} on the organic phase HHV was expected because the role of the catalyst was to promote deoxygenation of the organic compounds which in turn resulted in an increase in the energy content of the organic phase. It is interesting to note that the variation of the organic phase HHV with both temperature and C_{cat} was consistent with that of $Y_{P\text{-}WATER}$ as seen in ***Figure 5-4*** and ***Figure 5-5***.

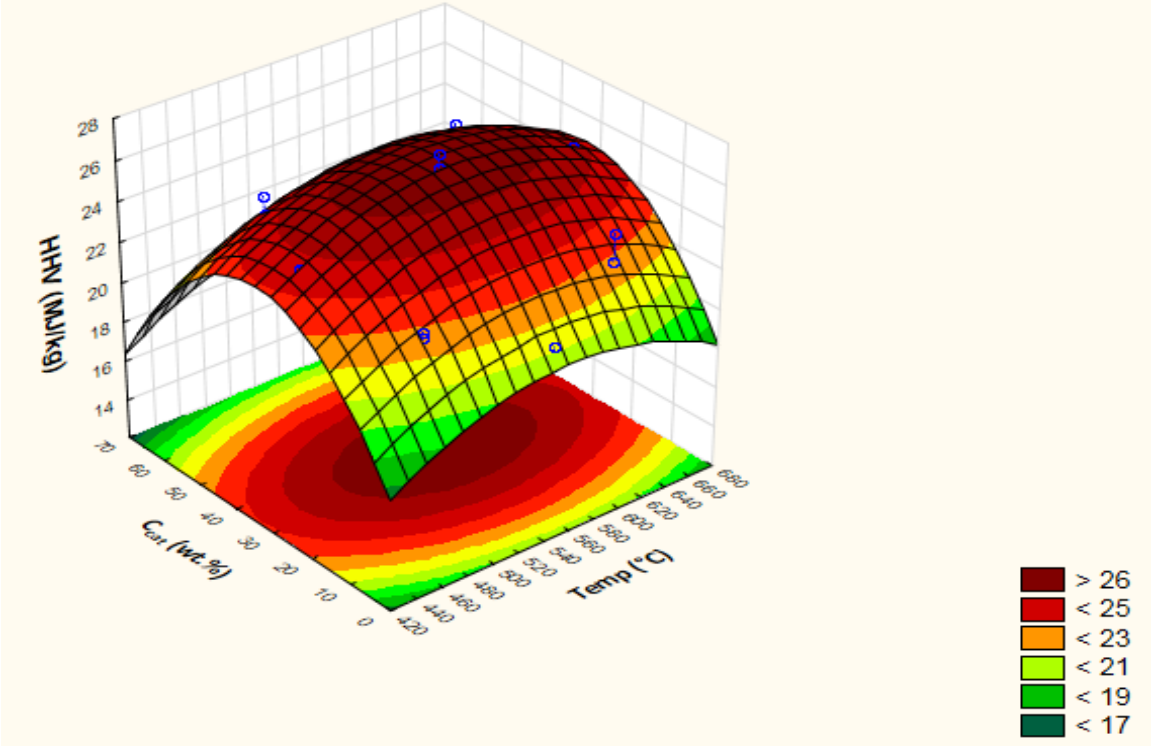

Figure 5-6: 3D surface plot of the organic phase HHV from MgO optimisation

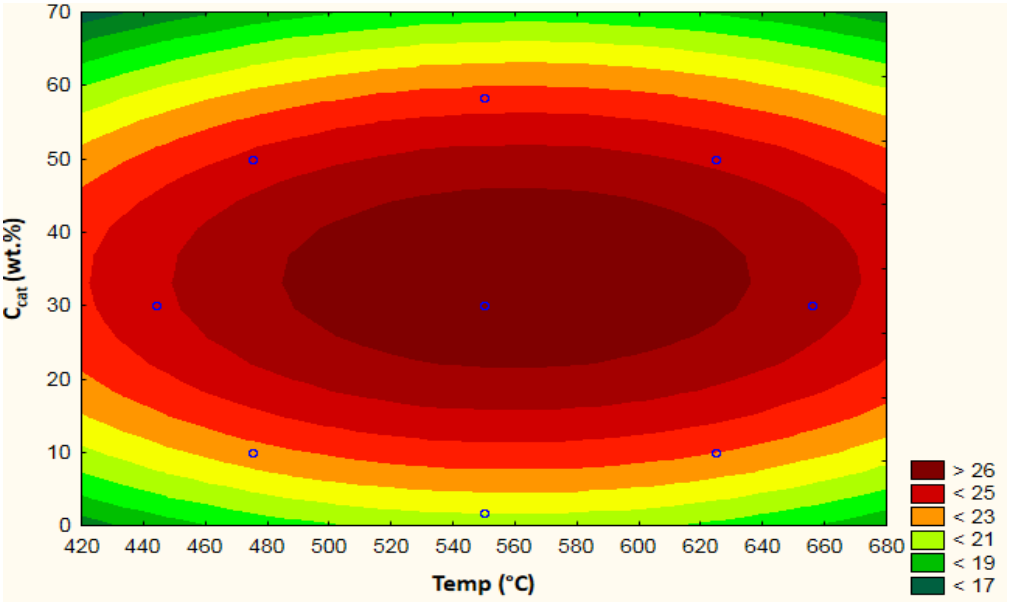

Figure 5-7: 2D surface plot of the organic phase HHV from MgO optimisation

Table 5-4: ANOVA for the organic phase HHV from MgO optimisation

	Factor	F value	p-value	Conclusion
	(1) Temperature (L)	2.4132	0.1443	insignificant
R^2 = 0.918	Temperature (Q)	15.1695	1.844E-3	significant
adjusted R^2 = 0.886	(2) C_{cat} (L)	31.9625	7.883E-5	significant
MS Residual = 0.361	C_{cat} (Q)	108.1313	1.147E-7	significant
	1L by 2L	0.0138	0.9082	insignificant

The model which relates the variation of the organic phase HHV ($HHV_{O\text{-}PHASE}$) with catalyst concentration and temperature is described below. It excludes the non-significant effect (1L by 2L) as seen in ***Table 5-4***. A high R^2 value of 0.918 and a low MS residual of 0.361 indicate that the model is sufficient to describe $HHV_{O\text{-}PHASE}$.

$$HHV_{O-PHASE} = -26.733 + 0.1684T - 0.0001502T^2 + 0.3807C_{cat} - 0.005638\,{C_{cat}}^2$$

Figure 5-8 displays the normal probability plot of the residuals of the organic phase HHV. The data points align well with the straight line which is characteristic of a good model.

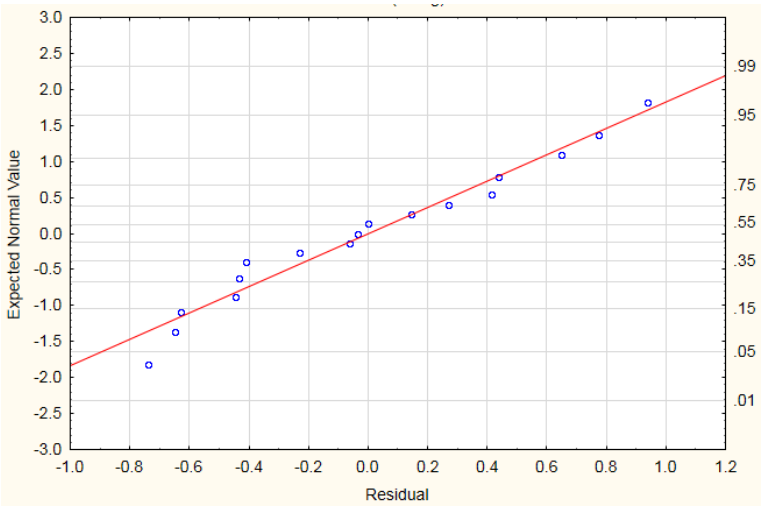

Figure 5-8: Normal probability plot of the organic phase HHV from MgO optimisation

The residual scatter plot for the organic phase HHV is shown in ***Figure 5-9***. The data appears homoscedastic which is another indicator that the model predicts the organic phase HHV well.

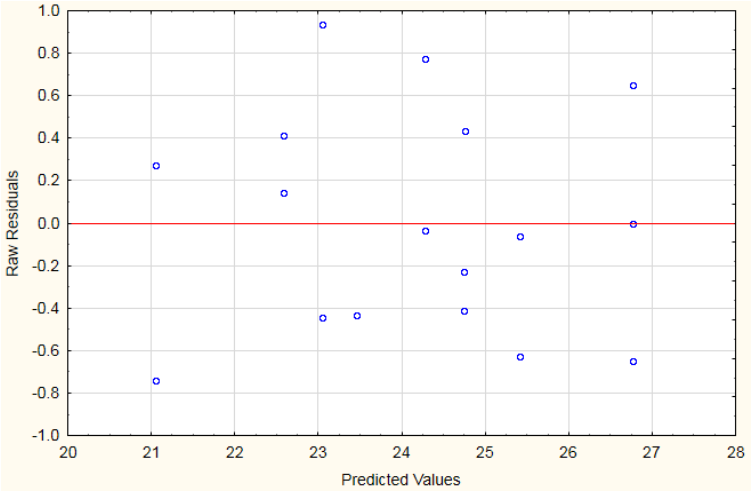

Figure 5-9: Residual scatter plot for the organic phase HHV from MgO optimisation

Figure 5-6 and ***Figure 5-7*** show that there was an increase in the organic phase HHV when C_{cat} increased from zero to around 35 wt.%. As the catalyst concentration increased to above 35 wt.%, the HHV was seen to decrease. There appeared to be an optimum catalyst concentration for the organic phase HHV similar to observations by Naqvi, Uemura, and Yusup (2014). These researchers studied the catalytic pyrolysis of paddy husk using zeolite catalyst in a fixed bed reactor. They found that a C/B ratio of 0.5 (corresponding to a C_{cat} of 33 wt.%) gave the highest deoxygenation of the bio-oil.

Temperature exhibited a similar effect to C_{cat} on the organic phase HHV. The organic phase HHV increased with temperature to a maximum of about 26 MJ/kg in the temperature range of 500 – 600 °C. Higher temperatures resulted in a decrease in the HHV. Similar observations are reported in literature (Naqvi, Uemura, and Yusup 2014; Sohaib et al. 2017). The effect of temperature in this study was less significant compared to the catalyst concentration effect as seen in ***Table 5-4***.

The following section gives a description of the gas yields from the MgO optimisation experiments. The major gas products determined by gas chromatography were CO_2, CO and CH_4 as well as minor amounts of hydrocarbon gases (C_2-C_4) and H_2.

5.3 Gas

5.3.1 CO_2

Figure 5-10 shows the 3D surface plot of the CO_2 yield, Y_{CO2} while ***Table 5-5*** gives the ANOVA results for Y_{CO2}.

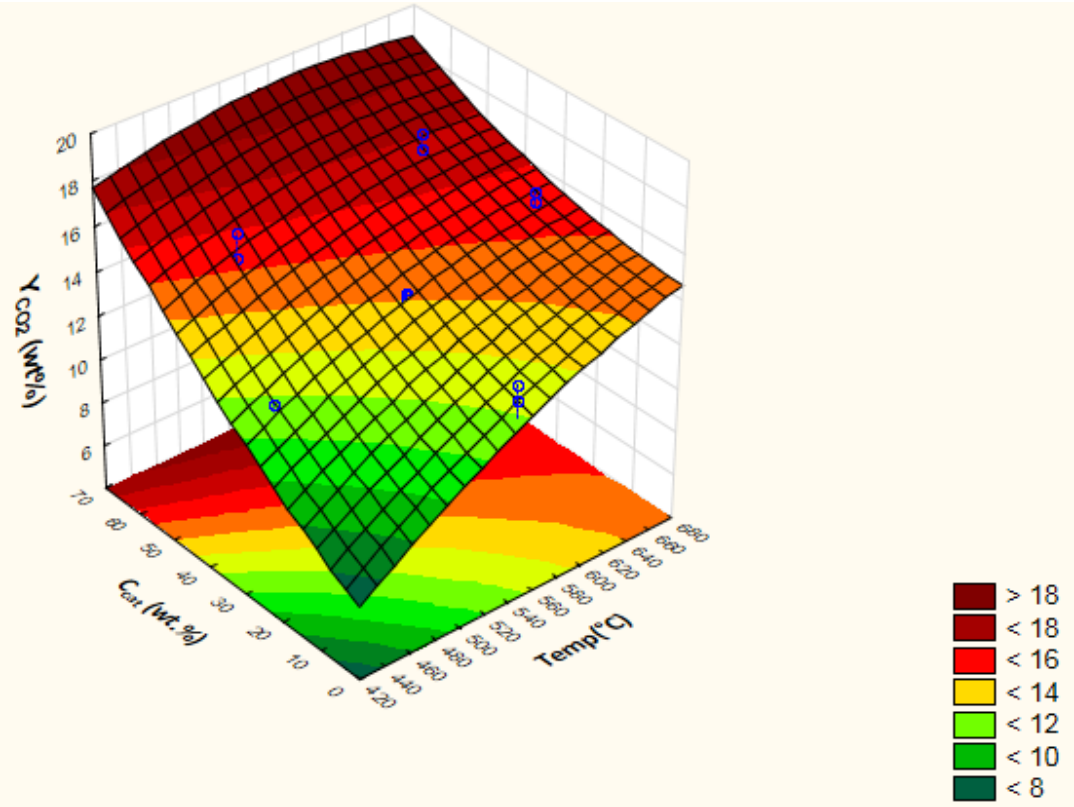

Figure 5-10: 3D surface plot of Y_{CO2} from MgO optimisation

Table 5-5: ANOVA for Y_{CO2} from MgO optimisation

	Factor	F value	p-value	Conclusion
	(1) Temperature (L)	36.7642	4.591E-5	significant
R^2 = 0.899	Temperature (Q)	0.8280	0.3794	insignificant
adjusted R^2 = 0.860	(2) C_{cat} (L)	73.8744	1.011E-6	significant
MS Residual = 0.794	C_{cat} (Q)	0.6595	0.4313	insignificant
	1L by 2L	2.8565	0.1148	insignificant

The ANOVA results showed that only the linear effects of temperature and catalyst concentration were statistically significant. It was seen that as either C_{cat} or temperature increased Y_{CO2} increased as well. The increase in Y_{CO2} with C_{cat} increase is evidence of deoxygenation via decarboxylation as was seen in the catalyst screening with MgO catalyst (Section 4.2.3.2). MgO is known to promote ketonisation reactions which produce CO_2 (Gliński, Kijeński, and Jakubowski 1995; Deng, Fu, and Guo 2009), while organic acids can also be cracked to produce CO_2 (Davidian et al. 2008; Li et al. 2012). From the data compiled by Neves et al. (2011) it was seen that in the temperature range from this study (444 to 660 °C) the was no significant change in Y_{CO2} with temperature increase. Interestingly in this study, Y_{CO2} doubled as temperature increased. This was probably due to the influence of the catalyst.

5.3.2 CO

Figure 5-11 shows the 3D surface plot for the CO yield, Y_{CO}. The figure shows that there is a general increase in Y_{CO} as temperature increases. At low temperatures, Y_{CO} increases with C_{cat} increases while at higher temperatures, Y_{CO} decreases as C_{cat} increases. ***Table 5-6*** shows the ANOVA results for Y_{CO}. According to the table above, temperature had the largest effect on Y_{CO}. CO is a major product of secondary volatile cracking, therefore an increase in temperature results in increased secondary reactions and a corresponding increase in Y_{CO} (Neves et al. 2011). The effect of C_{cat} on Y_{CO} was not statistically significant (probably overridden by the strong temperature effect) as evidenced in ***Table 5-6***, although increases in Y_{CO} were observed when C_{cat} increased. Limited CO increase was expected because MgO catalysts are known to promote decarboxylation reactions over decarbonylation ones (Stefanidis et al. 2011).

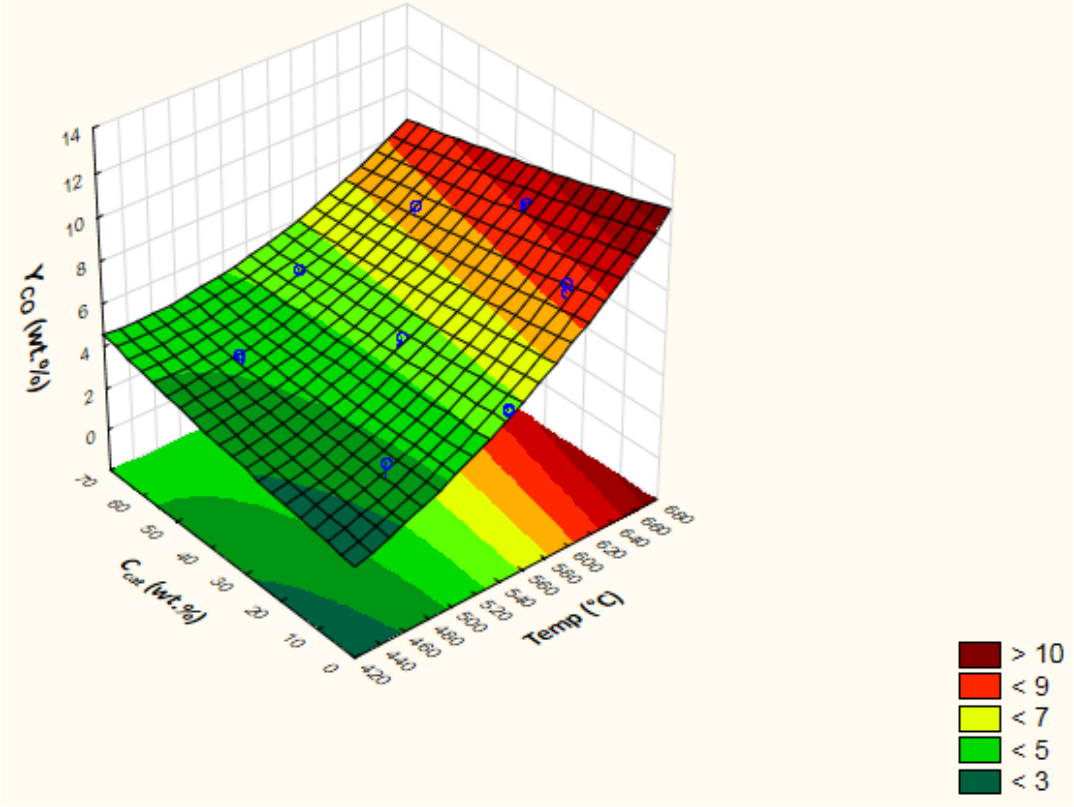

Figure 5-11: 3D surface plot of Y_{CO} from MgO optimisation

Table 5-6: ANOVA for Y_{CO} from MgO optimisation

	Factor	F value	p-value	Conclusion
	(1) Temperature (L)	352.890	8.361E-11	significant
R^2 = 0.9661	Temperature (Q)	6.376	0.0254	significant
adjusted R^2 = 0.9530	(2) C_{cat} (L)	1.344	0.267	insignificant
MS Residual = 0.188	C_{cat} (Q)	0.120	0.735	insignificant
	1L by 2L	8.313	0.0128	significant

5.3.3 CH_4

The 3D surface plot of the CH_4 yield, Y_{CH4} is illustrated in ***Figure 5-12***. The figure showed that at temperatures below 500 °C, Y_{CH4} was almost constant but increased exponentially at higher temperatures. The effect of C_{cat} appeared limited. An ANOVA test was also done for Y_{CH4} and the results are shown in ***Table 5-7***.

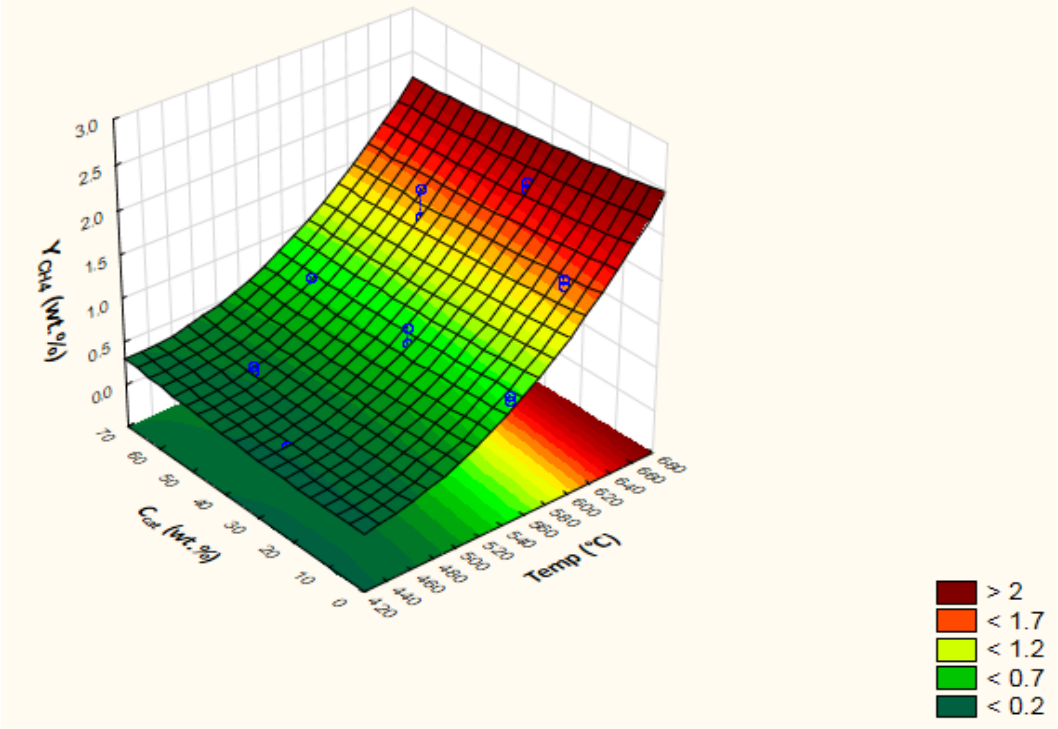

Figure 5-12: 3D surface plot of Y_{CH4} from MgO optimisation

Table 5-7: ANOVA for Y_{CH4} from MgO optimisation

	Factor	F value	p-value	Conclusion
	(1) Temperature (L)	364.4666	6.825E-11	significant
R^2 = 0.967	Temperature (Q)	12.9599	3.232E-3	significant
adjusted R^2 = 0.954	(2) C_{cat} (L)	0.8169	0.3825	insignificant
MS Residual = 0.0164	C_{cat} (Q)	0.1267	0.7276	insignificant
	1L by 2L	0.5146	0.4858	insignificant

Only temperature was statistically significant as seen in the table above. The variance of Y_{CH4} with temperature was very similar to the variation observed by Neves et al. (2011), with significant production only observed at temperatures > 500 °C. CH_4 is typically produced during char rearrangement and by secondary reactions (F.-X. Collard and Blin 2014). The catalyst concentration had a limited effect on Y_{CH4}, which is consistent with literature (Stefanidis et al. 2011).

5.3.4 C_2-C_4

The 3D surface plot of the C_2-C_4 hydrocarbon gases yield (Y_{C2-C4}) is shown in ***Figure 5-13***.

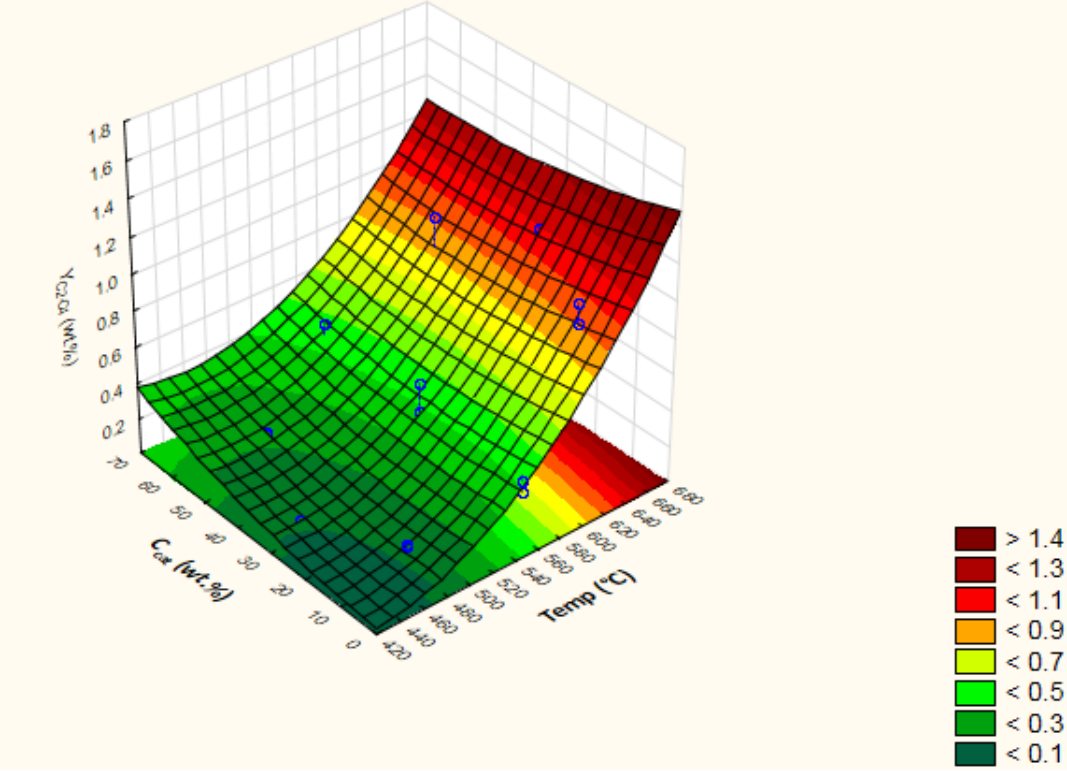

Figure 5-13: 3D surface profile of Y_{C2-C4} from MgO optimisation

Below 500 °C, Y_{C2-C4} did not change significantly and at temperatures above 500 °C, there was a linear increase in Y_{C2-C4} as temperature increased. It was reported that the mechanisms responsible for the formation of CH_4 and other hydrocarbon gases are similar (Neves et al. 2011). Therefore, as expected, the surface profile for Y_{C2-C4} looks almost identical to that for Y_{CH4} (Section 5.3.3). ANOVA analysis of Y_{C2-C4} (***Table 5-8***) showed that similar to Y_{CH4}, only temperature had a significant effect on Y_{C2-C4}.

Table 5-8: ANOVA for Y_{C2-C4} from MgO optimisation

	Factor	**F value**	**p-value**	**Conclusion**
	(1) Temperature (L)	194.6303	3.365E-9	significant
R^2 = 0.941	Temperature (Q)	9.0978	9.924E-3	significant
adjusted R^2 = 0.918	(2) C_{cat} (L)	0.1337	0.7205	insignificant
MS Residual = 0.0100	C_{cat} (Q)	0.3923	0.5419	insignificant
	1L by 2L	1.6196	0.2254	insignificant

5.3.5 H_2

The 3D surface profile of the hydrogen yield, Y_{H2} is shown in ***Figure 5-14***. This figure shows that under the studied conditions, Y_{H2} did not change significantly as it varied between 0.05 and 0.10 wt.%. Temperature appeared to have the main effect on Y_{H2}, and this was confirmed by the ANOVA results for Y_{H2} (***Table 5-10***). Below 500 °C, Y_{H2} was almost constant while for temperatures greater than 500 °C, H_2 production increased progressively

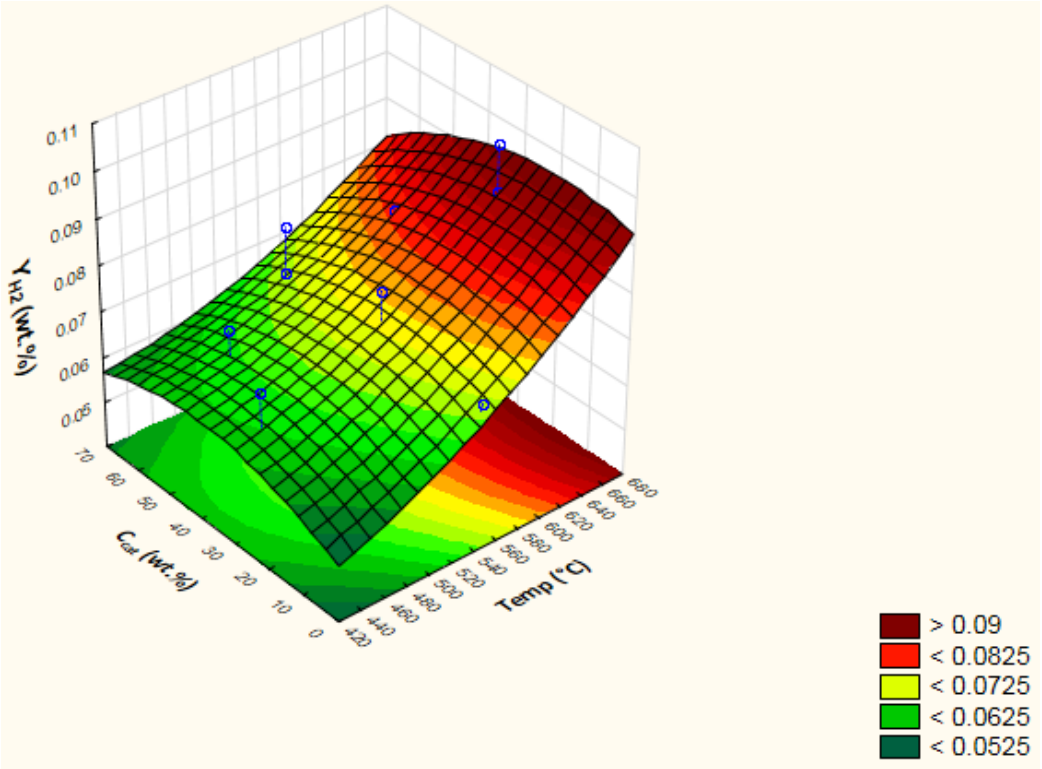

Figure 5-14: 3D surface profile of Y_{H2} from MgO optimisation

Table 5-9: ANOVA of Y_{H2} from MgO optimisation

	Factor	F value	p-value	Conclusion
	(1) Temperature (L)	26.2619	1.951E-4	significant
R^2 = 0.687	Temperature (Q)	0.2862	0.6017	insignificant
adjusted R^2 = 0.566	(2) C_{cat} (L)	0.01879	0.8931	insignificant
MS Residual = 5.71E-5	C_{cat} (Q)	0.7068	0.4157	insignificant
	1L by 2L	0.2190	0.2254	insignificant

When temperatures are low, primary reactions which do not produce H_2 are preponderant. At higher temperatures, H_2 is believed to be a product of char rearrangement and secondary cracking of organic volatiles (Neves et al. 2011). Similar to what was observed by Stefanidis et al. (2011), MgO as a catalyst does not promote H_2 production and therefore C_{cat} is an insignificant factor in the determination of Y_{H2} as shown in ***Table 5-9***.

5.4 Conclusions

The maximum organic phase HHV according to the regression model was 26.9 MJ/kg at 560 °C and 33.8 wt.% C_{cat}, while the corresponding $Y_{O\text{-}PHASE}$ at these conditions is 19.4 wt.%. These model-derived optimum conditions were very similar to the ones used for catalyst screening (550 °C and 30 wt.% C_{cat}), which resulted in a $Y_{O\text{-}PHASE}$ of 19.9 wt.% and an organic phase with an HHV of 26.8 MJ/kg. The regression models showed that the maximum HHV for the organic phase was achieved in the same range as that of the maximum organic phase yield; temperature range 530 – 560 °C and C_{cat} range 25 – 35 wt.%. Therefore, there was no need to develop a statistical desirability function to compromise between the organic phase HHV and $Y_{O\text{-}PHASE}$.

Ketonisation (producing H_2O and CO_2) is known to be catalysed by MgO. Based on the evolution of the organic phase HHV, pyrolytic water and CO_2 it appeared that ketonisation was the main mechanism by which deoxygenation took place. When temperature increases up to 530 – 560 °C and C_{cat} up to 25 – 35 wt.%, $Y_{P\text{-}WATER}$, Y_{CO2} yield and organic phase HHV increase in a similar way, showing that ketonisation could be one of the main catalysed mechanism. At higher temperatures and C_{cat}, while Y_{CO2} keeps increasing, both $Y_{P\text{-}WATER}$ and organic phase HHV were found to decrease. It means that other mechanisms, less efficient in terms of deoxygenation, were involved.

Values of the product yields at the optimum conditions were determined using the developed regression models and are shown in ***Table 5-10*** .

Table 5-10: Product yields at the optimum conditions for MgO catalytic pyrolysis (560 °C and 33.8 wt.% C_{cat})

Product	Y_{CHAR}	Y_{LIQUID}	$Y_{O\text{-}PHASE}$	Y_{CO2}	Y_{CO}	Y_{CH4}	$Y_{C2\text{-}C4}$	Y_{H2}
Yield (wt.%)	23.19	48.14	19.40	14.95	5.73	0.85	0.46	0.07

Based on the product yields above, the calculated gas calorific value is 5.95 MJ/kg which is comparable to the 6.16 MJ/kg obtained during the catalyst screening (temperature of 550 °C and C_{cat} of 30 wt.%). Not much energy can be obtained from the gas product because a huge proportion of it (52 vol.%) is CO_2, which does not contribute to the energy content of the gas.

6 CaO Optimisation Results

Chapter 6 describes the results of the optimisation experiments for CaO. Similar to the MgO optimisation, the statistical optimisation was based on a CCD of 2 factors; temperature and catalyst concentration, C_{cat}. The goal was to maximise the bio-oil quality (HHV) while achieving a sufficient bio-oil yield (> 15 wt.%). The effect of temperature was investigated in the range 444 – 656 °C, while that for C_{cat} in the range 1.7 – 58.3 wt.%. The heating rate was kept constant at around 300 °C/min and the carrier gas flow rate at 5 SLPM for all experiments.

The mass balance closure for the CaO optimisation experiments ranged from 90 – 92 wt.% which was consistent with the mass balances from the catalyst screening and the MgO optimisation. Similarly, the experiments were found to be repeatable with a standard deviation of less than 2 wt.% for all the yields. The variation of the different product yields: solid, liquid and gas from the CaO optimisation are discussed in Sections 6.1, 6.2 and 6.3 respectively. Regression models describing various response variables from the MgO optimisation experiments are given in Appendix C.

6.1 Char

6.1.1 Yield

The 3D surface plot of Y_{CHAR} from the CaO optimisation experiments is shown in ***Figure 6-1***. These char yields were generally higher than the ones obtained from the MgO optimisation experiments. The results of the ANOVA for Y_{CHAR} are tabulated in ***Table 6-1***. The ANOVA results shows that all the factors except the interaction parameter (1L by 2L) were statistically significant. An R^2 value > 0.98 shows that the model describes the variation of Y_{CHAR} well.

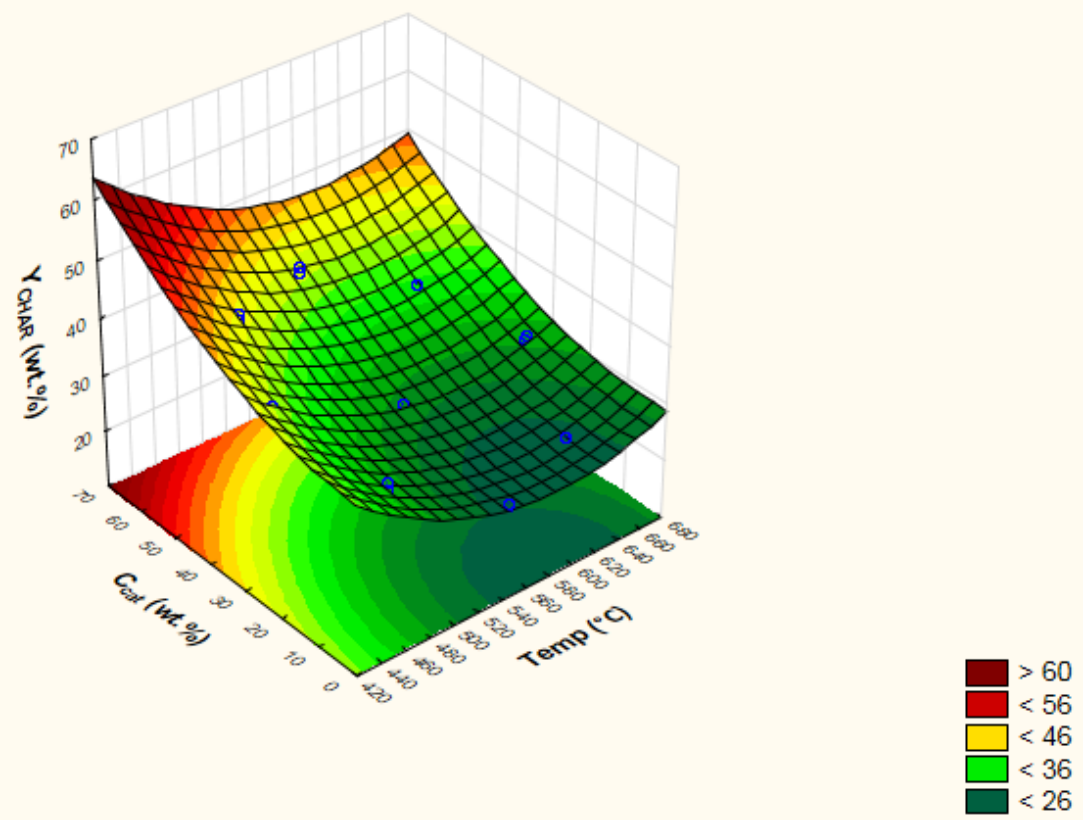

Figure 6-1: 3D surface profile of Y_{CHAR} from CaO optimisation

Table 6-1: ANOVA for Y_{CHAR} from CaO optimisation

	Factor	F value	p-value	Conclusion
	(1) Temperature (L)	255.8862	1.859E-9	significant
R^2 = 0.988	Temperature (Q)	67.6137	2.835E-6	significant
adjusted R^2 = 0.983	(2) C_{cat} (L)	660.9589	7.308E-12	significant
MS Residual = 0.749	C_{cat} (Q)	25.5171	2.838E-4	significant
	1L by 2L	1.2174	0.2915	insignificant

Figure 6-1 shows that there was an initial decrease in Y_{CHAR} as temperature increased to about 600 °C. At higher temperatures, Y_{CHAR} became almost constant. Below 600 °C, primary decomposition of the biomass occurs, leading to a decrease in Y_{CHAR} (Neves et al. 2011). At higher temperatures, the biomass matrix decomposition is almost complete and Y_{CHAR} does not vary much.

An increase in C_{cat} resulted in an increase in the char yield (***Figure 6-1***). It is well known that CaO as catalyst absorbs CO_2 during pyrolysis (Lin et al. 2010; Widyawati et al. 2011; Chen et al. 2017). CaO reacts with CO_2 forming $CaCO_3$ according to the equation below.

$$CaO + CO_2 \rightarrow CaCO_3 \qquad CO_2 \text{ absorption}$$

Presence of CO_2 as $CaCO_3$ in the char was shown in Section 4.2.2. As C_{cat} increased, there was more catalyst available to absorb CO_2, hence the increase in Y_{CHAR}. Therefore, the Y_{CHAR} from the CaO experiments was found to be higher than those from the MgO experiments.

6.2 Liquid

6.2.1 Total Yield

A plot of the variation of the total liquid yield, Y_{LIQUID} with temperature and C_{cat} for the CaO optimisation is presented in ***Figure 6-2***.

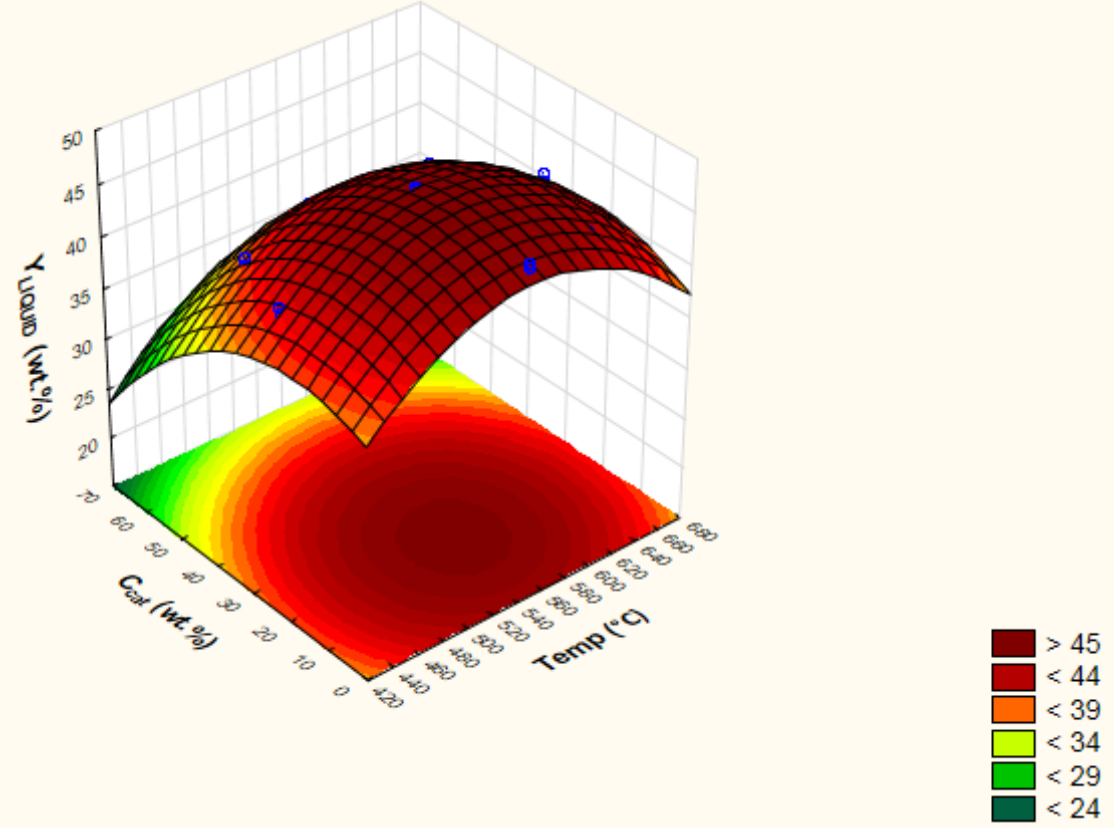

Figure 6-2: 3D surface profile of Y_{LIQUID} for CaO optimisation

Similar to the MgO optimisation, a maximum total liquid yield of 47.7 wt.% at 555 °C and 20.6 wt.% catalyst concentration is obtained using the developed regression model for Y_{LIQUID}. However, since the total liquid yield comprises of both the desirable organic phase and the undesirable aqueous phase, it will not be discussed in detail. Only the desirable organic phase, which suitable for co-processing with VGO in a crude oil refinery as it contains mostly organics will be discussed.

6.2.2 Organic Phase

The 3D surface plot of the organic phase yield, $Y_{O\text{-}PHASE}$ from the CaO optimisation is shown in ***Figure 6-3***. The ANOVA results for $Y_{O\text{-}PHASE}$ are shown in ***Table 6-2***. C_{cat} was seen to significantly affect $Y_{O\text{-}PHASE}$; there was a decrease in $Y_{O\text{-}PHASE}$ as C_{cat} increased. The quadratic effect of temperature describes the presence of a maximum $Y_{O\text{-}PHASE}$, which was reached between 500 and 550 °C. However, this effect was less pronounced compared to the effect of C_{cat}.

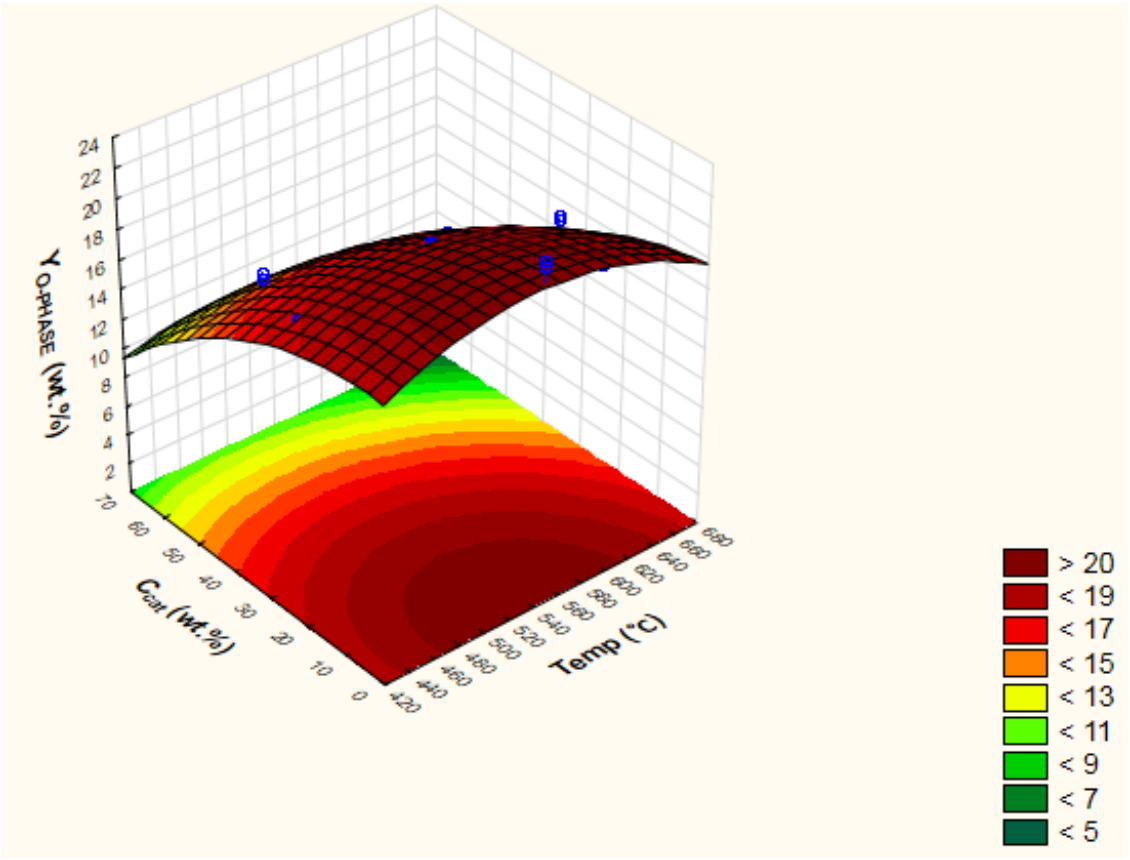

Figure 6-3: 3D surface profile of $Y_{O\text{-}PHASE}$ from CaO optimisation

Table 6-2: ANOVA for $Y_{O\text{-}PHASE}$ from CaO optimisation

	Factor	F value	p-value	Conclusion
	(1) Temperature (L)	7.8423	0.0160	significant
R^2 = 0.920	Temperature (Q)	6.0937	0.0296	significant
adjusted R^2 = 0.887	(2) C_{cat} (L)	122.9738	1.159E-7	significant
MS Residual = 0.933	C_{cat} (Q)	4.7447	0.005	significant
	1L by 2L	0.7337	0.4085	insignificant

With regards to $Y_{O\text{-}PHASE}$ variation with temperature, as temperature increased initially, volatiles were released from the solid biomass leading to an increase in Y_{LIQUID}. At higher temperatures, secondary cracking of the volatiles to produce permanent gas was enhanced, resulting in a decrease in Y_{LIQUID} (Neves et al. 2011). The cracking of volatiles was evidenced in this study by the increase in yields of the hydrocarbon gases and CO as will be discussed later in Section 6.3.

When the catalyst concentration is increased, some reactions are promoted, in particular the dehydration reactions known to be promoted by CaO (Lin et al. 2010; Chen et al. 2017). Therefore, produced water is transferred from the organic fraction to the aqueous fraction and hence $Y_{O\text{-}PHASE}$, decreases with increasing C_{cat}. This was evidenced by increase in $Y_{P\text{-}WATER}$ as C_{cat} increased (Section 6.2.3). It has also been reported that presence of large amounts of CaO catalysts results in severe cracking of organics into lower molecular weight compounds resulting in the reduction of the total organics and an increase in the incondensable gases (Widyawati et al. 2011; Li et al. 2012) as reported in Section 6.3.

The yield of pyrolytic water, $Y_{P\text{-}WATER}$ is discussed below to help explain the mechanisms occurring during the CaO catalysed pyrolysis of wood.

6.2.3 Pyrolytic Water

Figure 6-4 and ***Figure 6-5*** show the 3D and 2D surface profiles of $Y_{P\text{-}WATER}$ from the CaO optimisation. In general, $Y_{P\text{-}WATER}$ from the CaO optimisation was higher than that from the MgO optimisation because CaO is known to promote deoxygenation via dehydration reactions (Lin et al. 2010). A maximum $Y_{P\text{-}WATER}$ of 18 wt.% was seen for the MgO optimisation, while $Y_{P\text{-}WATER}$ as high as 28 wt.% was observed in the MgO optimisation.

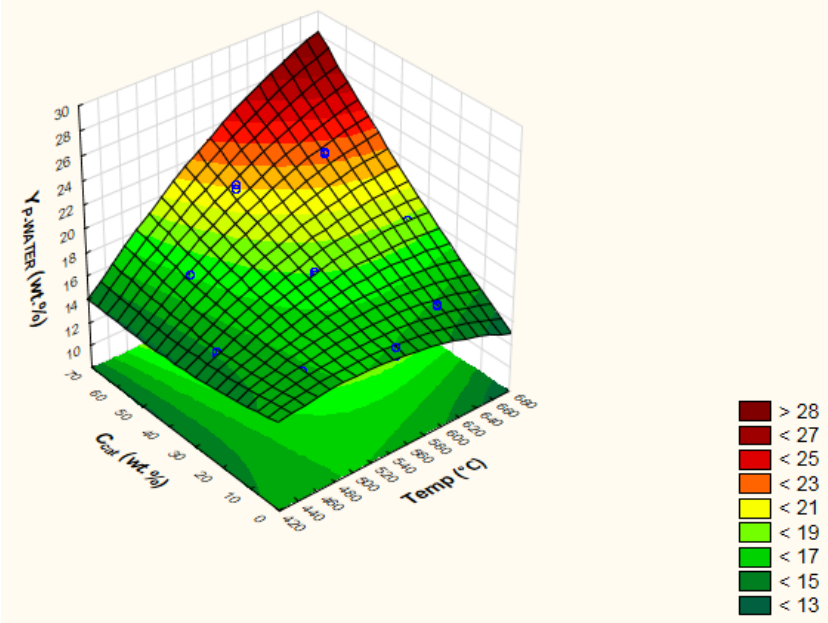

Figure 6-4: 3D surface profile of $Y_{P\text{-}WATER}$ from CaO optimisation

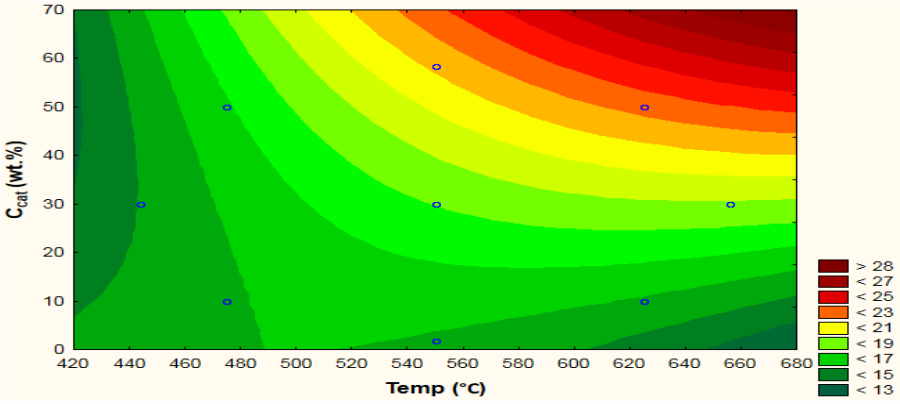

Figure 6-5: 2D surface plot of $Y_{P\text{-}WATER}$ from CaO optimisation

The 2 surface profiles above showed that for temperature higher than 450 °C, an increase in C_{cat} resulted in an increase in $Y_{P\text{-}WATER}$. At low C_{cat} (< 35 wt.%), temperature showed a minor effect on $Y_{P\text{-}WATER}$ while at higher catalyst concentrations, the effect of temperature became significant. The huge increase in $Y_{P\text{-}WATER}$ when both temperature and C_{cat} increased indicated a strong interaction between C_{cat} and temperature. This was confirmed by the ANOVA results for $Y_{P\text{-}WATER}$ at a 95 % confidence interval (***Table 6-3***) which showed a very small p-value for the interaction parameter (1L by 2L). As seen in the ANOVA table, R^2 is very high and MS residual is low indicating that the model is good enough to describe $Y_{P\text{-}WATER}$.

Table 6-3: ANOVA for $Y_{P\text{-}WATER}$ from CaO optimisation

	Factor	F value	p-value	Conclusion
	(1) Temperature (L)	329.8330	4.287E-10	significant
R^2 = 0.990	Temperature (Q)	18.1900	1.098E-3	significant
adjusted R^2 = 0.986	(2) C_{cat} (L)	618.2413	1.084E-11	significant
MS Residual = 0.0905	C_{cat} (Q)	3.9987	0.06870	insignificant
	1L by 2L	166.8517	2.120E-8	significant

As C_{cat} is increased, it is probable that more catalyst was available to react, which resulted in an increased rate of the dehydration reactions and therefore an increase in $Y_{P\text{-}WATER}$. This observation corroborates the findings of Lin et al. (2010) who also saw an increase in $Y_{P\text{-}WATER}$ as C_{cat} increased. In this study, this effect of C_{cat} was enhanced at higher temperatures (above 550 °C). This is possibly because at these higher temperatures, the activity of the CaO catalyst was enhanced and its propensity to promote dehydration reactions was enhanced. The above shows that elevated temperatures and high catalyst concentrations are favourable for dehydration reactions.

A discussion of the energy content of the organic phase from the CaO experiments follows in Section 6.2.3.

6.2.4 Higher Heating Value

The variation of the organic phase HHV (dry basis) with temperature and C_{cat} is shown by the surface profiles displayed by ***Figure 6-6*** and ***Figure 6-7***. It should be reiterated that the organic phase HHV is the most important measured response variable as it was used to assess the extent of the deoxygenation of the organic compounds, which was the main objective of this study.

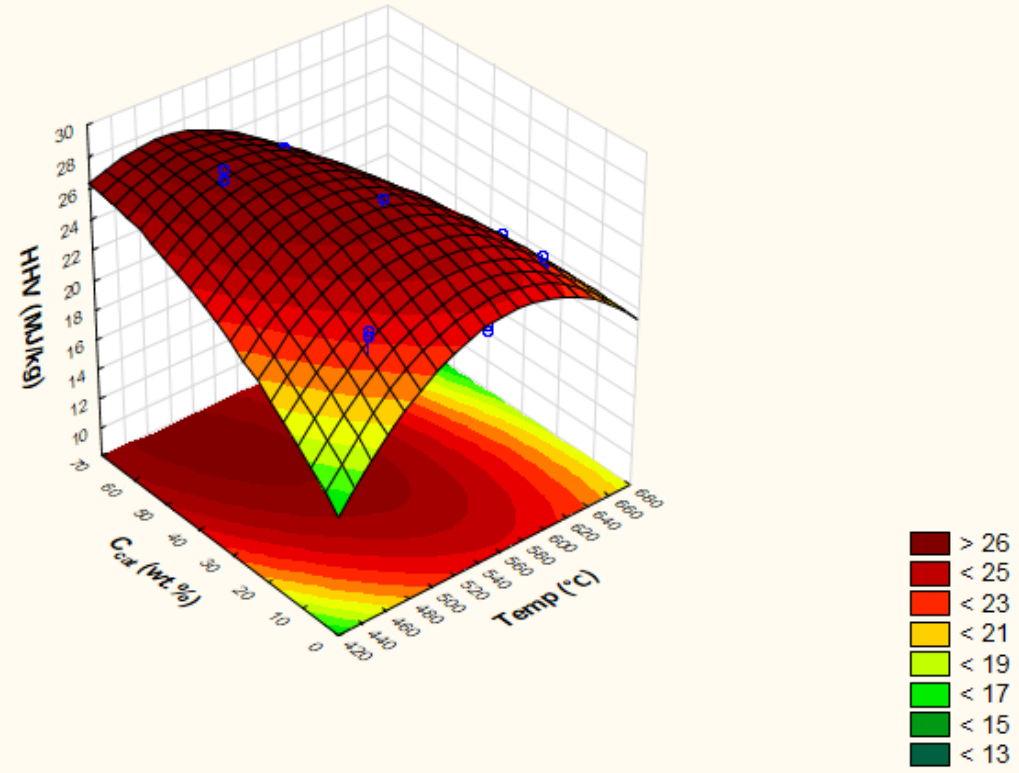

Figure 6-6: 3D surface plot of the organic phase HHV from CaO optimisation

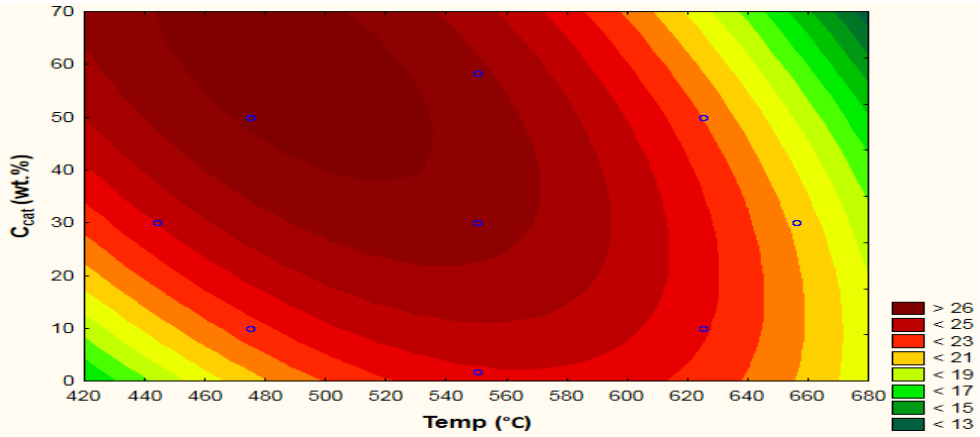

Figure 6-7: 2D surface plot of the organic phase HHV from CaO optimisation

From the surface plots above, it was seen that the variation of the organic phase HHV with C_{cat} is different to that from the MgO optimisation displayed by ***Figure 5-6***. In the MgO optimisation, there was an initial HHV increase with C_{cat} and then a decrease in HHV at higher C_{cat} for all temperatures. For the CaO optimisation, at lower temperatures (< 560 °C) there was a continuous increase in the HHV as C_{cat} increased. Above 560 °C, the HHV started decreasing at C_{cat} > 30 wt.%.

The temperature variation is however similar for both the CaO and MgO optimisations. There is an initial increase in the HHV until about 500 – 560 °C. At higher temperatures the HHV started decreasing. It was shown at a 95 % confidence, that all the effects except the quadratic effect of the catalyst concentration, C_{cat} (Q) were statistically significant (***Table 6-4***).

Table 6-4: ANOVA for the organic phase HHV from CaO optimisation

	Factor	F value	p-value	Conclusion
	(1) Temperature (L)	21.7538	5.470E-4	significant
R^2 = 0.865	Temperature (Q)	23.8639	3.753E-4	significant
adjusted R^2 = 0.809	(2) C_{cat} (L)	11.5436	5.293E-3	significant
MS Residual = 0.990	C_{cat} (Q)	2.7495	0.1232	insignificant
	1L by 2L	16.3480	1.630E-3	significant

The increase in the organic phase HHV with temperature up to 500 – 560 °C can be explained by the conversion of oxygenated groups into permanent gases such as carbon oxides, resulting in a liquid with increased carbon proportion as temperature increases. Demirbas (2007), reported that as temperature increased from 350 to 600 °C, deoxygenation of the oxygenated compounds was more and more intensive; while the proportions of stable aromatic compounds, such as alkylphenols increased. In this study, it was seen that as temperature increased above 560 °C, a large fraction of the permanent gases released is composed of CH_4, C_2-C_4 hydrocarbons and H_2 (see Section 6.3). The formation of some of these compounds could be due to cracking of the substituents of the aromatic rings and recombination reactions of the same aromatic rings, resulting in the formation of even more stable BTX and PAH respectively (Hervy et al. 2018). The loss of these compounds with high calorific value (CH_4, C_2-C_4 hydrocarbons and H_2) from the organic phase, results in an increased proportion of aromatic groups, which have a lower energy content than the alkyl groups. CH_4, C_2-C_4 hydrocarbons and H_2 all have calorific values > 49 MJ/kg while phenol and BTX have a calorific value < 43MJ/kg (Green and Perry 2007). This is probably because aromatic compounds have a much stronger C–C bond which requires more energy to break compared to the aliphatic C–C and C–H bonds (Kotz, Treichel, and Townsend 2010).

At low temperatures below 550 °C, as C_{cat} increased the organic phase HHV increased. This is probably because as the catalyst loading increased, more catalyst was available to promote deoxygenation reactions and hence the HHV increased. A similar observation was made by Lin et al. (2010) in the catalytic pyrolysis of pine using CaO at 520 °C. As the catalyst concentration was increased gradually from no catalyst to 83 wt.%, the bio-oil oxygen content decreased while the corresponding HHV calculated using Dulong's formula (Mason and Gandhi 1983) increased. However, it was seen in this study that conditions of temperatures above 560 °C and high C_{cat} (> 35 wt.%) resulted in a decrease in the organic phase HHV. It is possible that at higher temperatures, the activity of the catalyst to promote other reactions such as demethylation and dehydration was enhanced. Therefore, similar to the effect of high temperature on organic phase HHV discussed earlier, organics were lost as C_xH_y and H_2 gases, which resulted in a decrease in the organic phase HHV. This was evidenced by the increases in these gases at higher temperatures (> 560 °C) and C_{cat} greater than 35 wt.% as seen in Section 6.3.

Although C_{cat} (Q) was found in ***Table 6-4*** to be statistically insignificant, the p-value was small such that removing it from the model resulted in a decrease in the adjusted R^2 value. Hence C_{cat} (Q) was included in the regression model for the organic phase HHV, $HHV_{O\text{-}PHASE}$, which is given below.

$$HHV_{O-PHASE} = -91.8996 + 0.4071T - 0.0003583T^2 + 0.0009483T * C_{cat} + 0.6665C_{cat} - 0.00171{C_{cat}}^2$$

An R^2 value of 0.86 and an MS residual value <1 indicate that the model is sufficient to describe the organic phase HHV. The normal probability plot of the residuals illustrated in ***Figure 6-8***, shows that the residuals fit very well on the straight line. Therefore, the residuals were normally distributed proving that the model describes the variation of the organic phase HHV well. Similarly, the residual scatter plot (***Figure 6-9***) validates the model as it shows constant variation of the data across the studied range and no clear trends are noticeable from the data plot.

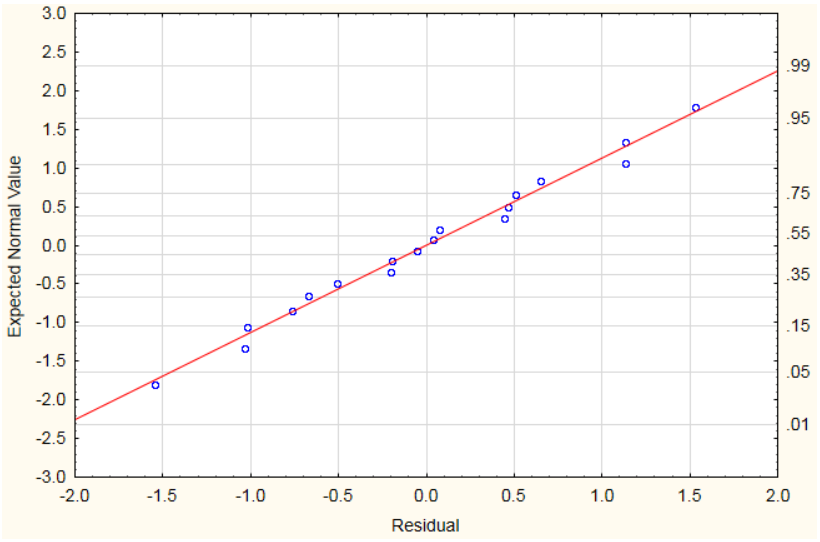

Figure 6-8: Normal probability plot of the organic phase HHV from CaO optimisation

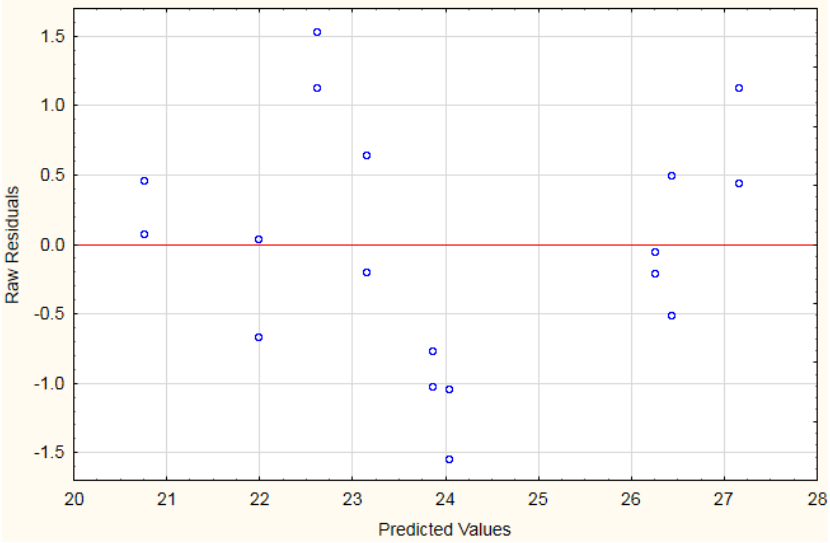

Figure 6-9: Residual scatter plot of the organic phase HHV from CaO optimisation

The optimum organic phase HHV based on this model was 27.5 MJ/kg at 490 °C and 59.0 wt.% C_{cat}. At these conditions the corresponding $Y_{O\text{-}PHASE}$ was 13.4 wt.%. This yield is too low to meet the target (15 wt.%) required for bio-oil blending at a 10 wt.% ratio (see Section 2.2.3.4). Therefore, a desirability function to find a compromise between a high HHV and a sufficient $Y_{O\text{-}PHASE}$ was developed in Section 6.4**.**

The gas products from the CaO optimisation are described next in Section 6.3.

6.3 Gas

6.3.1 CO_2

The 3D surface plot of the carbon dioxide yield, Y_{CO2} from the CaO optimisation is shown in ***Figure 6-10*** below. It was seen that as C_{cat} increased, Y_{CO2} decreased while temperature had a negligible effect on Y_{CO2}.

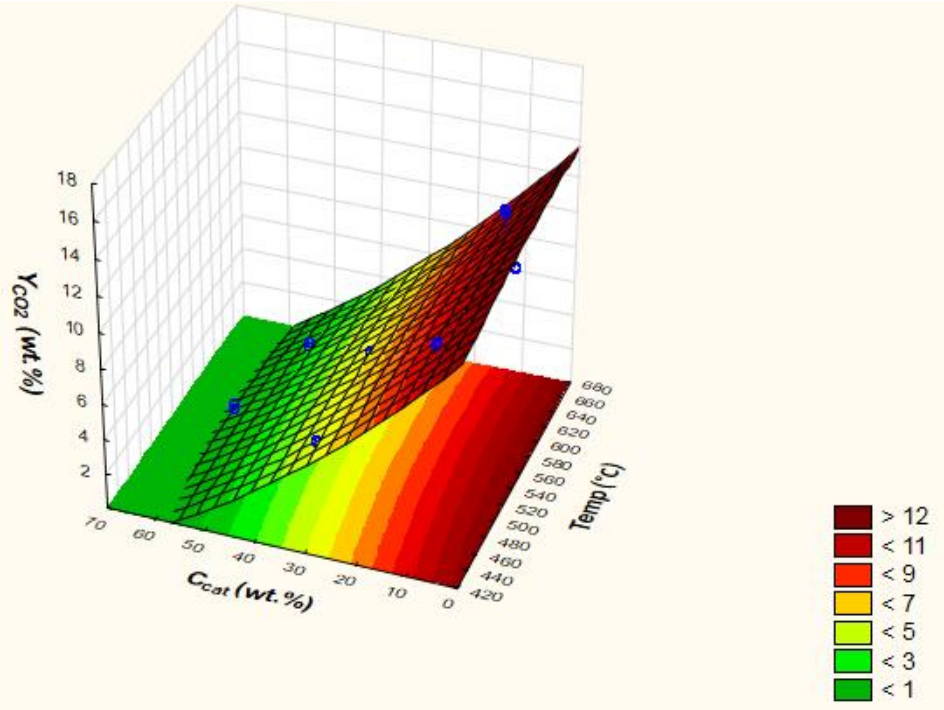

Figure 6-10: 3D surface plot of Y_{CO2} from CaO optimisation

An ANOVA analysis was done to test the statistical significance of the factors and the results are shown in ***Table 6-5*** below.

Table 6-5: ANOVA for Y_{CO2} from CaO optimisation

	Factor	F value	p-value	Conclusion
	(1) Temperature (L)	1.6310	0.2257	insignificant
R^2 = 0.984	Temperature (Q)	0.2348	0.6367	insignificant
adjusted R^2 = 0.977	(2) C_{cat} (L)	723.3286	4.291E-12	significant
MS Residual = 0.435	C_{cat} (Q)	2.6935	0.1267	insignificant
	1L by 2L	0.1531	0.7024	insignificant

As seen in ***Table 6-5***, only the linear effect of catalyst concentration, C_{cat} (L) was statistically significant. Y_{CO2} was observed to decrease as C_{cat} increased. This was most likely because as the amount of catalyst mixed with the initial biomass sample increased, the capacity of the char to absorb CO_2 increased, hence the decreases in Y_{CO2}. Similar observations were made by Lin et al. (2010) and Chen et al. (2017) who noticed a decrease in Y_{CO2} with increasing CaO concentration.

6.3.2 CO

The variation of the CO yield, Y_{CO} from the CaO optimisation is illustrated by ***Figure 6-11***. From the figure, Y_{CO} was seen to increase as both temperature and C_{cat} increased.

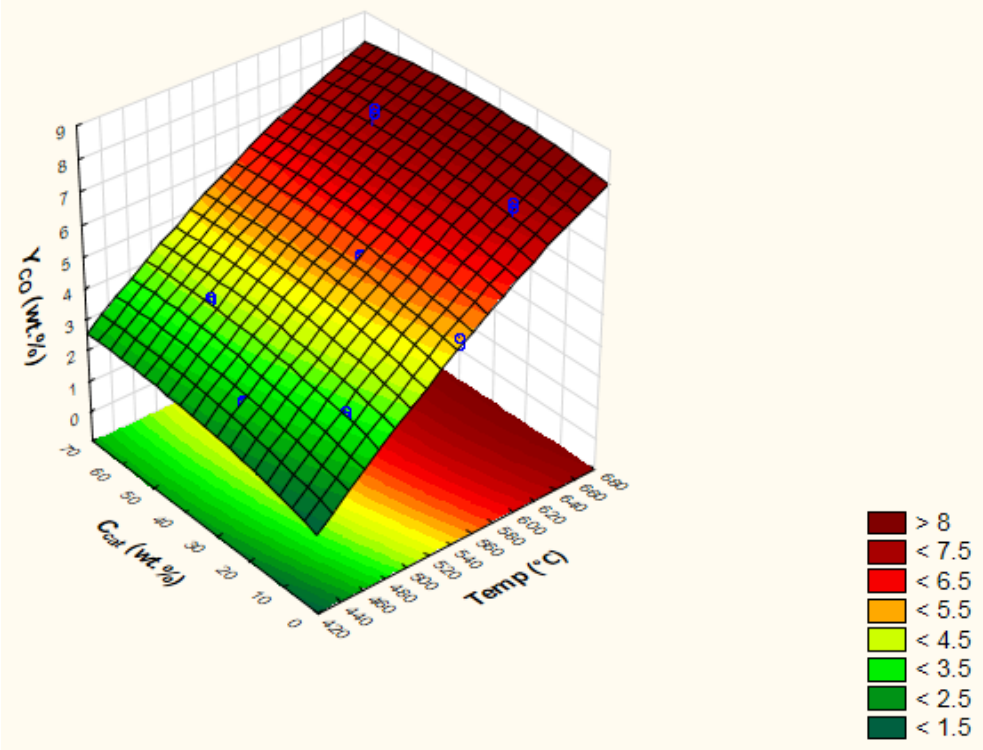

Figure 6-11: 3D surface profile of Y_{CO} from CaO optimisation

The statistical significance of the change in Y_{CO} was checked by an ANOVA test. The results of the ANOVA are detailed in ***Table 6-6*** and it showed that temperature had a more significant effect than C_{cat} on Y_{CO}.

Table 6-6: ANOVA for Y_{CO} from CaO optimisation

	Factor	F value	p-value	Conclusion
	(1) Temperature (L)	397.7178	1.442E-10	significant
R^2 = 0.971	Temperature (Q)	1.3983	0.2599	insignificant
adjusted R^2 = 0.959	(2) C_{cat} (L)	5.4540	0.0377	significant
MS Residual = 0.123	C_{cat} (Q)	0.5546	0.4708	insignificant
	1L by 2L	0.4965	0.4945	insignificant

Only the linear effects of temperature and C_{cat} were statistically significant as seen in the previous table. The increase in Y_{CO} with temperature was most likely due to the increased rate of secondary reactions at higher temperatures. CO was reported to be the primary product of secondary reactions (Neves et al. 2011). The observed increase in Y_{CO} as C_{cat} increased, supports what has been reported in literature. CaO is known to enhance the deoxygenation of organic pyrolysis volatiles via decarbonylation reactions resulting in an increased production of CO (Chen et al. 2017). However, the limited increase of CO with C_{cat} increase could be a result of CO absorption via the water-gas shift reaction.

6.3.3 CH_4

A 3D surface plot of Y_{CH4} from the CaO optimisation is shown in ***Figure 6-12***. Y_{CH4} was observed to increase as both C_{cat} and temperature increased, especially on the higher values of the respective ranges. Y_{CH4} can be multiplied by more than 10 times when both factors are increased. This indicated a strong interaction between temperature and the CaO concentration. An ANOVA test for Y_{CH4} was done, and the results are displayed in ***Table 6-7***. As seen in the ANOVA table, temperature and the catalyst concentration as well as the interaction between the two (1L by 2L) were statistically significant.

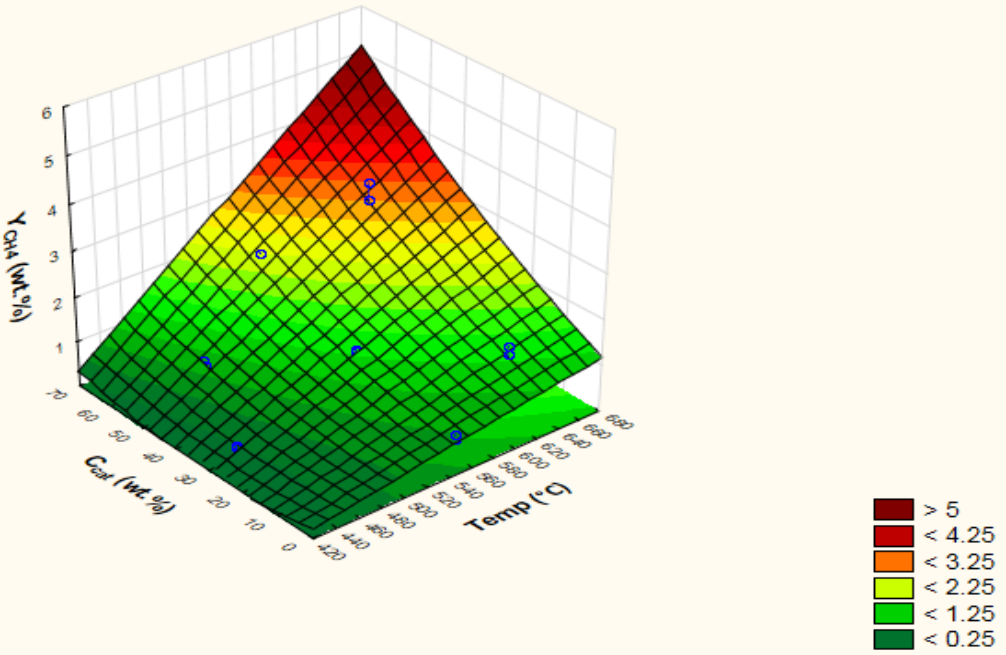

Figure 6-12: 3D surface profile of Y_{CH4} from CaO optimisation

Table 6-7: ANOVA for Y_{CH4} from CaO optimisation

	Factor	F value	p-value	Conclusion
	(1) Temperature (L)	235.5455	2.990E-9	significant
R^2 = 0.969	Temperature (Q)	0.0141	0.9075	insignificant
adjusted R^2 = 0.957	(2) C_{cat} (L)	120.3214	1.307E-7	significant
MS Residual = 0.0388	C_{cat} (Q)	1.5105	0.2426	insignificant
	1L by 2L	20.3182	7.171E-4	significant

At low temperatures (below 500 °C), Y_{CH4} was low, possibly because the secondary reactions, which are mostly responsible for CH_4 production, were limited at these temperatures (Neves et al. 2011). It is plausible that as temperature increased further, secondary cracking of volatiles was enhanced leading to higher CH_4 yields.

CaO was reported to catalyse the cracking of organic volatiles to produce methane and other light hydrocarbons (Widyawati et al. 2011). This could explain the increase in Y_{CH4} as C_{cat} increased, because more catalyst was available to promote the cracking reactions. In particular, Ellig et al. (1985) found that methyl substituted aromatic compounds could be cracked by CaO to produce methane and the parent aromatic compound.

Similar to this study, the same researchers found out that the effect of C_{cat} became more significant as the temperature increased. At higher temperatures, the activity of the catalyst is likely to be enhanced, favouring more volatile cracking (Chen et al. 2017), thus the significance of the interaction effect.

6.3.4 C_2-C_4

The 3D surface profile of Y_{C2-C4}, comparable to the one for Y_{CH4} is displayed in ***Figure 6-13***. Y_{C2-C4} increased as both C_{cat} and temperature increased. An ANOVA at of Y_{C2-C4} was conducted and the results are shown in ***Table 6-8***.

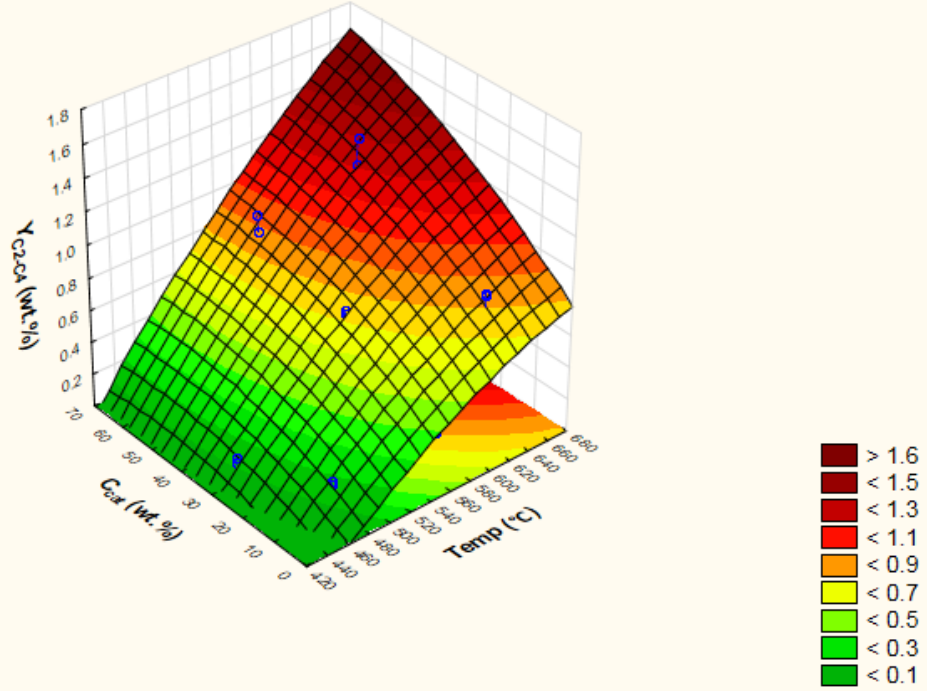

Figure 6-13: 3D surface profile of Y_{C2-C4} from CaO optimisation

Table 6-8: ANOVA for Y_{C2-C4} from CaO optimisation

	Factor	F value	p-value	Conclusion
	(1) Temperature (L)	549.7736	2.16E-11	significant
R^2 = 0.982	Temperature (Q)	2.6556	0.1291	insignificant
adjusted R^2 = 0.975	(2) C_{cat} (L)	105.8251	2.635E-7	significant
MS Residual = 0.00413	C_{cat} (Q)	1.8177	0.2025	insignificant
	1L by 2L	6.1233	0.0293	significant

The ANOVA analysis of Y_{C2-C4} displayed similar characteristics to that of Y_{CH4} (***Table 6-7***). All the factors were significant except C_{cat} (Q) and Temp (Q). The similarities in the variation of Y_{C2-C4} and Y_{CH4} with the catalyst concentration and temperature are because the mechanisms producing CH_4 and the other hydrocarbon gases, C_xH_y were reported to be similar (Neves et al. 2011). These mechanisms were described earlier for CH_4 in Section 6.3.3.

6.3.5 H_2

The surface profile of the hydrogen yield, Y_{H2} from the CaO optimisation is shown in ***Figure 6-14***.

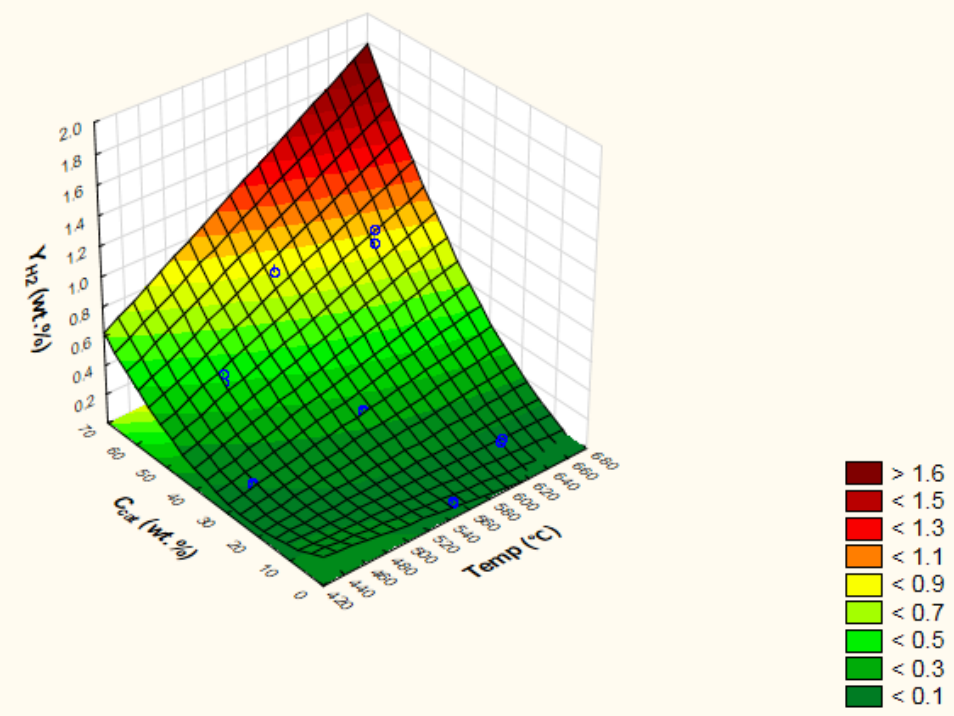

Figure 6-14: 3D surface profile of Y_{H2} from CaO optimisation

This profile was significantly different to the one for Y_{H2} from the MgO optimisation (***Figure 5-14***). In the CaO optimisation, C_{cat} was seen to influence Y_{H2}, while it was found to have no effect when MgO catalyst was used. In ***Figure 6-14***, it is seen that for C_{cat} > 35 wt.%, an increase in C_{cat} resulted in an increase in Y_{H2}. At lower C_{cat}, Y_{H2} was almost constant. Temperature appeared to only impact Y_{H2} at C_{cat} > 35 wt.%; an increase in temperature resulted in a linear increase in Y_{H2}. An ANOVA test (***Table 6-9***) was done to check the statistical significance of these effects. From the ANOVA, all the factors except temperature (Q), were found to be highly significant.

Table 6-9: ANOVA for Y_{H2} from CaO optimisation

	Factor	F value	p-value	Conclusion
	(1) Temperature (L)	63.5554	3.896E-6	significant
R^2 = 0.980	Temperature (Q)	0.0002	0.9886	insignificant
adjusted R^2 = 0.972	(2) C_{cat} (L)	458.4262	6.284E-11	significant
MS Residual = 0.00265	C_{cat} (Q)	22.3504	4.905E-4	significant
	1L by 2L	41.6445	3.145E-5	significant

The water-gas shift reaction (WGSR) was reported to be the main reaction by which H_2 is produced in the catalytic pyrolysis of wood using CaO (Widyawati et al. 2011; Chen et al. 2017).

$$CO + H_2O \rightarrow CO_2 + H_2 \qquad \text{(WGSR)}$$

The absorption of CO_2 by CaO and the increased production of pyrolytic water from catalytic dehydration reactions synergistically drive the WGSR towards hydrogen production according to the equilibrium principle. At C_{cat} < 35 wt.% and temperature < 600 °C, Y_{H2} appeared almost constant and only started to increase above this concentration. This was likely because, although the CO_2 was being absorbed as illustrated in ***Figure 6-10***, $Y_{P\text{-}WATER}$ was relatively low at these concentrations (***Figure 6-4***). As $Y_{P\text{-}WATER}$ started increasing at higher temperature and C_{cat}, it is probable that the WGSR became significant, resulting in an increase in Y_{H2}. It is worth noting that the 3D surface profile of $Y_{P\text{-}WATER}$ (***Figure 6-4***) is a close resemblance to that of Y_{H2} displayed by ***Figure 6-14***. This suggests that pyrolytic water was the limiting factor influencing hydrogen production. As seen from the surface profile of Y_{CO2} (***Figure 6-10***) the absorption of CO_2 was constant with changes in temperature and therefore was not likely to limit hydrogen formation. To further prove the existence of the WGSR, molar compositions of $Y_{P\text{-}WATER}$ and Y_{H2} from CaO optimisation were drawn (**Figure 6-15**). As seen in the figure, the increase in Y_{H2} is proportional to that of $Y_{P\text{-}WATER}$. $Y_{P\text{-}WATER}$ ranges from 0.8 to 1.6 mol. % and Y_{H2} from 0 to about 0.85 %. The almost 0.8 mol.% increases for each of Y_{H2} and $Y_{P\text{-}WATER}$ indicates the 1:1 stoichiometric relationship that exists between H_2 and H_2O in the WGSR.

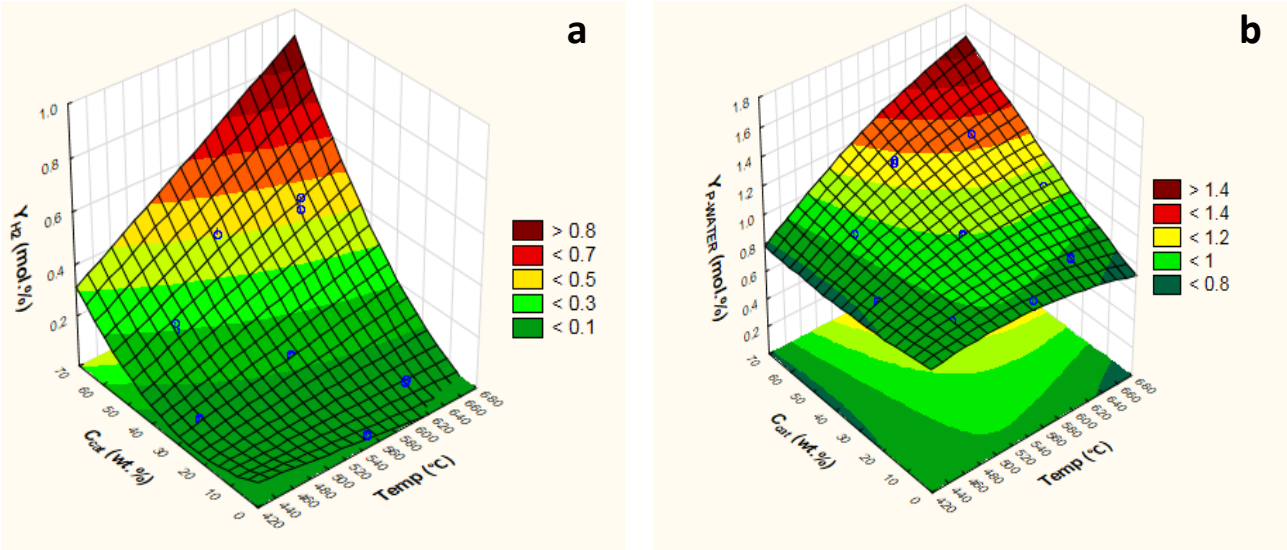

Figure 6-15: Molar yields of H_2 (a) and pyrolytic water (b) from CaO optimisation

In support of the increase in Y_{H2} observed in this study, Chen et al. (2017) observed a linear increase in the hydrogen gas composition as the catalyst concentration increased at 600 °C. Similarly, Guoxin and Hao (2009) and Widyawati et al. (2011) observed linear increases of Y_{H2} as temperature increased during the pyrolysis of wood in the presence of CaO. It is probable that MgO did not catalyse WGSR under the studied conditions, hence Y_{H2} did not change with changing C_{cat} in the MgO optimisation.

6.4 Conclusions

Using the developed regression model, the maximum organic phase HHV was 27.5 MJ/kg, obtained at 490 °C and 59.0 wt.% C_{cat}. Under these conditions, stronger deoxygenation was achieved than for MgO optimised conditions (26.9 MJ/kg), as evidenced by the higher HHV obtained. However, this deoxygenation occurred at a significant loss of the organics. At 490 °C and 59.0 wt.% CaO, $Y_{O\text{-}PHASE}$ was 13.4 wt.% which is below the 15 wt.% required for bio-oil co-processing at 10 % blending ratio in South Africa. The desirability function had to be used to make get a compromise between the organic phase HHV and $Y_{O\text{-}PHASE}$.

The desirability functions were defined to maximise both responses, $Y_{O\text{-}PHASE}$ and organic phase HHV. The desirability and predicted value profiles are shown in ***Figure 6-16***. From the above desirability profiles, it was seen that the optimum conditions for CaO catalysed in situ pyrolysis are the catalyst screening conditions (550 °C and 30 wt.% C_{cat}). At these conditions $Y_{O\text{-}PHASE}$ was 18.5 wt.%, while the organic phase HHV was 26.4 MJ/kg, which was similar to the organic phase results from the MgO optimum (26.9 MJ/kg at a $Y_{O\text{-}PHASE}$ of 19.9 wt.%). As a result, it was difficult to select a best performing catalyst and an energy conversion assessment (Section 7.1) was used to help select the best performing catalyst to be used on the pilot scale.

CaO was found to predominantly promote dehydration reactions as well as demethylation and secondary cracking of volatiles to produce C_xH_y gases. It was found that CaO was highly activated towards these reactions at temperatures above 560 °C and C_{cat} > 35 wt.% resulting in very low organic phase yields. Therefore, too high temperature and C_{cat} are not ideal for production of the organic phase.

Significant production of H_2 was obtained. According to literature, it was due to the WGSR catalysed by CaO (Lin et al. 2010; Widyawati et al. 2011; Chen et al. 2017). The production of pyrolytic water and absorption of CO_2 during CaO catalysed pyrolysis probably resulted in increased production of H_2 via the WGSR. The similarities in the surface profile of $Y_{P\text{-}WATER}$ and Y_{H2}, while the one for CO_2 showed that CO_2 absorption was constant, suggested that pyrolytic water was the limiting factor in the WGSR.

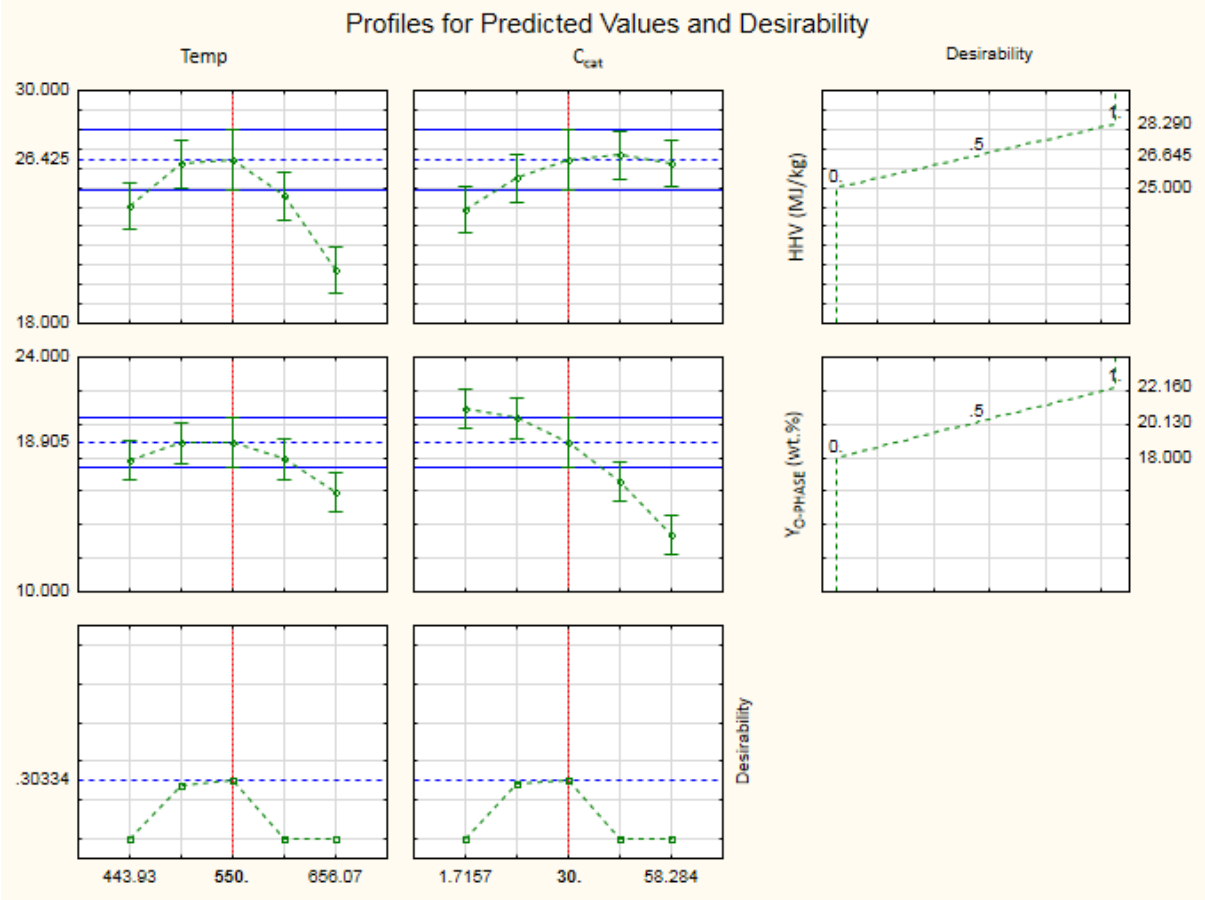

Figure 6-16: Desirability and predicted value profiles of $Y_{O\text{-}PHASE}$ and organic phase HHV from CaO optimisation

The calorific value of the gas calculated at the desirable optimum conditions for CaO is 13.7 MJ/kg (***Table 4-13***), which is more than double the typical gas calorific value from non-catalytic pyrolysis and from pyrolysis using MgO. This is due to the absorption of CO_2 by CaO as well as the increase in Y_{H2} due to the WGSR and the increased production of C_xH_y gases from the CaO catalysed cracking reactions. This higher calorific value gas can be used to meet some of the energy requirements of the pyrolysis process.

7 Pilot Scale Up

7.1 Selection of preferred catalyst from bench scale comparison of MgO and CaO

Similar $Y_{O\text{-}PHASE}$ and HHV values were obtained at the optimum conditions from MgO optimisation (Section 5.4), and at the desirable optimum from the CaO optimisation (Section 6.4), making it difficult to select a preferred catalyst for pilot study. An energy conversion (EC) assessment was also used to aid in determining the best performing catalyst. The energy conversion was calculated using the equation below.

$$EC = \frac{\sum Y_i * HHV_i}{HHV_{sample}} \qquad \text{EC assessment}$$

where $\mathbf{Y_i}$ is the yield of a specific pyrolysis product **i**, $\mathbf{HHV_i}$ is the calorific value of the pyrolysis product (wet basis) and $\mathbf{HHV_{sample}}$ is the calorific value of the biomass sample (wet basis).

Only the organic liquid phase and the gas products were considered for energy applications. As discussed in Section 4.2.2.2, the solid product/char is more efficiently used for soil amendment applications. As the aqueous phase contained mostly water and did not ignite when tested on the bomb calorimeter, it cannot be considered as a fuel source and was excluded from the energy assessment. ***Figure 7-1*** shows the energy conversion assessment of CaO and MgO based on the optimisation experiments.

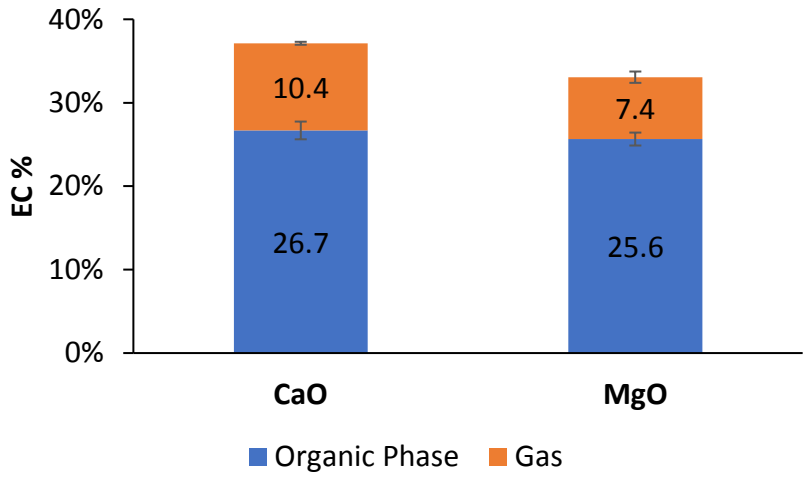

Figure 7-1: Energy conversion assessment of CaO and MgO based on the optimisations

From the diagram above, it is seen that overall, more energy could be recovered when CaO was used instead of MgO. The organic phase ECs were almost similar, although that of CaO was slightly higher because the water content of the organic phase at the CaO optimum (7.8 wt.%) was lower than that for MgO (approximately 12.6 wt.%) (Section 4.2.4.2). The biggest difference was in the gas EC which was a result of the cracking effect of CaO producing more hydrocarbon gases and the WGSR producing more hydrogen. Based on the above energy conversions, CaO is the more favourable catalyst as it recovers the most energy from the organic phase and gas products. In pyrolysis process, the gas product is often combusted to provide some heat for the energy process. A higher energy content of the gas product increases the potential of the process to be viable. In addition, as discussed in Section 4.2.2, the CaO derived solid product is the best in terms of applicability in soils. This was another reason why CaO was chosen over MgO as the catalyst to be scaled up for pilot scale experiments which are discussed next in Section 7.2.

7.2 Pilot Scale Results

In this part of the study, we are moving from batch bench scale to continuous process in the pilot. At bench scale, when the volatiles leave the sample boat, only secondary reactions between volatiles are possible, while in the pilot reactor contact between the volatiles with the char and the catalyst are occurring all along the reactor, making secondary reactions more likely to happen. Another major difference between the experimental setups is that on the pilot scale, the reactor was pre-heated, and the sample was introduced in the hot reactor. An increase in temperature automatically results in an increased heating rate.

A summary of the overall product yields from the pilot scale experiments is given in ***Figure 7-2***. The mass balance closure from the pilot results ranged from 89 – 91 %. A portion of the mass losses was ascribed to loss of volatiles from minor leaks on the pilot plant rig, as well as incomplete condensation of some volatiles, which was evidenced by the browning of the Tedlar bags during gas sampling. The typical liquid yield for intermediate pyrolysis for the non-catalytic runs were comparable to those reported elsewhere for biomass pyrolysis in an auger reactor (Puy et al. 2011; Veses et al. 2014).

Comparing the non-catalytic results on the bench (***Figure 4-2*** and ***Figure 4-3***) and pilot scale at 550 °C, it was seen that less liquid and more gas, especially CO, CH_4 and C_2-C_4, consistent with more secondary reactions were obtained on pilot scale (***Figure 7-2*** and ***Figure 7-9***). Pyrolysis char are known to have a cracking catalytic effect (Maneewan et al. 2014; Hervy et al. 2018; Fu et al. 2018), and with the likely greater contact between char/ catalyst mixture and volatiles in the pilot reactor, these cracking reactions were enhanced.

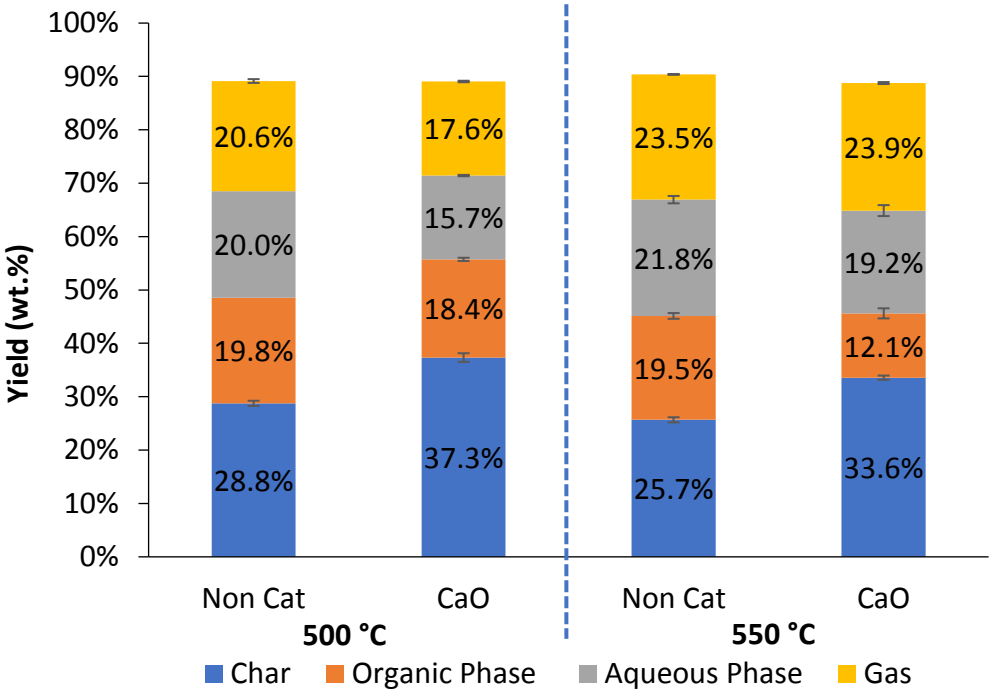

Figure 7-2: Overall pyrolysis product yields from pilot scale experiments

The desirable optimum conditions for CaO catalysed pyrolysis were 550 °C and 30 wt.% C_{cat}. The above conditions were applied to the pilot plant and compared to the non-catalytic case at 550 °C. While the organic phase yield was 19.5 wt.% for the non-catalytic test it was found to decrease to less than the targeted 15 wt.% (12.1 wt.%) with CaO catalyst (***Figure 7-2***). The significant decrease in the organic phase yield was interpreted to be a consequence of extensive secondary reactions (Section 7.2.2) and it was then decided to lower the reaction temperature. Veses et al. (2014) reported that 450 °C was optimum for CaO catalysed biomass pyrolysis in their auger reactor setup which included a heat carrier to achieve a high biomass heating rate.

It was reported that higher temperatures resulted in significant cracking of volatiles, leading to low yield of the organic phase (Veses et al. 2014). Poor mass balances were also reported at higher temperatures. In our pilot reactor setup, there was no heat carrier. To counteract the potential over cracking effect, it was decided to lower the catalytic pyrolysis temperature from 550 to 500 °C, where acceptable organic phase yields were obtained. A non-catalytic test at 500 °C was also done as a reference.

A detailed discussion of the pyrolysis products is given in Sections 7.2.1 – 7.2.3.

7.2.1 Char

The yield of char, Y_{CHAR} reported in ***Figure 7-2*** was given on a catalyst free basis. In the non-catalytic case, Y_{CHAR} decreased with an increase in temperature; at 500 °C, Y_{CHAR} was 28.8 wt.% while it was 25.7 wt.% at 550 °C. It is well known that higher temperatures and heating rates favour volatile production over char formation (Bridgwater 2003; Goyal, Seal, and Saxena 2008). For the pilot tests, the sample was introduced in the hot reactor. Higher reactor temperature automatically resulted in higher heating rate of the sample particles. Comparing Y_{CHAR} at 550 °C on the bench and pilot scales, it was seen that the bench-scale yield was slightly smaller (24.4 wt.%) than the pilot yield (25.6 wt.%). The close char yield means heating rates at bench and pilot scales were probably similar. However, it is probable that there was more secondary char generated in the pilot reactor due to a higher probability of secondary reactions, as a result of a longer volatile/solid (char or catalyst) contact. On the pilot plant rig, the solid phase moves along the reactor together with the gas phase from the inlet to the outlet, resulting in a greater likelihood of contact between the two, than in the batch setup.

When CaO was used as the catalyst, a significant rise in Y_{CHAR} was observed at both 500 and 550 °C and this was likely a result of the absorption of CO_2 by CaO to form $CaCO_3$. This was confirmed through much lower CO_2 yield when CaO catalyst was used (Section 7.2.3.1). Similar increases in Y_{CHAR} with CaO were also seen on the bench scale (Section 4.2.2). However, at same catalyst content the increase in Y_{CHAR} on the pilot scale was greater than that on the bench scale. On the pilot scale, Y_{CHAR} increased by between 7.9 and 8.5 wt.% (at 500 and 550 °C respectively, see ***Figure 7-2***) compared to just 4.8 wt.% on the bench scale (at 550 °C, see ***Figure 4-2***).

This difference was most likely due to the greater contact between the gas phase and the solid phase in the pilot reactor which resulted in the absorption of more CO_2. This was confirmed by the proximate analyses of the pilot scale chars as described in Section 7.2.1.1.

7.2.1.1 Proximate Analysis

Table 7-1 gives the proximate analyses of chars from the pilot scale experiments. While the amount of volatiles generated at T < 650 °C, is relatively close for the chars produced with and without catalyst, volatile production at T > 650 °C (where CO_2 is released from $CaCO_3$) was more than 5 times higher for the chars obtained from catalytic pyrolysis. This result is characteristic of the presence of $CaCO_3$ in the catalytic pyrolysis char. It was observed that the volatiles released at T > 650 °C from the char produced by the catalytic runs on the pilot (above 27 wt.%) were greater than those produced by the bench scale experiments (18.9 wt.%). This confirmed that more CO_2 was absorbed on the pilot scale setup than the batch setup. The low fixed carbon and organics content (volatiles) of the catalytic pyrolysis chars confirm that fuel application would not be recommended.

Table 7-1: Altered proximate analysis of chars from pilot scale experiments (dry basis)

	500 °C		**550 °C**	
	Non-Cat	CaO	Non-Cat	CaO
Volatiles, < 650 °C (wt.%)	14.7	9.2	5.7	5.4
Volatile, > 650 °C (wt.%)	4.5	27.6	5.8	31.0
Fixed Carbon (wt.%)	77.0	11.6	83.9	10.2
Inorganics (wt.%)	3.8	51.6	4.6	53.4

7.2.2 Liquid

As seen in ***Figure 7-2***, for non-catalytic runs, the total liquid yield, Y_{LIQUID} was greater at 550 °C (41.3 wt.%) than at 500 °C (39.8 wt.%), suggesting that for non-catalytic runs 550 °C is more preferred for liquid production. However, the organic phase yields, $Y_{O\text{-}PHASE}$ were similar for the two temperatures. When catalysts were used, a decrease in Y_{LIQUID} was observed. This decrease was more severe at 550 °C where Y_{LIQUID} decreased by 10.0 wt.%.

At 500 °C, Y_{LIQUID} decreased by 5.7 wt.%. On the bench scale, Y_{LIQUID} was comparable for both catalytic and non-catalytic pyrolysis at 550 °C (***Figure 4-2***). The differences could be explained by the better mixing or contact between the catalyst and volatiles in the pilot reactor. Because of this, it is plausible that the catalytic cracking effect was greater in the pilot reactor than in the batch reactor at the same temperature, leading to a significant decrease in liquid yields. This was further evidenced by the larger increase in the yields of gas products characteristic of cracking (CO, CH_4 and C_2-C_4) on the pilot scale (***Figure 7-9***) compared to the bench scale (***Figure 4-3***).

7.2.2.1 Organic Phases

Figure 7-3 shows the bio-oil as obtained from non-catalytic pyrolysis at 550 °C. C1, C2, C3 and C4 denote condensers 1, 2, 3 and 4 respectively. Although not visible in ***Figure 7-3***, condenser 2 had two phases, a top aqueous phase which will be denoted "C2A" and a bottom organic phase denoted "C2O" which were separated easily be decanting. Similar product repartition was found for the catalytic tests. The total organic phase was the sum of the individual liquid products from C1, C2O, C3 and C4, while the aqueous phase was comprised solely of C2A.

Figure 7-3*:* Bio-oil from the different condensers obtained from pilot scale non-catalytic pyrolysis at 550 °C

The distribution of the yields of the different organic phases is given in ***Figure 7-4***. From this illustration, it was seen that generally the main organic fraction was found in C1 while C2O, C3 and C4 contained lower amounts of organics.

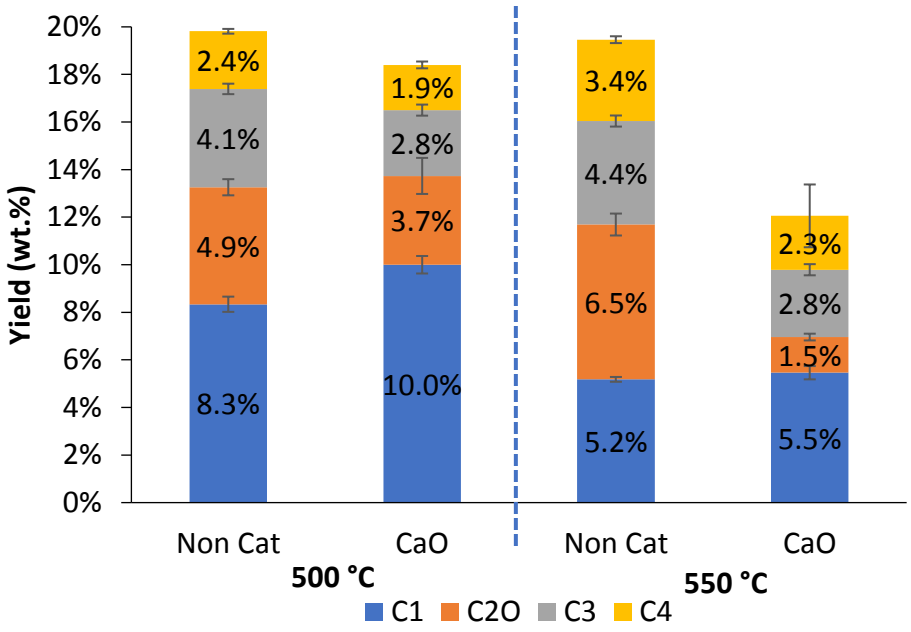

Figure 7-4: Distribution of the organic phases from pilot scale experiments

The water content of the liquid products from the different condensers is given in ***Figure 7-5***.

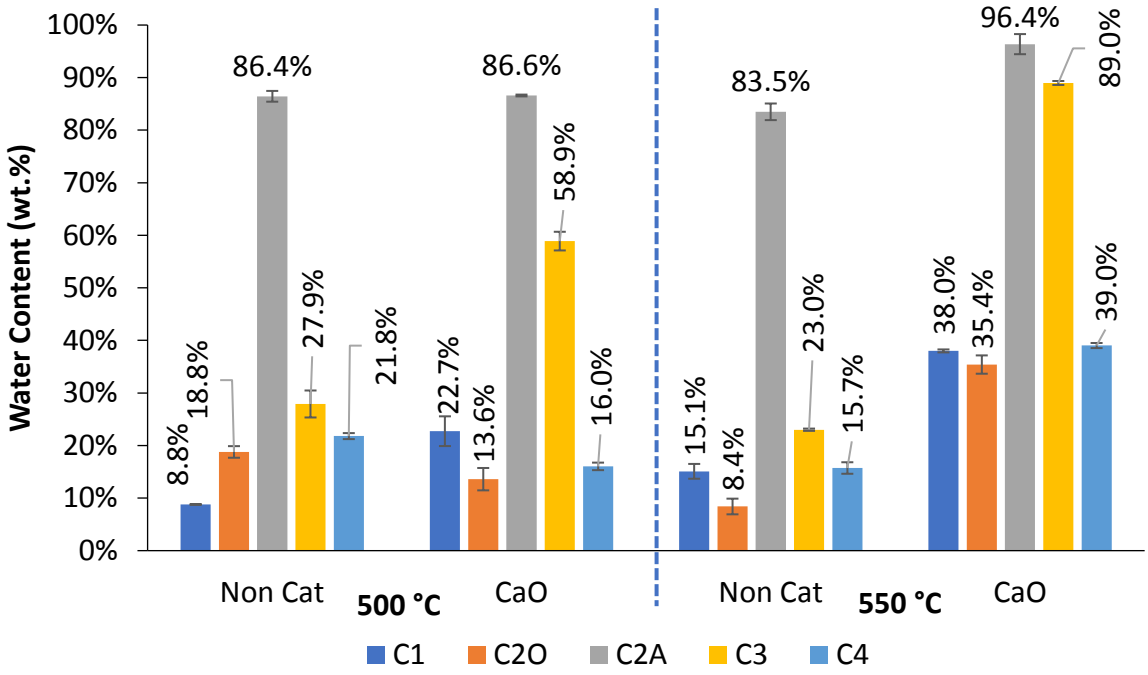

Figure 7-5: Water content of the organic and aqueous (C2A) products collected in the different condensers from pilot scale experiments

As expected, the aqueous fraction in condenser 2 was characterised by high water content (≥ 80 wt.%) for all the experiments. Generally, the water contents of the organic fractions were found to be lower than 40 wt.%, even less than 30 wt.% for non-catalytic tests. In the catalytic runs, it was observed that C3 had a significant increase in the water content of the organic fraction (≥ 50 wt.%). Based on the study by De Rezende Pinho et al. (2017) it can be assumed that a maximum bio-oil water content of 31.9 wt.% can be fed to an FCC during bio-oil co-processing. However, it is better to have a water content as low as possible, so that more organics can be recovered in the gasoline and diesel products from the FCC. The organic phases produced at 500 °C and 30 wt.% CaO were attractive because their water contents were all < 32 wt.% (except for C3) and could therefore be successfully co-processed in an FCC. The overall organic phase water content including C3 is 25.6 wt.% (at 500 °C and 30 wt.% CaO). If C3 is excluded, the overall organic phase water content is 19.7 wt.%. Therefore, it would be beneficial to exclude the liquid fraction from C3 from the total organic phase, as the organic phase water content will be decreased by my more than 5 wt.%, with only a 2.8 wt.% loss in the organic phase yield. The organic phase produced by catalytic pyrolysis at 550 °C is less suitable for co-processing in a crude oil refinery because it has a high overall water content (> 32 wt.%), even when excluding the product in C3. It can be noted that the water contents from the non-catalytic organic phases at 500 °C are low enough (< 28 wt.%) to allow for blending at the maximum blending ratio for crude bio-oil (5 wt.%).

7.2.2.2 Pyrolytic Water and Organics

Using the water contents displayed in ***Figure 7-5***, the pyrolytic water yield, $Y_{P\text{-}WATER}$ as well as the organics yields were calculated, and these are shown in ***Figure 7-6***. The low organics yield (6.8 wt.%) at 550 °C when CaO was used, indicated the excessive volatile cracking which occurred at this temperature. It was found from the regression modelling, (Chapters 5 and 6) that higher temperatures enhanced the activity of the catalysts towards volatile cracking. Hence decreasing the reaction temperature to 500 °C at the same C_{cat} for CaO resulted in a much higher organics yield (15.8 wt.%) compared to that at 550 °C (6.8 wt.%). The excessive volatile cracking was evidenced by the increase in the yields of CO, CH_4 and C_2-C_4, which are products of volatile cracking (see Section 7.2.3).

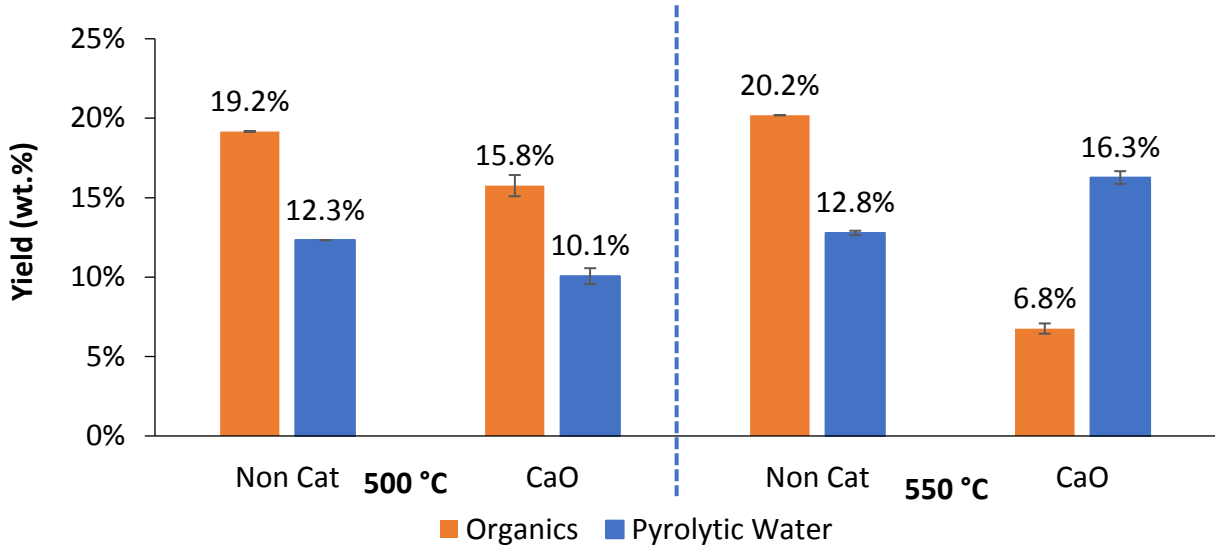

Figure 7-6: Pyrolytic water and organics yield from pilot scale experiments

$Y_{P\text{-}WATER}$ at 500 and 550 °C were similar when no catalyst was used. This concurs with the data compiled by Neves et al. (2011) which showed that at slow/intermediate heating rates, $Y_{P\text{-}WATER}$ is relatively constant in the temperature range of 400 – 700 °C. When CaO catalyst was used at 500 °C, a decrease in $Y_{P\text{-}WATER}$ compared to the non-catalytic case was observed. It was expected that due to the known dehydrating ability of CaO (Lin et al. 2010), $Y_{P\text{-}WATER}$ would increase, similar to what was seen on the bench scale (***Figure 4-7***). The different observations were probably due to more contact between catalyst and volatiles on the pilot scale, which shifted the WGSR more towards H_2 production and H_2O consumption, due to more CO_2 being absorbed (see Section 7.2.1.1). At 550 °C and 30 wt.% catalyst, $Y_{P\text{-}WATER}$ was higher than that of the non-catalytic case at the same temperature. It is likely that at 550 °C, the catalyst activity was enhanced such that the dehydration reactions were promoted to a greater extent, than at 500 °C resulting in a higher $Y_{P\text{-}WATER}$.

7.2.2.3 Higher Heating Value

The HHVs (dry basis) of the organic fractions from the different condensers are shown in ***Figure 7-7***. The HHV for C3 fraction at 550 °C and 30 wt.% C_{cat} could not be measured due to the presence of substantial amounts of water in that condensers. HHVs for C2A for all runs could also not be determined for the same reason.

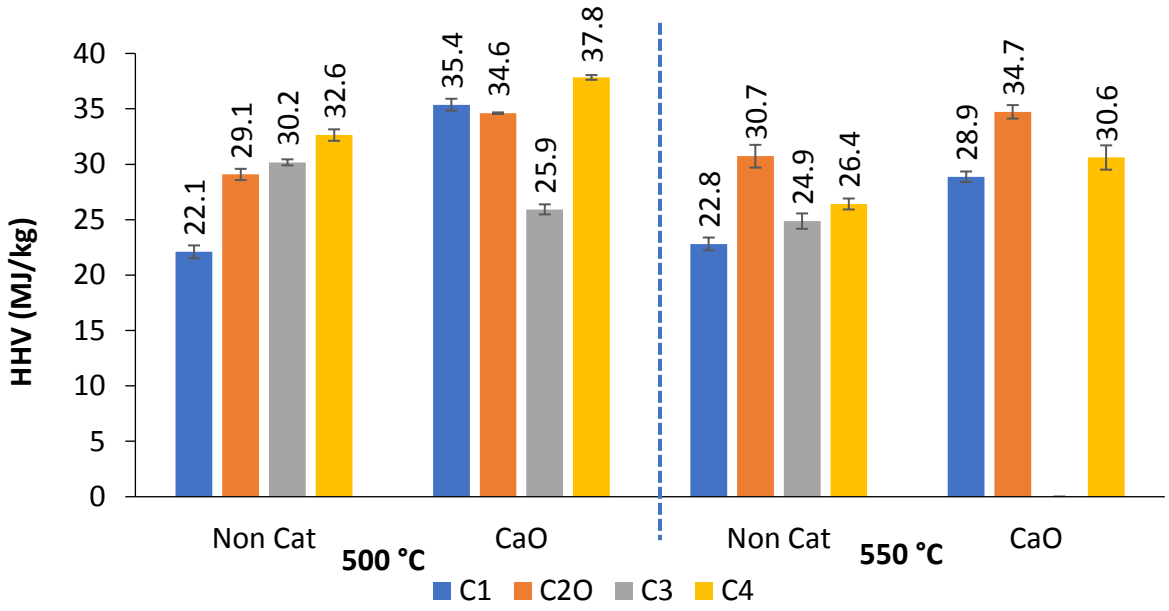

Figure 7-7: HHV of the organic products collected in the different condensers from pilot scale experiments

To compare the HHVs in this study to the ones reported in literature, overall HHVs were calculated and are shown in ***Figure 7-8***. The overall HHV values shown in the figure are reported for two different scenarios. In the first scenario, the overall HHV was calculated based on the total organics collected from all the condensers, similar to what was reported in most literature. Since the energy content of the organic compounds found in the aqueous fraction (C2A and C3 for the catalytic tests) could not be determined, because the aqueous fraction did not combust in the bomb calorimeter, they were assigned an HHV of zero. In the second scenario, the overall HHV was calculated based on the combustible organic fractions i.e. organics collected from C1, C2O, C3 (except for the catalytic tests where C3 had a high water content) and C4.

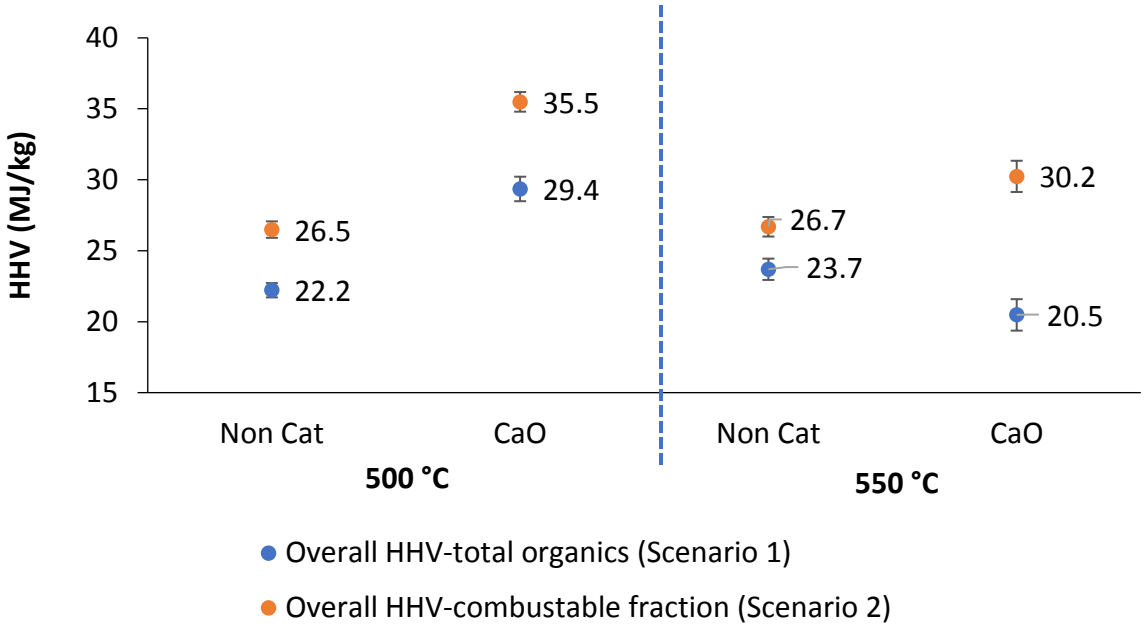

Figure 7-8: Overall organics HHV from pilot scale experiments reported based on total organics (Scenario 1) and based on combustible fraction only (Scenario 2)

The largest overall organics HHV was 29.4 MJ/kg, which was achieved at 500 °C and 30 wt.% CaO concentration. This HHV was comparable to the HHVs reported in the reviewed literature (**Table 2-11**) for total bio-oil organics on a dry basis. Veses et al. (2014) reported a calorific value of 30.2 MJ/kg for bio-oil produced from catalytic pyrolysis using CaO in an auger reactor at 450 °C. A recent study by Ly et al. (2018) showed that a bio-oil HHV of 28.0 MJ/kg could be achieved in a fluidised bed reactor in the pyrolysis of tulip tree using calcined dolomite catalyst.

The overall HHV of the combustible organic fractions was seen to be relatively high, with an overall HHV of 35.5 MJ/kg achieved at 500 °C and 30 wt.% C_{cat}. This shows that the fractionation condensation system designed in this study was very efficient in terms of separating the different organic phases and achieving a bio-oil with a very high HHV.

The elemental analyses of the organic phases from the pilot scale experiments were determined and this is reported in Section 7.2.2.4.

7.2.2.4 Elemental Analysis

The overall elemental composition of the organics is given in ***Table 7-2*** below. The elemental analysis of the liquid product from the different condensers is given in Appendix D.1.

Table 7-2: Elemental analysis of organics from the pilot scale experiments (wt.%, db)

		Test			
	Temperature	500 °C	500 °C	550 °C	550 °C
	Catalyst	Non-Cat	CaO	Non-Cat	CaO
C		53.74	72.04	57.27	63.00
H		7.10	6.76	6.63	5.85
N		0.05	0.45	0.65	0.92
O[a]		39.10	20.70	35.45	30.22

[a] Determined by difference

The table above shows that the elemental composition of the non-catalytic bio-oil found in this study corresponded to the typical elemental composition for bio-oil reported in literature (Czernik and Bridgwater 2004) i.e. C: 54 – 58 wt.%, H: 5.5 – 7.0 wt.%, O: 35 – 40 wt.%. A decrease in the O content of the organics from 39.10 wt.% to 35.45 wt.% was seen when the reaction temperature increased from 500 to 550 °C. This was similar to the observation by Ly et al. (2018) who reported a decrease in the oxygen content of the bio-oil from 38.71 to 34.71 wt.% when the temperature was increased to 500 °C from 550 °C. This decrease in the oxygen content might be due to cracking of the oxygenated volatiles which was promoted at higher temperatures (Neves et al. 2011). Such cracking is generally accompanied by an increase in CO production. As seen in Section 7.2.3, under non-catalytic conditions, the CO yield increased when the temperature was increased from 500 to 550 °C.

Table 7-2 shows that although deoxygenation was promoted at 550 °C under the influence of catalyst, oxygen content of the oil was observed to be higher than that at 500 °C. This observation supports what was seen in the bench scale optimisation experiments; that calorific value and hence deoxygenation, of the organics decreased at higher temperatures (> 550 °C). This was probably due to the nature of the cracking reactions at higher temperatures. At 500 °C, a large proportion of the oxygenated groups of biomass have been converted. The oxygenated groups remaining, the bond 4-O-5 diarylether for instance are particularly stable (Sergeev and Hartwig 2011). It is likely that amongst additional reactions catalysed at 550 °C, reactions leading to the loss of carbon and/or hydrogen (demethylation for instance) become preponderant, thereby resulting in an increased oxygen content. This hypothesis is consistent with the significant increase in the production of hydrocarbon gases, C_xH_y observed when catalytic pyrolysis temperature increased from 500 to 550 °C (Section 7.2.3).

The overall bio-oil elemental analysis results obtained from this study are comparable to those from other biomass pyrolysis studies using metal oxide catalysts as illustrated in ***Table 7-3***. The results from this study are seen to be even slightly better.

Table 7-3: Comparison between elemental analysis (wt.%) of organics from this study and literature

	Reaction Conditions		
Temperature	*[b]500 °C*	*[c]500 °C*	*[d]450 °C*
Catalyst	MgO	CaO	CaO
C	70.1	72.0	67.9
H	8.0	6.8	7.5
N	-	0.5	0.3
O[a]	21.9	20.7	24.2

[a] Determined by difference

[b] Stefanidis et al. (2011) [c] This study [d] Veses et al. (2014)

Desirable organic fraction

In this study, due to the design of the condensation system, organic fractions separate from the aqueous fractions and it was possible to determine the elemental composition of the organic phase only. At the preferred reaction conditions found on the pilot scale, 500 °C and 30 wt.% C_{cat}, the desirable phases to be fed into an oil refinery were C1, C2O and C4 due to their relatively low water contents (< 23 wt.%). These phases had a total yield of 15.6 wt.% which is sufficient to feed in an oil refinery according to the literature reviewed in Section 2.2.3. When only these 3 phases are considered, their overall elemental composition on a dry basis is given in ***Table 7-4***.

Table 7-4: Elemental analysis of organic fraction that will be fed into oil refinery

Element	**C**	**H**	**O**	**N**
Composition (wt.%, db)	80.2	6.9	12.6	0.3

According to Section 2.2.3, to achieve a 10 wt.% blending ratio in an oil refinery, the bio-oil should have an oxygen content of < 17 wt.% dry basis and a water content below 32 wt.%. The organic fraction comfortably meets this oxygen content requirement while its moisture content was < 20 wt.% (see Section 7.2.2.1). Therefore these 3 fractions could be successfully co-processed in an oil refinery. However, the yield of 15.6 wt.% is just above the targeted value and the possibility to improve it by doing an optimisation work on the pilot scale could be considered.

7.2.3 Gas

The yields of the different gases making up the gas products from the entire pilot scale runs on this study is shown in ***Figure 7-9***. Gas product analysis helped to explain the mechanisms through which deoxygenation was occurring.

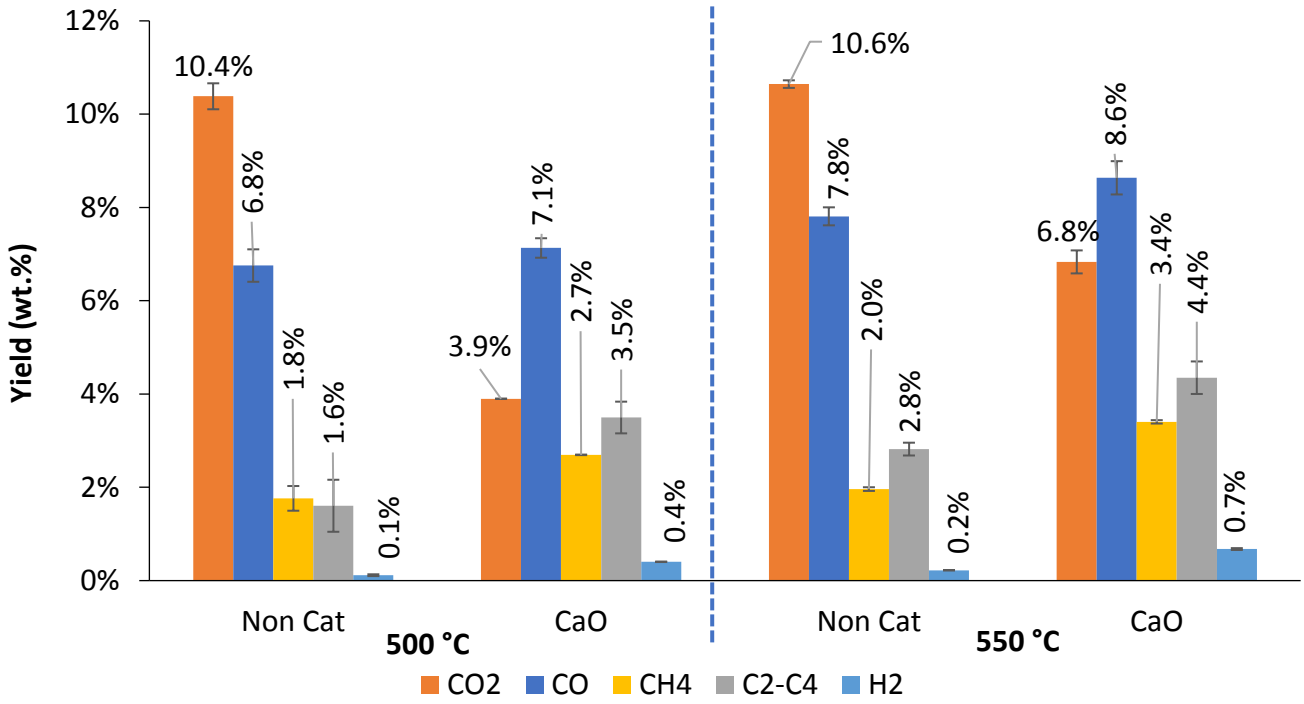

Figure 7-9: Gas product yields from pilot scale runs

7.2.3.1 CO_2

The yield of CO_2, Y_{CO2} for the non-catalytic runs on the pilot scale at 550 °C (10.6 wt.%) was comparable to that on the bench scale (11.2 wt.%) at the same temperature. This corresponded to the data compiled by Neves et al. (2011) which showed that temperature in the range 450 – 800 °C had a limited effect on Y_{CO2}. When catalyst was used, a decrease in the CO_2 yields was observed. This was most likely a result of CO_2 absorption by CaO as discussed in Section 7.2.1.

7.2.3.2 CO and H_2

Figure 7-9 shows that in the non-catalytic case, there was a 1 wt.% increase in the CO yield, Y_{CO} when the temperature changed from 500 °C to 550 °C. Higher temperature promoted secondary reactions, of which CO is a major product (Neves et al. 2011). The increase in Y_{CO} indicates that some deoxygenation has occurred, hence a higher HHV of the organic phase also recorded when the temperature was increased (***Figure 7-8***).

A lower increase in Y_{CO} was observed on the pilot scale compared to the bench scale in the CaO catalysed experiments. Y_{CO} increased by 1.7 wt.% on the bench scale and by only 0.8 wt.% on the pilot reactor at 550 °C. Again, this could be due to the WGSR being driven more towards H_2 production due to a greater extent of CO_2 absorption by CaO. The H_2 yield, Y_{H2} at the pilot scale increased by 0.1 wt.% more than that on the bench scale, which helps support the assumption that WGSR occurred more on the pilot scale.

7.2.3.3 *CH_4 and C_xH_y*

When compared to the bench scale results, Y_{CH4} and Y_{CxHy} are much greater on the pilot scale. For example, in the non-catalytic case at 550 °C on the pilot scale (***Figure 7-9***), yield of CH_4 was multiplied by a factor 4 and almost 10 for C_2-C_4 when compared to the bench scale (***Figure 4-3***). This is evidence of enhanced secondary reactions on the pilot, which are likely due to the cracking effect of char as mentioned at the beginning of section 7.2.

At 550 °C, Y_{CH4} increased by 1.4 wt.% when CaO was used on pilot scale, compared to 0.8 wt.% on the bench scale. Similarly, the other hydrocarbon gases increased by 1.6 wt.% for the pilot compared to 0.4 wt.% on bench scale. Hydrocarbon gases are also major products from cracking and demethylation of organic volatiles (Neves et al. 2011). CaO and MgO are both known to promote these reactions (Lin et al. 2010; Chen et al. 2017). The higher increases of these gases on the pilot reactor compared to the bench scale, further gives evidence of stronger catalytic effect on the pilot scale.

Due to the substantial absorption of CO_2 on the pilot reactor as well as the increased production of H_2 and C_xH_y hydrocarbons (even higher than the production at 550 °C for the catalytic test at bench scale) a relatively high gas calorific value of 23.1 MJ/kg was achieved at 500 °C and 30 wt.% C_{cat}.

7.2.4 Conclusions

It was found that the bench scale conditions could not be directly upscaled to the pilot plant rig and achieve the same results as on the fixed-bed reactor and adjustments had to be made to the reactor temperature. It appeared that the pilot scale reactor allowed for a greater contact time between the volatiles and catalyst compared to the bench scale. This resulted in more CO_2 absorption and severe volatile cracking at temperatures of 550 °C, resulting in high gas yields and low organic phase yields (6.6 wt.%). As a result, a lower temperature (500 °C) was used to limit the volatile cracking, which resulted in a much higher organic phases yield (15.6 wt.%) being achieved.

The greater contact between volatiles and catalyst on the pilot scale also meant that the deoxygenation of the organics was enhanced compared to the bench scale, resulting in a higher organic phase HHV (up to 35.5 MJ/kg) on the pilot scale compared to a maximum of 27.5 MJ/kg on the bench scale. The oxygen content of this organic phase (12.6 wt.% on a dry basis) was below the minimum threshold of 17 wt.% required for a 10 wt.% blending ratio in an oil refinery and therefore it is suitable for blending purposes. The organic phase had an overall water content of 19.7 wt.%, which is also suitable for blending with VGO in a crude oil refinery. A comparison of the desirable organic fraction in this study to literature was done (***Table 7-5***). This table shows that the fractionation condensation system designed in this study was efficient in the isolation of a highly deoxygenated organic-rich phase.

Table 7-5: Comparison of the organic fraction in this study to literature in terms of HHV and oxygen content (dry basis)

Catalyst	HHV	O-content	Reference
CaO	20.5	41.1	Li et al. (2012)
CaO	29.9	31.0	Lin et al. (2010)
CaO	30.2	24.2	Veses et al. (2014)
MgO	31.2	21.9	Stefanidis et al. (2011)
CaO	35.5	12.6	This study

The organic phase oxygen content without catalyst at 500 °C was 39.10 wt.% and with catalyst at the same temperature it was 20.70 wt.%. Without catalyst at 550 °C, organic phase oxygen content was 35.45 wt.%. Therefore, much higher temperature would be required for similar deoxygenation without catalyst. Thus, the use of catalyst has an advantage in terms of energy efficiency of the process.

8 Conclusions and Recommendations

8.1 Overall Conclusions

This study has shown that a bio-oil of sufficient quality for co-processing with VGO in a crude oil refinery can be produced by *in situ* catalytic pyrolysis of forest residues using intermediate pyrolysis technology. It was found out that bio-oil could be deoxygenated to 12.6 wt.% oxygen (dry basis) via catalytic pyrolysis using CaO on a pilot scale reactor at 500 °C and 30 wt.% catalyst concentration. The yield of this oil was 15.6 wt.%, enough to achieve bio-oil co-processing at a 10 wt.% blending ratio at the Enref crude oil refinery in South Africa. The bio-oil had a water content of 19.7 wt.% which is acceptable in an oil refinery.

Prior to the pilot scale runs, a catalyst screening study was done on bench scale to assess the ability of Al_2O_3, CaO and MgO for bio-oil deoxygenation. This was followed by optimisation experiments, also on bench scale, to determine the conditions which result in highest bio-oil quality at a sufficient yield. From the bench experiments, Al_2O_3 was found to promote mostly decarbonylation reactions, CaO dehydration reactions and MgO decarboxylation reactions. It was difficult to select a best performing catalyst at bench scale, as the 3 catalysts selected from literature had the similar performances at 550 °C and 30 wt.% C_{cat} (HHV between 26.3 – 26.8 MJ/kg). CaO was the preferred catalyst because it had the highest gross energy yield as calculated by an energy conversion assessment.

The char product from *in situ* catalytic pyrolysis is not ideal for energy generation due to low overall calorific value because of its high content of inorganics. It is more suitable for soil amendment applications with the char from catalytic pyrolysis using CaO being the most suitable for such applications due to similarities with agricultural lime. MgO derived char has the potential to neutralise soil acidity and improve the magnesium content of the soil. Char containing Al_2O_3 should not be used for such applications as it can potentially increase the toxicity of the soil. This consideration comforted the selection of CaO catalyst.

The MgO optimisation experiments showed that the optimum bio-oil yield occurred in the temperature range of 530 – 560 °C and a catalyst range of 25 – 35 wt.%, which were also the ranges for maximum bio-oil HHV. Based on the experimental data, it appeared that ketonisation was the main mechanism by which deoxygenation occurred when MgO catalyst was used. For CaO, the maximum bio-oil HHV was 27.5 MJ/kg at a yield of 13.4 wt.% (obtained at 490 °C and 59.0 wt.% C_{cat}). This bio-oil yield was too low to meet the blending ratio requirements in South Africa. Therefore, desirability function analysis was used to find a compromise optimum, which was 26.4 MJ/kg bio-oil HHV and 18.5 wt.% bio-oil yield, at 550 °C and 30 wt.% C_{cat} (catalyst screening conditions).

CaO absorbed CO_2 during pyrolysis and coupled with the water production, it influenced the equilibrium of the gaseous phase via the water-gas shift reaction (WGSR) leading to a significant production of hydrogen. Because of the CO_2 absorption by CaO, a significant increase in the char yield was observed as C_{cat} increased. The results from the study suggested that water production is the limiting factor in the WGSR. Besides the promotion of dehydration reactions, CaO was found to significantly promote decarbonylation and cracking reactions as well. The activity of the catalyst was found to be dependent on temperature. When the catalyst loading was high (> 30 wt.%), elevated temperatures (≥ 550 °C) resulted in the production of significant amounts of water, CO and C_xH_y gases. When considering the gas product for combustion to provide some heat for the process, the relatively high proportion of fuel gas appears as another advantage of the CaO catalytic conversion.

The conditions on the bench scale could not be upscaled directly on to the pilot due to the significant difference between the volatile and char/catalyst contact between the two reactors. Better contact on the pilot meant that a lower temperature (500 °C from 550 °C on bench scale) had to be used, to minimise the catalytic cracking effect. Because of the greater volatile/catalyst contact on the pilot, volatile deoxygenation was enhanced on pilot scale, resulting in a bio-oil with a much higher HHV (35.5 MJ/kg) compared to a maximum bio-oil HHV of 27.5 MJ/kg on bench scale.

8.2 Recommendations

Based on the reviewed literature, the quality of the bio-oil found in this study, 12.6 wt.% oxygen and < 20 wt.% water content, is good enough for co-processing in an oil refinery at a 10 wt.% blending ratio. However, it is recommended that this oil be tested in an FCC to confirm that it is indeed suitable.

The results obtained at 500 °C and 30 wt.% C_{cat} on the pilot scale were satisfactory. However, fine-tuning of these reaction conditions is still possible for and could lead to improved results, for example a higher bio-oil yield.

The condensation system of the pilot plant rig could be improved by designing an ESP which may lead to the condensation of more volatiles and improve the mass balance closure.

Gas chromatography – mass spectrometry (GC-MS) to identify compounds in pyrolysis liquid products was not done in this study. It is recommended that it be done to confirm the proposed reaction mechanisms.

References

Ackerman, Pierre, Cori Ham, Steven Dovey, Ben Du Toit, John De Wet, Anton Kunneke, and Thomas Seifert. 2013. "State of the Art Use of Forest Residues for Bioenergy in Southern Africa." Stellenbosch.

Adjaye, J D, and N N Bakhshi. 1995. "Production of Hydrocarbons by Catalytic Upgrading of a Fast Part I : Conversion over Various Catalysts." *Fuel Processing Technology* 45: 161–83.

Aguado, Roberta, Martin Olazar, María José San José, Gorka Aguirre, and Javier Bilbao. 2000. "Pyrolysis of Sawdust in a Conical Spouted Bed Reactor. Yields and Product Composition." *Industrial and Engineering Chemistry Research* 39 (6): 1925–33. doi:10.1021/ie990309v.

Alakangas, Eija, and Risto Impola. 2015. "Quality Guidelines for Wood Fuels in Finland." Espoo. doi:10.13140/RG.2.1.3290.3127.

AlGhamdi, K, Justin S J Hargreaves, and S David Jackson. 2009. "Base Catalysis with Metal Oxides." In *Metal Oxide Catalysis*, edited by S. David Jackson and Justin S J Hargreaves, 1–2:819–66. Weinheim: WILEY-VCH. doi:10.1002/9783527626113.

Alves, S. S., and J. L. Figueiredo. 1989. "A Model for Pyrolysis of Wet Wood." *Chemical Engineering Science* 44 (12): 2861–69. doi:10.1016/0009-2509(89)85096-1.

Auta, M., L. M. Ern, and B. H. Hameed. 2014. "Fixed-Bed Catalytic and Non-Catalytic Empty Fruit Bunch Biomass Pyrolysis." *Journal of Analytical and Applied Pyrolysis* 107. Elsevier B.V.: 67–72. doi:10.1016/j.jaap.2014.02.004.

Aysu, Tevfik. 2015. "Catalytic Pyrolysis of Eremurus Spectabilis for Bio-Oil Production in a Fixed-Bed Reactor: Effects of Pyrolysis Parameters on Product Yields and Character." *Fuel Processing Technology* 129: 24–38. doi:10.1016/j.fuproc.2014.08.014.

Balat, Mustafa, Mehmet Balat, Elif Kirtay, and Havva Balat. 2009. "Main Routes for the Thermo-Conversion of Biomass into Fuels and Chemicals. Part 1: Pyrolysis Systems." *Energy Conversion and Management* 50 (12). Elsevier Ltd: 3147–57. doi:10.1016/j.enconman.2009.08.014.

Benallal, B., C. Roy, H. Pakdel, S. Chabot, and M. A. Poirier. 1995. "Characterization of Pyrolytic Light Naphtha from Vacuum Pyrolysis of Used Tyres Comparison with Petroleum Naphtha." *Fuel* 74 (11): 1589–94. doi:10.1016/0016-2361(95)00165-2.

Bridgwater, A. V. 2003. "Renewable Fuels and Chemicals by Thermal Processing of Biomass." *Chemical Engineering Journal* 91 (2–3): 87–102. doi:10.1016/S1385-8947(02)00142-0.

———. 2012. "Review of Fast Pyrolysis of Biomass and Product Upgrading." *Biomass and Bioenergy* 38. Elsevier Ltd: 68–94. doi:10.1016/j.biombioe.2011.01.048.

Burkhardt, Sabrina, Linoj Kumar, Richard Chandra, and Jack Saddler. 2013. "How Effective Are Traditional Methods of Compositional Analysis in Providing an Accurate Material Balance for a Range of Softwood Derived Residues?" *Biotechnology for Biofuels* 6 (1): 90–100. doi:10.1186/1754-6834-6-90.

Carrier, Marion, Thomas Hugo, Johann Gorgens, and Hansie Knoetze. 2011. "Comparison of Slow and Vacuum Pyrolysis of Sugar Cane Bagasse." *Journal of Analytical and Applied Pyrolysis* 90 (1). Elsevier B.V.: 18–26. doi:10.1016/j.jaap.2010.10.001.

Chen, Xu, Yingquan Chen, Haiping Yang, Wei Chen, Xianhua Wang, and Hanping Chen. 2017. "Fast Pyrolysis of Cotton Stalk Biomass Using Calcium Oxide." *Bioresource Technology* 233. Elsevier Ltd: 15–20. doi:10.1016/j.biortech.2017.02.070.

Collard, François-Xavier, and Joël Blin. 2014. "A Review on Pyrolysis of Biomass Constituents: Mechanisms and Composition of the Products Obtained from the Conversion of Cellulose, Hemicelluloses and Lignin." *Renewable and Sustainable Energy Reviews* 38. Elsevier: 594–608. doi:10.1016/j.rser.2014.06.013.

Collard, François Xavier, Joël Blin, Ammar Bensakhria, and Jérémy Valette. 2012. "Influence of Impregnated Metal on the Pyrolysis Conversion of Biomass Constituents." *Journal of Analytical and Applied Pyrolysis* 95 (January). Elsevier B.V.: 213–26. doi:10.1016/j.jaap.2012.02.009.

Cosimo, Juana I. Di, and Carlos R. Apesteguía. 1998. "Study of the Catalyst Deactivation in the Base-Catalyzed Oligomerization of Acetone." *Journal of Molecular Catalysis A: Chemical*

130 (1–2): 177–85. doi:10.1016/S1381-1169(97)00204-5.

Czernik, Stefan, and A. V. Bridgwater. 2004. "Overview of Applications of Biomass Fast Pyrolysis Oil." *Energy & Fuels* 18 (2): 590–598. doi:10.1021/ef034067u.

Davidian, Thomas, Nolven Guilhaume, Cécile Daniel, and Claude Mirodatos. 2008. "Continuous Hydrogen Production by Sequential Catalytic Cracking of Acetic Acid. Part I. Investigation of Reaction Conditions and Application to Two Parallel Reactors Operated Cyclically." *Applied Catalysis A: General* 335 (1): 64–73. doi:10.1016/j.apcata.2007.11.010.

Demirbas, Ayhan. 2007. "The Influence of Temperature on the Yields of Compounds Existing in Bio-Oils Obtained from Biomass Samples via Pyrolysis." *Fuel Processing Technology* 88 (6): 591–97. doi:10.1016/j.fuproc.2007.01.010.

Deng, Li, Yao Fu, and Qing Xiang Guo. 2009. "Upgraded Acidic Components of Bio-Oil through Catalytic Ketonic Condensation." *Energy and Fuels* 23 (1): 564–68. doi:10.1021/ef800692a.

Dhyani, Vaibhav, and Thallada Bhaskar. 2018. "A Comprehensive Review on the Pyrolysis of Lignocellulosic Biomass." *Renewable Energy* 129. Elsevier Ltd: 695–716. doi:10.1016/j.renene.2017.04.035.

Dielbold, J.; 2000. "A Review of the Chemical and Physical Mechanisms of the Storage Stability of Fast Pyrolysis Bio-Oils; Report No. NREL/ SR-570-27613." Golden. doi:10.2172/753818.

Díez, V. K., C. R. Apesteguía, and J. I. Di Cosimo. 2006. "Aldol Condensation of Citral with Acetone on MgO and Alkali-Promoted MgO Catalysts." *Journal of Catalysis* 240 (2): 235–44. doi:10.1016/j.jcat.2006.04.003.

Dovey, S B. 2009. "Estimating Biomass and Macronutrient Content of Some Commercially Important Plantation Species in South Africa." *Southern Forests: A Journal of Forest Science* 71 (921023905): 245–51. doi:10.2989/SF.2009.71.3.9.921.

Du, Shoucheng, Julia Valla, and George M Bollas. 2010. "Characteristics and Origin of Char and Coke from Fast and Slow, Catalytic and Thermal Pyrolysis of Biomass and Relevant Model Compounds." *Green Chemistry* 15 (11): 3214–29. doi:10.1039/C3GC41581C.

Ellig, Daniel L., Chiu K. Lai, David W. Mead, John P. Longwell, and William A. Peters. 1985. "Pyrolysis of Volatile Aromatic Hydrocarbons and N-Heptane Over Calcium Oxide and Quartz." *Industrial and Engineering Chemistry Process Design and Development* 24 (4): 1080–87. doi:10.1021/i200031a031.

Emmel, Alexandre, Alvaro L. Mathias, Fernando Wypych, and Luiz P. Ramos. 2003. "Fractionation of Eucalyptus Grandis Chips by Dilute Acid-Catalysed Steam Explosion." *Bioresource Technology* 86 (2): 105–15. doi:10.1016/S0960-8524(02)00165-7.

Encinar, J M, J F Gonzalez, and J Gonzalez. 2000. "Fixed-Bed Pyrolysis of Cynara Cardunculus L. Product Yields and Compositions." *Fuel Processing Technology* 68 (3): 209–22. doi:10.1016/S0378-3820(00)00125-9.

Ertaş, Murat, and M. Hakki Alma. 2010. "Pyrolysis of Laurel (Laurus Nobilis L.) Extraction Residues in a Fixed-Bed Reactor: Characterization of Bio-Oil and Bio-Char." *Journal of Analytical and Applied Pyrolysis* 88 (1): 22–29. doi:10.1016/j.jaap.2010.02.006.

European Biomass Industry Assocition. 2017. "Recovery of Forest Residues." http://www.eubia.org/cms/wiki-biomass/biomass-procurement/recovery-of-forest-residues/.

Fogassy, Gabriella, Nicolas Thegarid, Guy Toussaint, Andre C. van Veen, Yves Schuurman, and Claude Mirodatos. 2010. "Biomass Derived Feedstock Co-Processing with Vacuum Gas Oil for Second-Generation Fuel Production in FCC Units." *Applied Catalysis B: Environmental* 96 (3–4). Elsevier B.V.: 476–85. doi:10.1016/j.apcatb.2010.03.008.

Forestry Economics Services. 2015. "Report on Commercial Timber Resources and Primary Roundwood Processing in South Africa." Vol. 00. Pretoria. doi:10.1163/9789004272224_029.

Fu, Da qing, Xiao hong Li, Wen ying Li, and Jie Feng. 2018. "Catalytic Upgrading of Coal Pyrolysis Products over Bio-Char." *Fuel Processing Technology* 176 (January). Elsevier: 240–48. doi:10.1016/j.fuproc.2018.04.001.

Funke, Axel, Marco Tomasi Morgano, Nicolaus Dahmen, and Hans Leibold. 2017. "Experimental Comparison of Two Bench Scale Units for Fast and Intermediate Pyrolysis." *Journal of*

Analytical and Applied Pyrolysis 124. Elsevier B.V.: 504–14. doi:10.1016/j.jaap.2016.12.033.

Garcìa-Pérez, M., A. Chaala, H. Pakdel, D. Kretschmer, and C. Roy. 2007. "Vacuum Pyrolysis of Softwood and Hardwood Biomass. Comparison between Product Yields and Bio-Oil Properties." *Journal of Analytical and Applied Pyrolysis* 78 (1): 104–16. doi:10.1016/j.jaap.2006.05.003.

Garcia-Perez, Manuel, Xiao Shan Wang, Jun Shen, Martin J. Rhodes, Fujun Tian, Woo Jin Lee, Hongwei Wu, and Chun Zhu Li. 2008. "Fast Pyrolysis of Oil Mallee Woody Biomass: Effect of Temperature on the Yield and Quality of Pyrolysis Products." *Industrial and Engineering Chemistry Research* 47 (6): 1846–54. doi:10.1021/ie071497p.

Gellerstedt, Göran, Monica Ek, and Gunnar Henriksson. 2009. *Wood Chemistry and Biotechnology*. *Wood Chemistry and Biotechnology*. Vol. 1. Berlin. doi:10.1515/9783110213409.

Gliński, M., J. Kijeński, and A. Jakubowski. 1995. "Ketones from Monocarboxylic Acids: Catalytic Ketonization over Oxide Systems." *Applied Catalysis A, General* 128 (2): 209–17. doi:10.1016/0926-860X(95)00082-8.

Goyal, H. B., Diptendu Seal, and R. C. Saxena. 2008. "Bio-Fuels from Thermochemical Conversion of Renewable Resources: A Review." *Renewable and Sustainable Energy Reviews* 12 (2): 504–17. doi:10.1016/j.rser.2006.07.014.

Green, Don W, and Robert H Perry. 2007. *Perry's Chemical Engineers' Handbook (8th Edition)*. 8th ed. Blacklick: McGraw-Hill Professional Publishing.

Guoxin, Hu, and Huang Hao. 2009. "Hydrogen Rich Fuel Gas Production by Gasification of Wet Biomass Using a CO2 Sorbent." *Biomass and Bioenergy* 33 (5). Elsevier Ltd: 899–906. doi:10.1016/j.biombioe.2009.02.006.

Hervy, Maxime, Audrey Villot, Claire Gérente, Doan Pham Minh, Elsa Weiss-Hortala, Ange Nzihou, and Laurence Le Coq. 2018. "Catalytic Cracking of Ethylbenzene as Tar Surrogate Using Pyrolysis Chars from Wastes." *Biomass and Bioenergy* 117 (August). Elsevier Ltd:

86–95. doi:10.1016/j.biombioe.2018.07.020.

Hill, Dennis. 2011. "Oil & Natural Gas Technology North Dakota Refining Capacity Study." Mandan. https://www.netl.doe.gov/file library/Research/oil-gas/FE0000516_FinalReport.pdf.

Hornung, A, A Apfelbacher, and S Sagi. 2011. "Intermediate Pyrolysis: A Sustainable Biomass-to-Energy Concept-Biothermal Valorisation of Biomass (BtVB) Process." *Journal of Scientific and Industrial Research* 70 (8): 664–67.

Huber, George W., Iborra Sara, and Avelino Corma. 2006. "Synthesis of Transportation Fuels from Biomass." *Chem Rev.* 2 (106): 4044–98.

Hui-Peng, L, S Jian, Z Hua, Z Li, and Q Yu-Tai. 2009. "Effects of Phenols on the Stability of Fcc Diesel Fuel." *Petroleum Science and Technology* 27 (5): 486–97. doi:10.1080/10916460802097269.

Imran, Ali, Eddy A. Bramer, Kulathuiyer Seshan, and Gerrit Brem. 2014. "High Quality Bio-Oil from Catalytic Flash Pyrolysis of Lignocellulosic Biomass over Alumina-Supported Sodium Carbonate." *Fuel Processing Technology* 127. Elsevier B.V.: 72–79. doi:10.1016/j.fuproc.2014.06.011.

Inalbon, María C., Paulina Mocchiutti, Miguel A. Zanuttini, Pedro A. Balatti, Mario Rajchenberg, and Mario C.N. Saparrat. 2015. "Applying Ligninolytic Fungi on Eucalyptus Grandis Wood for Pulping Pretreatment or Fractionation." *Procedia Materials Science* 8. Elsevier B.V.: 1099–1107. doi:10.1016/j.mspro.2015.04.173.

Joubert, Jan-Erns. 2013. "Pyrolysis of Eucalyptus Grandis." Stellenbosch University.

Junginger, Martin, C S Goh, and A Faaij. 2014. *International Bioenergy Trade: History Status & Outlook on Securing Sustainable Bioenergy Supply, Demand and Markets*. *Lecture Notes in Energy 17*. doi:10.1007/978-94-007-6982-3.

Kim, Pyoungchung, Samuel Weaver, and Nicole Labbé. 2016. "Effect of Sweeping Gas Flow Rates on Temperature-Controlled Multistage Condensation of Pyrolysis Vapors in an Auger Intermediate Pyrolysis System." *Journal of Analytical and Applied Pyrolysis* 118. Elsevier

B.V.: 325–34. doi:10.1016/j.jaap.2016.02.017.

Kookana, R. S., A. K. Sarmah, L. Van Zwieten, E. Krull, and B. Singh. 2011. *Biochar Application to Soil. Agronomic and Environmental Benefits and Unintended Consequences*. *Advances in Agronomy*. 1st ed. Vol. 112. Elsevier Inc. doi:10.1016/B978-0-12-385538-1.00003-2.

Kotz, John C, Paul M Treichel, and John R Townsend. 2010. *Chemistry & Chemical Reactivity*. 7th ed. Belmont: Cengage Learning. doi:10.1016/B978-0-12-810425-5.00002-3.

Lappas, A. A., M. C. Samolada, D. K. Iatridis, S. S. Voutetakis, and I. A. Vasalos. 2002. "Biomass Pyrolysis in a Circulating Fluid Bed Reactor for the Production of Fuels and Chemicals." *Fuel* 81 (16): 2087–95. doi:10.1016/S0016-2361(02)00195-3.

Li, R., Z. P. Zhong, B. S. Jin, and A. J. Zheng. 2012. "Application of Mineral Bed Materials during Fast Pyrolysis of Rice Husk to Improve Water-Soluble Organics Production." *Bioresource Technology* 119: 324–30. doi:10.1016/j.biortech.2012.05.099.

Lin, Yuyu, Chu Zhang, Mingchuan Zhang, and Jian Zhang. 2010. "Deoxygenation of Bio-Oil during Pyrolysis of Biomass in the Presence of CaO in a Fluidized-Bed Reactor." *Energy & Fuels* 24 (10): 5686–95. doi:10.1021/ef1009605.

Ly, Hoang Vu, Dong-Hyeon Lim, Jae Wook Sim, Seung-Soo Kim, and Jinsoo Kim. 2018. "Catalytic Pyrolysis of Tulip Tree (Liriodendron) in Bubbling Fluidized-Bed Reactor for Upgrading Bio-Oil Using Dolomite Catalyst." *Energy* 162. Elsevier Ltd: 564–75. doi:10.1016/j.energy.2018.08.001.

Maneewan, Kodchanipa, Supachita Krerkkaiwan, Sasithorn Sunphorka, Tharapong Vitidsant, and Prapan Kuchonthara. 2014. "Catalytic Effect of Biomass Pyrolyzed Char on the Atmospheric Pressure Hydrogasification of Giant Leucaena (Leucaena Leucocephala) Wood." *Industrial and Engineering Chemistry Research* 53 (30): 11913–19. doi:10.1021/ie501805e.

Mannekus & Co. B.V., Van. 2013. "Feritilizers." http://www.mannekus.com/fertilizers/.

Mante, Ofei D, and F A Agblevor. 2014. "Catalytic Pyrolysis for the Production of Refinery-Ready Biocrude Oils from Six Different Biomass Sources." *Green Chemistry* 16 (6): 3364. doi:10.1039/c4gc00555d.

Marinangeli, Richard, Terry Marker, John Petri, Tom Kalnes, Mike Mccall, Dave Mackowiak, Bob Jerosky, Bill Reagan, Lazlo Nemeth, and Mark Krawczyk. 2005. "OPPORTUNITIES FOR BIORENEWABLES IN OIL REFINERIES."

Mason, David M., and Kiran N. Gandhi. 1983. "Formulas for Calculating the Calorific Value of Coal and Coal Chars: Development, Tests, and Uses." *Fuel Processing Technology* 7 (1): 11–22. doi:10.1016/0378-3820(83)90022-X.

Melzer, Michael, Joël Blin, Ammar Bensakhria, Jeremy Valette, and François Broust. 2013. "Pyrolysis of Extractive Rich Agroindustrial Residues." *Journal of Analytical and Applied Pyrolysis* 104: 448–60. doi:10.1016/j.jaap.2013.05.027.

Miguel Mercader, F. de, M. J. Groeneveld, S. R A Kersten, N. W J Way, C. J. Schaverien, and J. A. Hogendoorn. 2010. "Production of Advanced Biofuels: Co-Processing of Upgraded Pyrolysis Oil in Standard Refinery Units." *Applied Catalysis B: Environmental* 96 (1–2). Elsevier B.V.: 57–66. doi:10.1016/j.apcatb.2010.01.033.

Mihalcik, David J., Charles A. Mullen, and Akwasi A. Boateng. 2011. "Screening Acidic Zeolites for Catalytic Fast Pyrolysis of Biomass and Its Components." *Journal of Analytical and Applied Pyrolysis* 92 (1): 224–32. doi:10.1016/j.jaap.2011.06.001.

Morf, Philipp, Philipp Hasler, and Thomas Nussbaumer. 2002. "Mechanisms and Kinetics of Homogeneous Secondary Reactions of Tar from Continuous Pyrolysis of Wood Chips." *Fuel* 81 (7): 843–53. doi:10.1016/S0016-2361(01)00216-2.

Nambiar, E K Sadanandan, and M H Kallio. 2008. "Increasing and Sustaining Productivity in Subtropical and Tropical Plantation Forests: Making a Difference through Research Partnership." In *Site Management and Productivity in Tropical Plantation Forests: Proceedings of Workshops in Piracicaba (Brazil) 22-26 November 2004 and Bogor (Indonesia) 6-9 November 2006*, edited by E K Sadanandan Nambiar, 205–27. Bogor: Center For International Forestry Research (CIFOR).

Naqvi, Salman Raza, Yoshimitsu Uemura, and Suzana Bt Yusup. 2014. "Catalytic Pyrolysis of Paddy Husk in a Drop Type Pyrolyzer for Bio-Oil Production: The Role of Temperature and Catalyst." *Journal of Analytical and Applied Pyrolysis* 106. Elsevier B.V.: 57–62.

doi:10.1016/j.jaap.2013.12.009.

Ndou, A. S., and N. J. Coville. 2004. "Self-Condensation of Propanol over Solid-Base Catalysts." *Applied Catalysis A: General* 275 (1–2): 103–10. doi:10.1016/j.apcata.2004.07.025.

Neves, Daniel, Henrik Thunman, Arlindo Matos, Luis Tarelho, and Alberto Gomez-Barea. 2011. "Characterization and Prediction of Biomass Pyrolysis Products." *Progress in Energy and Combustion Science* 37 (5). Elsevier Ltd: 611–30. doi:10.1016/j.pecs.2011.01.001.

"NIST/SEMATECH e-Handbook of Statistical Methods." 2012. http://www.itl.nist.gov/div898/handbook/.

Nowakowski, Daniel J., and Jenny M. Jones. 2008. "Uncatalysed and Potassium-Catalysed Pyrolysis of the Cell-Wall Constituents of Biomass and Their Model Compounds." *Journal of Analytical and Applied Pyrolysis* 83 (1): 12–25. doi:10.1016/j.jaap.2008.05.007.

Nsaful, Frank, François Xavier Collard, and Johann F. Görgens. 2018. "Lignocellulose Thermal Pretreatment and Its Effect on Fuel Properties and Composition of the Condensable Products (Tar Precursors) from Char Devolatilization for Coal Substitution in Gasification Application." *Fuel Processing Technology* 179 (March). Elsevier: 334–43. doi:10.1016/j.fuproc.2018.07.015.

Oasmaa, Anja, and E. Kuoppala. 2003. "Fast Pyrolysis of Forestry Residue. 3. Storage Stability of Liquid Fuel." *Energy and Fuels* 17 (4): 1075–84. doi:10.1021/ef030011o.

Oasmaa, Anja, E. Kuoppala, S. Gust, and Y. Solantausta. 2003. "Fast Pyrolysis of Forestry Residue. 1. Effect of Extractives on Phase Separation of Pyrolysis Liquids." *Energy and Fuels* 17 (1): 1–12. doi:10.1021/ef020088x.

Oasmaa, Anja, Solanta, Yrjö Usta, Vesa Arpiainen, Eeva Kuoppala, and Kai Sipilä. 2010. "Fast Pyrolysis Bio-Oils from Wood and Agricultural Residues." *Energy and Fuels* 24 (2): 1380–88. doi:10.1021/ef901107f.

Paasikallio, Ville, Christian Lindfors, Eeva Kuoppala, Yrjo Solantausta, Anja Oasmaa, Jani Lehto, and Juha Lehtonen. 2014. "Product Quality and Catalyst Deactivation in a Four Day Catalytic Fast Pyrolysis Production Run." *Green Chemistry* 16 (7): 3549–59. doi:10.1039/c4gc00571f.

PAMSA. 2016. "South African and Global Forest Products Industry Welcomes UN Climate Change Agreement Signing." http://www.thepaperstory.co.za/2016/04/south-african-and-global-forest-products-industry-welcomes-un-climate-change-agreement-signing/.

Park, Ji Yeon, Minsu Kang, Jun Seok Kim, Joon Pyo Lee, Won Il Choi, and Jin Suk Lee. 2012. "Enhancement of Enzymatic Digestibility of Eucalyptus Grandis Pretreated by NaOH Catalyzed Steam Explosion." *Bioresource Technology* 123. Elsevier Ltd: 707–12. doi:10.1016/j.biortech.2012.07.091.

Pattiya, Adisak, James O. Titiloye, and A. V. Bridgwater. 2008. "Fast Pyrolysis of Cassava Rhizome in the Presence of Catalysts." *Journal of Analytical and Applied Pyrolysis* 81 (1): 72–79. doi:10.1016/j.jaap.2007.09.002.

Patwardhan, Pushkaraj R., Justinus A. Satrio, Robert C. Brown, and Brent H. Shanks. 2010. "Influence of Inorganic Salts on the Primary Pyrolysis Products of Cellulose." *Bioresource Technology* 101 (12). Elsevier Ltd: 4646–55. doi:10.1016/j.biortech.2010.01.112.

Pham, Tu N., Tawan Sooknoi, Steven P. Crossley, and Daniel E. Resasco. 2013. "Ketonization of Carboxylic Acids: Mechanism, Catalysts, and Implications for Biomass Concersion." *American Chemical Society Catalysis* 3: 2456–73.

Phillips, Lloyd. 2017. "How Biorefineries Can Add Value to Forestry Waste." *Farmer's Weekly*. http://www.farmersweekly.co.za/agri-business/agribusinesses/how-biorefineries-can-add-value-to-forestry-waste/.

Pütün, Ersan. 2010. "Catalytic Pyrolysis of Biomass: Effects of Pyrolysis Temperature, Sweeping Gas Flow Rate and MgO Catalyst." *Energy* 35 (7). Elsevier Ltd: 2761–66. doi:10.1016/j.energy.2010.02.024.

Puy, Neus, Ramón Murillo, María V. Navarro, José M. López, Joan Rieradevall, G. Fowler, Ignacio Aranguren, Tomás García, Jordi Bartrolí, and Ana M. Mastral. 2011. "Valorisation of Forestry Waste by Pyrolysis in an Auger Reactor." *Waste Management* 31 (6). Elsevier Ltd: 1339–49. doi:10.1016/j.wasman.2011.01.020.

Rezende Pinho, Andrea De, Marlon B B De Almeida, Fabio Leal Mendes, Vitor Loureiro

Ximenes, and Luiz Carlos Casavechia. 2015. "Co-Processing Raw Bio-Oil and Gasoil in an FCC Unit." *Fuel Processing Technology* 131. Elsevier B.V.: 159–66. doi:10.1016/j.fuproc.2014.11.008.

Rezende Pinho, Andrea De, Marlon B B DeAlmeida, Fabio Leal Mendes, Luiz Carlos Casavechia, S Talmadge Michael, Christopher M Kinchin, and Helena L Chum. 2017. "Fast Pyrolysis Oil from Pinewood Chips Co-Processing with Vacuum Gas Oil in an FCC Unit for Second Generation Fuel Production." *Fuel* 188. The Authors: 462–73. doi:10.1016/j.fuel.2016.10.032.

Richardson, Yohan, Joël Blin, Ghislaine Volle, Julius Motuzas, and Julbe. Anne. 2010. "In Situ Generation of Ni Metal Nanoparticles as Catalyst for H 2-Rich Syngas Production from Biomass Gasification." *Applied Catalysis A: General* 382: 220–30. doi:10.1016/j.apcata.2010.04.047.

Ridout, Angelo J., Marion Carrier, François Xavier Collard, and Johann Görgens. 2016. "Energy Conversion Assessment of Vacuum, Slow and Fast Pyrolysis Processes for Low and High Ash Paper Waste Sludge." *Energy Conversion and Management* 111. Elsevier Ltd: 103–14. doi:10.1016/j.enconman.2015.12.043.

Rowell, Roger M, Roger Pettersen, James S Han, Jeffrey S Rowell, and Mandla A Tshabalala. 2005. "Cell Wall Chemistry." In *Handbook of Wood Chemistry and Wood Composites*, edited by Roger M Rowell. Boca Raton: CRC Press. doi:10.1016/j.jclepro.2015.07.070.

Roy, C, M Hebert, W Kalkreuth, A E Schwerdtfeger, W Kalkreuthc, and A E Schwerdtfegera. 1998. "Conversion Characteristics Of Canadian Coals Subjected to Vacuum Pyrolysis Treatment." *Fuel* 77 (3): 197–208.

Russell, Scott H., Juan Luis Turrion-Gomez, Will Meredith, Paul Langston, and Colin E. Snape. 2017. "Increased Charcoal Yield and Production of Lighter Oils from the Slow Pyrolysis of Biomass." *Journal of Analytical and Applied Pyrolysis*. Elsevier B.V., 1–6. doi:10.1016/j.jaap.2017.01.028.

Samac, D a, and M Tesfaye. 2003. "Plant Impovement for Tolerance to Aluminum in Acid Soils - a Review." *Plant Cell, Tissue and Organ Culture* 75: 189–207.

Sergeev, Alexey G., and John F. Hartwig. 2011. "Selective, Nickel-Catalyzed Hydrogenolysis of Aryl Ethers." *Science* 332 (June): 439–43.

Serrano-Ruiz, Juan Carlos, and James A Dumesic. 2012. "Catalytic Production of Liquid Hydrocarbon Transportation Fuels." In *Catalysis for Alternative Energy Generation*, edited by Laszlo Guczi and Erdohelyi Andras, 29–56. New York: Springer. doi:10.1007/978-1-4614-0344-9.

Shadangi, Krushna Prasad, and Kaustubha Mohanty. 2014a. "Comparison of Yield and Fuel Properties of Thermal and Catalytic Mahua Seed Pyrolytic Oil." *Fuel* 117 (PART A). Elsevier Ltd: 372–80. doi:10.1016/j.fuel.2013.09.001.

———. 2014b. "Thermal and Catalytic Pyrolysis of Karanja Seed to Produce Liquid Fuel." *Fuel* 115. Elsevier Ltd: 434–42. doi:10.1016/j.fuel.2013.07.053.

Shen, Jun, Xiao-Shan Wang, Manuel Garcia-Perez, Daniel Mourant, Martin J Rhodes, and Chun-Zhu Li. 2009. "Effects of Particle Size on the Fast Pyrolysis of Oil Mallee Woody Biomass." *Fuel* 88 (10). Elsevier Ltd: 1810–17. doi:10.1016/j.fuel.2009.05.001.

Sjöström, E. 1993. *Wood Chemistry, Fundamentals and Applications*. *Carbohydrate Research*. 2nd ed. Vol. 252. San Diego: ACADEMIC PRESS, INC. doi:10.1016/0008-6215(94)90030-2.

Sluiter, A., B. Hames, R. Ruiz, C. Scarlata, J. Sluiter, D. Templeton, and D. Crocker. 2012. "Determination of Structural Carbohydrates and Lignin in Biomass: Laboratory Analytical Procedure (LAP)." *Technical Report NREL/TP-510-42618*. Golden. doi:NREL/TP-510-42618.

Sluiter, A., R. Ruiz, C. Scarlata, J . Sluiter, and D. Templeton. 2008. "Determination of Extractives in Biomass: Laboratory Analytical Procedure (LAP)." *Technical Report NREL/TP-510-42619*. Golden. doi:NREL/TP-510-42621.

Sluiter, A, B Hames, D Hyman, C Payne, R Ruiz, C Scarlata, J Sluiter, D Templeton, and J Wolfe Nrel. 2008. "Determination of Total Solids in Biomass and Total Dissolved Solids in Liquid Process Samples." *National Renewable Energy Laboratory (NREL)*. doi:NREL/TP-510-

42621.

Sluiter, A, B Hames, R Ruiz, C Scarlata, J Sluiter, and D Templeton. 2008. "Determination of Ash in Biomass: Laboratory Analytical Procedure (LAP)." *Nrel/Tp-510-42622*. doi:NREL/TP-510-42619.

Sohaib, Qazi, Muddasar Habib, Syed Fawad Ali Shah, Unsia Habib, and Sana Ullah. 2017. "Fast Pyrolysis of Locally Available Green Waste at Different Residence Time and Temperatures." *Energy Sources, Part A: Recovery, Utilization and Environmental Effects* 39 (15). Taylor & Francis: 1639–46. doi:10.1080/15567036.2017.1363830.

Sohi, S. P., E. Krull, E. Lopez-Capel, and R. Bol. 2010. "A Review of Biochar and Its Use and Function in Soil." *Advances in Agronomy* 105 (1): 47–82. doi:10.1016/S0065-2113(10)05002-9.

South African Petroleum Industry Association. 2014. "South African Fuel Industry." http://www.sapia.org.za/Overview/South-African-fuel-industry.

Stefanidis, S. D., K. G. Kalogiannis, E. F. Iliopoulou, A. A. Lappas, and P. A. Pilavachi. 2011. "In-Situ Upgrading of Biomass Pyrolysis Vapors: Catalyst Screening on a Fixed Bed Reactor." *Bioresource Technology* 102 (17). Elsevier Ltd: 8261–67. doi:10.1016/j.biortech.2011.06.032.

Stefanidis, S. D., S. A. Karakoulia, K. G. Kalogiannis, E. F. Iliopoulou, A. Delimitis, H. Yiannoulakis, T. Zampetakis, A. A. Lappas, and K. S. Triantafyllidis. 2016. "Natural Magnesium Oxide (MgO) Catalysts: A Cost-Effective Sustainable Alternative to Acid Zeolites for the in Situ Upgrading of Biomass Fast Pyrolysis Oil." *Applied Catalysis B: Environmental* 196. Elsevier B.V.: 155–73. doi:10.1016/j.apcatb.2016.05.031.

Stillwell, Ashlynn, and Michael Webber. 2016. "Predicting the Specific Energy Consumption of Reverse Osmosis Desalination." *Water* 8 (12): 601. doi:10.3390/w8120601.

Thegarid, N., G. Fogassy, Y. Schuurman, C. Mirodatos, S. Stefanidis, E. F. Iliopoulou, K. Kalogiannis, and A. A. Lappas. 2014. "Second-Generation Biofuels by Co-Processing Catalytic Pyrolysis Oil in FCC Units." *Applied Catalysis B: Environmental* 145. Elsevier

B.V.: 161–66. doi:10.1016/j.apcatb.2013.01.019.

Tripathi, Manoj, J. N. Sahu, and P. Ganesan. 2016. "Effect of Process Parameters on Production of Biochar from Biomass Waste through Pyrolysis: A Review." *Renewable and Sustainable Energy Reviews* 55. Elsevier: 467–81. doi:10.1016/j.rser.2015.10.122.

Veses, A., M. Aznar, J. M. López, M. S. Callén, R. Murillo, and T. García. 2015. "Production of Upgraded Bio-Oils by Biomass Catalytic Pyrolysis in an Auger Reactor Using Low Cost Materials." *Fuel* 141. Elsevier Ltd: 17–22. doi:10.1016/j.fuel.2014.10.044.

Veses, A., M. Aznar, I. Martínez, J. D. Martínez, J. M. López, M. V. Navarro, M. S. Callén, R. Murillo, and T. García. 2014. "Catalytic Pyrolysis of Wood Biomass in an Auger Reactor Using Calcium-Based Catalysts." *Bioresource Technology* 162. Elsevier Ltd: 250–58. doi:10.1016/j.biortech.2014.03.146.

Wang, Xiaoquan, Sascha R. a. Kersten, Wolter Prins, and Wim P. M. van Swaaij. 2005. "Biomass Pyrolysis in a Fluidized Bed Reactor. Part 2: Experimental Validation of Model Results." *Ind. Eng. Chem. Res.* 44 (23): 8786–95. doi:10.1021/ie050486y.

Widyawati, Meilina, Tamara L Church, Nicholas H Florin, and Andrew T Harris. 2011. "Hydrogen Synthesis from Biomass Pyrolysis with in Situ Carbon Dioxide Capture Using Calcium Oxide." *International Journal of Hydrogen Energy* 36 (8). Elsevier Ltd: 4800–4813. doi:10.1016/j.ijhydene.2010.11.103.

Wiedenhoeft, Alex C, and Regis B Miller. 2005. "Structure and Function of Wood." In *Handbook of Wood Chemistry and Wood Composites*, edited by Roger M Rowell. Boca Raton: CRC Press. doi:10.1016/j.jclepro.2015.07.070.

Xiao, Yang, and Arvind Varma. 2015. "Catalytic Deoxygenation of Guaiacol Using Methane." *ACS Sustainable Chemistry and Engineering* 3 (11): 2606–10. doi:10.1021/acssuschemeng.5b00669.

Yan, Hao, Xiang Feng, Yibin Liu, Chaohe Yang, and Honghong Shan. 2017. "Catalytic Cracking of Acetic Acid and Its Ketene Intermediate over HZSM-5 Catalyst: A Density Functional Theory Study." *Molecular Catalysis* 437. Elsevier B.V.: 11–17.

doi:10.1016/j.mcat.2017.04.038.

Yildiz, Güray, Marty Pronk, Marko Djokic, Kevin M. Van Geem, Frederik Ronsse, Ruben Van Duren, and Wolter Prins. 2013. "Validation of a New Set-up for Continuous Catalytic Fast Pyrolysis of Biomass Coupled with Vapour Phase Upgrading." *Journal of Analytical and Applied Pyrolysis* 103. Elsevier B.V.: 343–51. doi:10.1016/j.jaap.2013.02.001.

Yildiz, Güray, Frederik Ronsse, Ruben Van Duren, and Wolter Prins. 2016. "Challenges in the Design and Operation of Processes for Catalytic Fast Pyrolysis of Woody Biomass." *Renewable and Sustainable Energy Reviews* 57. Elsevier: 1596–1610. doi:10.1016/j.rser.2015.12.202.

Yu, Qiang, Xinshu Zhuang, Zhenhong Yuan, Qiong Wang, Wei Qi, Wen Wang, Yu Zhang, Jingliang Xu, and Huijuan Xu. 2010. "Two-Step Liquid Hot Water Pretreatment of Eucalyptus Grandis to Enhance Sugar Recovery and Enzymatic Digestibility of Cellulose." *Bioresource Technology* 101 (13). Elsevier Ltd: 4895–99. doi:10.1016/j.biortech.2009.11.051.

Zhang, Huiyan, Jian Zheng, Rui Xiao, Yixuan Jia, Dekui Shen, Baosheng Jin, and Guomin Xiao. 2014. "Study on Pyrolysis of Pine Sawdust with Solid Base and Acid Mixed Catalysts by Thermogravimetry − Fourier Transform Infrared Spectroscopy and Pyrolysis − Gas Chromatography / Mass Spectrometry." *Energy & Fuels* 28: 4294–99. doi:doi.org/10.1021/ef500176w.

Zimdahl, Robert L. 2015. *Six Chemicals That Changed Agriculture*. London: ACADEMIC PRESS, INC.

Appendices

Appendix A: Forestry residue estimation data

A.1 Volume of sawlogs and poles sold from plantations by region (Forestry Economics Services 2015)

	Saw logs and poles (m3)					
Region	**Softwoods**	***E. grandis***	**Other gum**	**Wattle**	**Other hardwoods**	**Total**
Limpopo Province	234 214	79 021	38 006	0	0	351 241
Mpumalanga North	1 148 595	86 994	238	0	0	1 235 827
Central Districts	61 112	0	0	0	0	61 112
Mpumalanga South	776 294	10 939	5 927	0	4 320	797 480
Maputaland	0	47	0	0	0	47
Zululand	8 337	0	0	0	0	8 337
KZN Midlands	359 763	41 924	10 893	0	6	412 586
KZN North	93 121	9 928	433	0	0	103 482
KZN South	372 092	31 910	3 603	0	600	408 205
Eastern Cape	650 261	53 252	12 046	589	0	716 148
Southern Cape	557 563	7 451	0.00	0	0	565 014
Western Cape	160 943		450	0	0	161 393

A.2 Volume and mining timber sold from plantations by region (Forestry Economics Services 2015)

	Mining timber and pulpwood (m3)					
Region	**Softwoods**	***E. grandis***	**Other gum**	**Wattle**	**Other hardwoods**	**Total**
Limpopo Province	55 127	53 472	1 070	0	0	109 669
Mpumalanga North	407 311	455 547	15 774	0	0	878 632
Central Districts	277 170	0	36 402	330	0	313 901
Mpumalanga South	647 879	258 858	402 169	41 482	0	1 350 388
Maputaland	0	0	0	0	0	0
Zululand	3 175	898 451	325 358	19 575	0	1 246 560
KZN Midlands	479 863	800 435	697 688	327 238	0	2 305 225
KZN North	77 199	162 761	88 316	101 187	4 256	433 719
KZN South	485 548	372 248	418 978	100 030	1 555	1 378 359
Eastern Cape	360 130	162 498	35 766	1 395	3 726	563 516
Southern Cape	0	0	0	0	0	0
Western Cape	0	0	0	0	0	0

A.3 Volume of charcoal, firewood and other products sold from plantations by region

(Forestry Economics Services 2015)

	Charcoal, Firewood & Other Products (m3)					
Region	**Softwoods**	***E. grandis***	**Other gum**	**Wattle**	**Other hardwoods**	**Total**
Limpopo Province	15 980	10 342	4 752	0	0	31 074
Mpumalanga North	9 224	5 476	585	0	0	15 285
Central Districts	156	0	2 577	0	0	2 733
Mpumalanga South	4 780	6 070	8 270	8 194	640	27 954
Maputaland	0	0	0	0	0	0
Zululand	0	0	0	494	0	494
KZN Midlands	186	727	5 070	25 429	0	31 412
KZN North	912	3 462	3 770	61 439	0	69 584
KZN South	5 722	413	8	216	0	6 359
Eastern Cape	10 667	44 294	186	2 887	0	58 034
Southern Cape	0	0	0	0	0	0
Western Cape	0	0	0	0	0	0

A.4 Total volume of timber products sold from plantations by region

	Combined timber volume (m3)					
Region	**Softwoods**	***E. grandis***	**Other gum**	**Wattle**	**Other hardwoods**	**Total**
Limpopo Province	305 321	142 835	43 828	0	0	491 984
Mpumalanga North	1 565 130	548 017	16 596	0	0	2 129 744
Central Districts	338 438	0	38 978	330	0	377 746
Mpumalanga South	1 428 953	275 866	416 366	49 677	4 960	2 175 822
Maputaland	0	47	0	0	0	47
Zululand	11 512	898 451	325 358	20 069	0	1 255 390
KZN Midlands	839 812	843 086	713 651	352 667	6	2 749 222
KZN North	171 232	176 151	92 519	162 626	4 256	606 785
KZN South	863 362	404 571	422 589	100 246	2 155	1 792 923
Eastern Cape	1 021 058	260 043	47 999	4 871	3 726	1 337 698
Southern Cape	557 563	7 451	0	0	0	565 014
Western Cape	160 943	0	450	0	0	161 393

A.5 Total branch residues produced by region

	Branch residue (ton)					
Region	**Softwoods**	**E. grandis**	**Other gum**	**Wattle**	**Other hardwoods**	**Total**
Limpopo Province	33 794	8 484	5 823	0	0	48 101
Mpumalanga North	173 232	32 552	2 205	0	0	207 989
Central Districts	37 459	0	5 179	62	0	42 699
Mpumalanga South	158 159	16 386	55 318	9 292	928	240 083
Maputaland	0	3	0	0	0	3
Zululand	1 274	53 368	43 226	3 754	0	101 622
KZN Midlands	92 952	50 079	94 814	65 964	1	303 811
KZN North	18 952	10 463	12 292	30 418	796	72 922
KZN South	95 559	24 032	56 144	18 750	403	194 888
Eastern Cape	113 013	15 447	6 377	911	697	136 444
Southern Cape	61 712	443	0	0	0	62 155
Western Cape	17 813	0	60	0	0	17 873

A.6 Bark residue and total forest residues produced by region

	Bark residue (ton)						
	Softwood	***E. grandis***	**Other gum**	**Wattle**	**Other hardwood**	**Total Bark**	**Total Bark & Branch**
Limpopo Province	11 698	8 484	3 441	0	0	23 623	71 724
Mpumalanga North	59 965	32 552	1 303	0	0	93 820	301 809
Central Districts	12 967	0	3 060	31	0	16 057	58 757
Mpumalanga South	54 747	16 386	32 688	4 646	464	108 931	349 014
Maputaland	0	3	0	0	0	3	6
Zululand	441	53 368	25 543	1 877	0	81 229	182 851
KZN Midlands	32 176	50 079	56 027	32 982	1	171 264	475 075
KZN North	6 560	10 463	7 263	15 209	398	39 894	112 816
KZN South	33 078	24 032	33 176	9 375	202	99 862	294 750
Eastern Cape	39 120	15 447	3 768	456	349	59 139	195 583
Southern Cape	21 362	443	0	0	0	21 805	83 959
Western Cape	6 166	0	35	0	0	6 202	24 075

Appendix B: Regression models from MgO optimisation

Response	Coefficients					
	β_0	β_1	β_2	β_3	β_4	β_5
Y_{CHAR}	103.0796	-0.2429	1.815E-4	-	-0.0531	8.867E-4
Y_{LIQUID}	-72.2565	0.4684	4.595E-4	8.925E-4	-0.2882	4.34E-3
$Y_{O\text{-}PHASE}$	-27.6813	0.2316	2.166E-4	3.422E-2	-	-1.996E-3
$Y_{P\text{-}WATER}$	-70.0515	0.3099	-2.867E-4	4.25E-4	4.517E-2	-2.554E-3
$HHV_{O\text{-}PHASE}$	-26.733	0.1684	-1.502E-4	-	0.3807	-5.638E-3
Y_{CO2}	-27.081	0.1122	-7.616E-5	-3.66E-4	0.291	-
Y_{CO}	5.606	-0.0358	6.53E-5	2.95E-4	0.156	-
Y_{CH4}	4.771	-2.272E-2	2.807E-5	-	-	-
$Y_{C2\text{-}C4}$	3.0794	1.434E-2	1.726E-5	-	-	-
Y_{H2}	1.657E-3	1.290E-4	-	-	-	-

Appendix C: Regression models from CaO optimisation

Response	Coefficients					
	β_0	β_1	β_2	β_3	β_4	β_5
Y_{CHAR}	205.3069	-0.6161	5.243E-4	2.25E-4	0.13	4.53E-3
Y_{LIQUID}	-97.8717	0.5213	4.748E-4	2.583E-4	9.03E-2	5.67E-3
$Y_{O\text{-}PHASE}$	-30.4588	0.1901	1.757E-4	1.950E-4	0.1402	2.18E-3
$Y_{P\text{-}WATER}$	-7.7210	9.475E-2	9.456E-5	9.158E-4	0.4476	6.234E-4
$HHV_{O\text{-}PHASE}$	-91.8996	0.4071	-3.583E-4	9.483E-4	0.6665	1.71E-3
Y_{CO2}	11.8393	2.808E-3	-	-	0.3017	1.333E-3
Y_{CO}	-7.5839	2.335E-2	-	-	1.025E-2	-
Y_{CH4}	-1.378	3.797E-3	-	2.092E-4	0.1040	2.662E-4
$Y_{C2\text{-}C4}$	-4.080	1.239E-2	7.722E-6	3.75E-5	6.967E-3	8.984E-5
Y_{H2}	0.6034	9.81E-4	-	7.833E-5	4.447E-2	2.53E-4

Appendix D: Uncertainty analysis for energy conversion assessment

$$EC = \frac{Y_i * HHV_i}{HHV_{sample}}$$

$$\Delta EC = EC * \sqrt{\left(\frac{\Delta Y_i}{Y_i}\right)^2 + \left(\frac{\Delta HHV_i}{HHV_i}\right)^2 + \left(\frac{\Delta HHV_{sample}}{HHV_{sample}}\right)^2}$$

CaO Organic Phase: $\Delta EC = 26.7\ \% * \sqrt{\left(\frac{0.5}{18.5}\right)^2 + \left(\frac{0.7}{24.4}\right)^2 + \left(\frac{0.1}{17.7}\right)^2}$ = 1.1%

MgO Organic Phase: $\Delta EC = 25.6\ \% * \sqrt{\left(\frac{0.3}{19.9}\right)^2 + \left(\frac{0.6}{23.4}\right)^2 + \left(\frac{0.1}{17.7}\right)^2}$ = 0.8 %

CaO Gas: $\Delta EC = 10.4\ \% * \sqrt{\left(\frac{0.2}{14.0}\right)^2 + \left(\frac{0.1}{13.7}\right)^2 + \left(\frac{0.1}{17.7}\right)^2}$ = 0.2 %

MgO Gas: $\Delta EC = 7.4\ \% * \sqrt{\left(\frac{0.9}{20.7}\right)^2 + \left(\frac{0.5}{6.2}\right)^2 + \left(\frac{0.1}{17.7}\right)^2}$ = 0.7 %

Appendix E: Elemental analysis of pilot scale organics

E.1 Elemental analysis of organics from the different condensers from the pilot scale runs (wt.%, db)

Reaction Conditions		Condenser				
		C1	C2A	C2O	C3	C4
500 °C Non-Cat	C	44.3	42.5	71.8	67.5	74.2
	H	8.0	5.0	6.7	8.7	6.9
	N	-	-	0.2	-	-
	O[a]	47.7	52.5	21.3	23.8	18.9
550 °C Non-Cat	C	49.6	40.4	75.8	59.7	74.2
	H	7.8	0.5	7.6	7.3	6.9
	N	0.4	2.6	0.2	0.3	-
	O[a]	42.3	56.5	16.4	32.7	18.9
500 °C 30 % CaO	C	79.7	28.9	80.6	60.6	82.1
	H	7.1	6.5	6.1	6.1	7.3
	N	0.4	1.4	-	0.9	0.2
	O[a]	12.8	63.3	13.3	32.4	10.4
550 °C 30 % CaO	C	66.8	32.5	75.6	39.5	65.3
	H	6.0	1.0	7.4	3.3	7.4
	N	1.0	2.6	0.4	1.4	0.3
	O[a]	26.2	63.9	16.6	55.9	27.0

Appendix F: Raw data from MgO optimisation

F.1 Overall product yields

Conditions		Y_{CHAR} (wt.%)			Y_{LIQUID} (wt.%)			Y_{GAS} (wt.%)		
T (°C)	C_{cat} (wt.%)	1	2	Avg.	1	2	Avg.	1	2	Avg.
444	30	30.1	31.4	30.7	45.6	44.1	44.9	14.3	15.3	14.8
475	10	27.5	28.0	27.8	48.3	47.7	48.0	13.6	14.4	14.0
475	50	28.0	27.8	27.9	41.8	40.9	41.3	20.7	21.5	21.1
550	1.7	23.7	24.9	24.3	45.1	45.8	45.4	20.1	19.7	19.9
550	30	23.2	24.0	23.6	49.1	48.1	48.6	20.1	21.4	20.7
550	58.3	24.3	24.0	24.1	44.0	45.2	44.6	23.2	22.4	22.8
625	10	21.4	21.9	21.7	44.1	44.6	44.3	24.6	23.7	24.1
625	50	21.9	22.6	22.2	43.1	43.0	43.0	27.3	26.3	26.8
656	30	20.9	20.4	20.7	41.1	42.7	41.9	27.9	28.7	28.3

F.2 Aqueous and organic phases and pyrolytic water yields

Conditions		$Y_{A\text{-}PHASE}$ (wt.%)			$Y_{O\text{-}PHASE}$ (wt.%)			$Y_{P\text{-}WATER}$ (wt.%)		
T (°C)	C_{cat} (wt.%)	1	2	Avg.	1	2	Avg.	1	2	Avg.
444	30	26.6	24.9	25.8	19.0	19.2	19.1	14.3	13.5	13.9
475	10	25.2	25.0	25.1	23.1	22.7	22.9	13.7	13.5	13.6
475	50	25.9	24.8	25.4	15.9	16.1	16.0	13.5	12.3	12.9
550	1.7	22.0	21.6	21.8	23.1	24.2	23.7	13.0	13.8	13.4
550	30	29.1	28.4	28.5	20.0	19.7	19.9	17.3	16.7	17.0
550	58.3	27.3	28.8	28.1	16.7	16.4	16.6	16.3	16.9	16.6
625	10	25.6	24.4	25.0	18.5	20.2	19.4	14.8	14.4	14.6
625	50	27.9	28.3	28.1	15.2	14.6	14.9	16.5	17.4	17.0
656	30	24.5	25.1	24.8	16.6	17.6	17.1	13.5	14.0	13.7

F.3 Organic Phase HHV, CO_2 and CO yields

Conditions		HHV (MJ/kg, db)			Y_{CO2} (wt.%)			Y_{CO} (wt.%)		
T (°C)	C_{cat} (wt.%)	1	2	Avg.	1	2	Avg.	1	2	Avg.
444	30	24.5	24.3	24.4	10.9	12.0	11.4	3.1	2.9	3.0
475	10	23.0	22.7	22.9	9.8	9.7	9.8	3.3	4.2	3.7
475	50	24.3	25.1	24.7	15.4	16.5	16.0	4.5	4.3	4.4
550	1.7	20.3	21.3	20.8	12.7	13.3	13.0	6.1	5.6	5.8
550	30	27.4	26.1	26.8	14.0	14.3	14.1	5.2	5.7	5.4
550	58.3	23.0	23.9	23.5	16.4	16.8	16.6	5.4	4.7	5
625	10	22.6	24.0	23.3	13.4	12.6	13.0	8.6	8.2	8.4
625	50	25.2	24.7	25.0	16.7	17.4	17.1	7.9	6.8	7.3
656	30	25.4	24.8	25.1	15.7	16.1	15.9	9.1	9.3	9.2

F.4 CH_4, C_2-C_4 and H_2 yields

Conditions		Y_{CH4} (wt.%)			Y_{C2-C4} (wt.%)			Y_{H2} (wt.%)		
T (°C)	C_{cat} (wt.%)	1	2	Avg.	1	2	Avg.	1	2	Avg.
444	30	0.2	0.2	0.2	0.08	0.15	0.12	0.06	0.07	0.06
475	10	0.3	0.3	0.3	0.13	0.18	0.15	0.06	0.06	0.06
475	50	0.4	0.4	0.4	0.22	0.23	0.22	0.05	0.07	0.06
550	1.7	0.9	0.8	0.9	0.42	0.39	0.38	0.07	0.07	0.07
550	30	0.5	0.9	0.7	0.26	0.54	0.40	0.09	0.07	0.08
550	58.3	0.8	0.5	0.7	0.47	0.37	0.42	0.08	0.07	0.07
625	10	1.6	1.5	1.5	0.91	1.42	1.17	0.08	0.08	0.08
625	50	1.7	1.3	1.5	0.99	0.72	0.86	0.07	0.08	0.07
656	30	1.9	2.0	1.9	1.01	1.09	1.05	0.09	0.10	0.09

Appendix G: Raw data from CaO optimisation

G.1 Overall product yields

Conditions		Y_{CHAR} (wt.%)			Y_{LIQUID} (wt.%)			Y_{GAS} (wt.%)		
T (°C)	C_{cat} (wt.%)	1	2	Avg.	1	2	Avg.	1	2	Avg.
444	30	40.0	39.3	39.7	41.0	41.5	41.3	8.7	8.9	8.8
475	10	31.4	32.8	32.1	43.7	43.5	43.6	14.9	14.4	14.7
475	50	42.9	43.9	43.4	39.9	39.1	39.5	6.9	6.8	6.8
550	1.7	24.7	25.2	25.0	46.4	46.8	46.6	18.4	18.2	18.3
550	30	29.7	28.7	29.2	46.9	47.2	47.1	13.9	14.1	14.0
550	58.3	40.8	41.9	41.3	38.7	39.4	39.1	10.3	10.1	10.2
625	10	24.7	25.2	25.0	43.6	43.9	43.8	21.9	21.4	21.6
625	50	34.4	35.4	34.9	41.2	41.3	41.3	15.0	14.9	15.0
656	30	30.8	31.6	31.2	43.1	42.4	42.8	16.5	16.0	16.2

G.2 Aqueous and organic phases and pyrolytic water yields

Conditions		$Y_{A\text{-}PHASE}$ (wt.%)			$Y_{O\text{-}PHASE}$ (wt.%)			$Y_{P\text{-}WATER}$ (wt.%)		
T (°C)	C_{cat} (wt.%)	1	2	Avg.	1	2	Avg.	1	2	Avg.
444	30	23.3	24.3	23.8	17.7	17.3	17.5	15.3	14.8	15.0
475	10	24.0	23.9	23.9	19.7	19.6	19.6	15.7	15.9	15.8
475	50	23.5	23.1	23.3	16.4	16.0	16.2	17.4	16.7	17.1
550	1.7	24.2	24.8	24.5	22.3	22.0	22.1	15.7	16.4	15.8
550	30	28.7	28.3	28.5	18.2	18.9	18.6	17.9	18.8	18.4
550	58.3	25.9	27.0	26.4	12.8	12.4	12.6	20.7	21.1	20.9
625	10	25.5	26.0	25.7	18.1	18.0	18.0	15.9	16.7	16.3
625	50	27.5	28.1	27.8	13.7	13.2	13.5	22.5	22.5	22.5
656	30	26.3	25.7	26.0	16.8	16.7	16.8	18.8	18.8	18.8

G.3 Organic Phase HHV, CO_2 and CO yields

Conditions		HHV (MJ/kg, db)			Y_{CO2} (wt.%)			Y_{CO} (wt.%)		
T (°C)	C_{cat} (wt.%)	1	2	Avg.	1	2	Avg.	1	2	Avg.
444	30	23.0	22.5	22.8	5.3	5.4	5.4	3.0	2.9	2.9
475	10	23.8	24.2	24.0	10.7	10.5	10.6	3.6	3.5	3.5
475	50	27.6	28.3	28.0	0.9	1.0	1.0	4.3	4.2	4.2
550	1.7	22.8	23.1	23.0	12.0	12.1	12.1	5.2	5.0	5.1
550	30	25.9	26.9	26.4	5.8	5.7	5.8	5.8	6.1	5.9
550	58.3	26.2	26.1	26.1	0.6	1.0	0.8	5.7	5.5	5.6
625	10	23.0	23.8	23.4	11.8	11.6	11.7	7.6	7.5	7.5
625	50	22.0	21.3	21.7	1.9	1.6	1.7	7.9	7.8	7.8
656	30	20.8	21.2	21.0	5.3	5.0	5.2	7.5	7.5	7.5

G.4 CH_4, C_2-C_4 and H_2 yields

Conditions		Y_{CH4} (wt.%)			Y_{C2-C4} (wt.%)			Y_{H2} (wt.%)		
T (°C)	C_{cat} (wt.%)	1	2	Avg.	1	2	Avg.	1	2	Avg.
444	30	0.3	0.3	0.3	0.12	0.15	0.13	0.11	0.12	0.11
475	10	0.4	0.3	0.3	0.19	0.17	0.18	0.08	0.06	0.07
475	50	0.9	0.8	0.8	0.31	0.37	0.34	0.45	0.40	0.43
550	1.7	0.8	0.7	0.7	0.37	0.37	0.37	0.07	0.06	0.07
550	30	1.3	1.3	1.3	0.71	0.74	0.72	0.26	0.24	0.25
550	58.3	2.2	2.0	2.1	0.97	0.87	0.92	0.79	0.79	0.79
625	10	1.5	1.4	1.4	0.87	0.88	0.87	0.10	0.08	0.09
625	50	3.0	3.4	3.2	1.34	1.18	1.26	0.87	0.96	0.91
656	30	2.2	2.1	2.1	1.10	1.15	1.12	0.35	0.32	0.33